NASA/CR-1998-206940

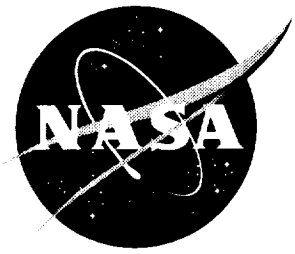

Magellan Aerodynamic Characteristics During the Termination Experiment Including Thruster Plume-Free Stream Interaction

Francisco J. Cestero and Robert H. Tolson
Joint Institute for Advancement of Flight Sciences
The George Washington University
Langley Research Center, Hampton, Virginia

National Aeronautics and
Space Administration

Langley Research Center
Hampton, Virginia 23681-2199

Prepared for Langley Research Center
under Cooperative Agreement NCC1-104

March 1998

Available from the following:

NASA Center for AeroSpace Information (CASI)
800 Elkridge Landing Road
Linthicum Heights, MD 21090-2934
(301) 621-0390

National Technical Information Service (NTIS)
5285 Port Royal Road
Springfield, VA 22161-2171
(703) 487-4650

Abstract

Results are presented for the study of the aerodynamic characteristics of the Magellan spacecraft during the October 1994 Termination Experiment. Also studied are the effects of the thruster engine exhaust plumes upon the molecular free stream around the spacecraft and upon the aerodynamics coefficients. As Magellan passed through the carbon dioxide region of the Venusian atmosphere, the solar array panels were turned in opposite directions relative to the free stream creating a torque on the spacecraft. The spacecraft control system was programmed to counter the effects of this torque with attitude control engines to maintain an inertially fixed attitude. The orientation and reaction engine telemetry returned from Magellan are used to create a model of the aerodynamic torques.

Presented are new geometric models of the Magellan spacecraft. These are analyzed with the aid of both free molecular and Direct Simulation Monte Carlo codes over a range of momentum accommodation coefficients. The aerodynamic torques determined from these simulations are compared to the torques derived from the telemetry data. The Direct Simulation Monte Carlo method is also used to model the attitude engine exhaust plumes, the free stream disturbance caused by these plumes, and the resulting torques acting on the spacecraft compared to no-exhaust plume cases. The effect of the exhaust plumes was found to be approximately a factor of two for the cases studied.

In addition, flight telemetry data was used in an attempt to calibrate the attitude control engines yielding varying thrust levels (20%) from engine to engine.

Table of Contents

List of Figures

List of Tables

Abbreviations

AT	Atmospheric Torque
AACS	Articulation and Attitude Control System
ARU	Attitude Reference Unit
BUS	Propulsion bus.
DSMC	Direct Simulation Monte Carlo
FEM	Forward Equipment Module
FMS	Free Molecular Simulation
Freemac	Free molecular flow simulation software
Freemol/DSMC	Free molecular code and DSMC code designed with the same modeling and similar discretization conventions.
HGA	High Gain Antenna
MGA	Medium Gain Antenna
OTM	Orbital Trim Maneuver
PA	Plume Analysis
REA	Reaction Engine Assembly
REC	Reaction Engine Calibration
REM	Reaction Engine Motor
RWA	Reaction Wheel Assembly
SRM	Solid Rocket Motor
TE	Termination Experiment
VIRA	Venus International Reference Atmosphere

Nomenclature

A_{ref}	Reference area, meters^2
Cx, Cy, Cz	Aerodynamic force coefficients
Cmx, Cmy, Cmz	Aerodynamic moment coefficients
d	Diameter of free stream particle, meters
$\varepsilon_x, \varepsilon_y, \varepsilon_z$	Direction cosines of free stream along each coordinate axis
F_x, F_y, F_z	Forces acting in direction of coordinate axis, Newtons.
Freemac TRASYS	Model of Magellan in Freemac conventions using TRASYS dimensions
Freemol/DSMC Didier	Model of Magellan in Freemol/DSMC conventions developed by D. Rault.
Freemac Didier	Freemol/DSMC Didier model converted to Freemac conventions
I	Moment of inertia, kg-meters^2
J2000	Inertial reference frame
k	Boltzmann constant, k = 1.3806 x 10^{-23} J/ K
Kn	Knudsen number
L	Characteristic length of Magellan, L = 10.0 meters
L_{ref}	Reference length, meters
m_{av}	Weighted average of gas specie mass, kg
N	Torque vector, Newton-meters
n	Particle density, particles/meters^3
θ, ϕ	Angles that describe the orientation of a model in Freemac to the free stream, degrees
ρ	Atmospheric density, kg/meters^3
S	Molecular speed ratio
σ_n, σ_t	Normal and tangential accommodation coefficients
T	Surface temperature, Kelvins
T_∞	Ambient atmospheric temperature, Kelvins
T_x, T_y, T_z	Torques acting along direction of coordinate axis, Newton-meters
U	Free stream velocity, meters/second
u	Free stream unit vector
φ	Spacecraft attitude angular error from nominal orientation, radians
ω	Spacecraft attitude angular velocity error from nominal, radians/sec

I. Introduction

Introductory material on the background of the Magellan spacecraft and the mission to Venus are presented with an emphasis on the Termination Experiment. In addition, the purpose of this study and the research methodology are introduced.

I.1 Background

The Magellan spacecraft was launched on a 15 month voyage to the planet Venus from the Space Shuttle on May 5, 1989.. The mission was designed to map the surface topology hidden beneath the clouds of Venus using a synthetic aperture radar and to measure variations in the Venus gravity field that would provide data on its interior structure[1]. Arriving on August 10, 1990, Magellan assumed an initial orbit of approximately 8500 km x 170 km inclined 85.5° from the equator. The first three Venus sidereal days were spent radar mapping 98% of the surface. During the fourth Venusian day Magellan measured the variations in the Venus gravitational field, but the elliptic orbit limited the area of good data acquisition to the equatorial region. To improve the quality of the polar data, Magellan performed an aerobraking maneuver in the summer of 1993 that placed the spacecraft in a more circular 700 km x 250 km orbit[2]. The primary mission goals successfully completed, two additional experiments were performed including the September Windmill Experiment[3,4] and the Termination Experiment (TE).

The Termination Experiment was the last mission performed by the Magellan spacecraft. The experiment involved multiple passes through Venus' upper atmosphere ranging from altitudes of 140 km where the current atmospheric model predicts primarily carbon dioxide to 170 km where the primary specie is atomic oxygen. These passes were to continue until Magellan entered the Venus atmosphere and burned up. The intent of the Termination Experiment was that the data returned from the Magellan spacecraft as it

swept through the CO_2 region of Venus atmosphere, would increase our understanding of the behavior of carbon dioxide under free molecular conditions and transitional flow. With the solar array panels turned in opposite directions relative to the free stream the atmosphere induced a torque on the spacecraft. In this sense Magellan behaved like a windmill. The spacecraft's control system was programmed to counter the effects of this torque with the Reaction Engine Assemblies (REA) to maintain an inertially fixed attitude. Given knowledge of the timing and thrust level of each motor the total torque acting upon the spacecraft can be determined.

The flow field around the Magellan spacecraft during the TE has been characterized with a Knudsen number varying between 1 and 10, placing the flow field between the regions described by continuum and free molecular flow physics. At the molecular level the forces acting on Magellan in a free molecular environment and their resulting torques are a function of the normal and tangential momentum accommodation coefficients. These coefficients represent the fraction of free stream particles that reflect diffusely in a collision with the surfaces of the spacecraft.

I.2 Purpose of Study

The purposes of this study are two fold. To use aerodynamic data from the Magellan Termination Experiment (TE) to study the free molecular flow characteristics of the spacecraft in a carbon dioxide environment. And to investigate the effects the engine exhaust plumes, by disturbing the free stream, had upon the aerodynamic torques experienced by the spacecraft, and by implication, future spacecraft in similar situations.

I.3 Methodology

This investigation into the accommodation coefficients of the Magellan spacecraft during the Termination Experiment is organized into four broad phases. The first phase is the Reaction Engine Calibration (REC) analysis which uses telemetry data provided by the attitude control system to calibrate the attitude control engines. This is accomplished by differentiating the attitude error with respect to time and comparing the change in the error rate before and after an isolated engine firing. Modeling the engine firings as pulses, the change in the attitude rate of change produced by an engine firing is directly related to the thrust level by solving the Euler equations of motion for a rigid body.

The second phase is the Atmospheric Torque (AT) analysis which determines the aerodynamic forces acting upon the Magellan spacecraft. The aerodynamic torques are obtained by analyzing the telemetry data in conjunction with the results from the REC phase to determine the total of all torques acting on the spacecraft. This is done by differentiating the attitude errors twice with respect to time and multiplying by the assumed moments of inertia. To this is added the calibrated torque from the REC phase. Gravity gradient and solar pressure torque models are introduced and their effects subtracted from the total torque. From this the aerodynamic torque is determined.

Phase three, the Free Molecule Simulation analysis (FMS), uses a free molecular simulation of a geometric model of the Magellan spacecraft to numerically determine the aerodynamic coefficients for a given set of accommodation coefficients. The simulation is implemented using the free molecular analysis program Freemac[5,6] as presented in chapter VI. Two cases are simulated, the first with all accommodation values (normal and tangential, equal over the surface of the spacecraft) at 1.0 and the second with all the accommodation coefficients set to 0.8. The results of the FMS phase for both

accommodation models are compared to the AT results in order to estimate the average accommodation coefficient through interpolation.

The fourth phase, the Plume Analysis (PA), involves using a Direct Simulation Monte Carlo (DSMC) code, called DSMC[7] to investigate the effects of interactions between the incoming free stream and attitude control engine exhaust[8] on the spacecraft's aerodynamic coefficients. Simulation cases are first run without exhaust plume modeling and without modeling free stream interparticle collisions for comparison to the free molecular results in the FMS phase. Then simulations are performed in which interparticle collisions are modeled, and lastly full up cases with both collisions and exhaust plumes are done. The same accommodation coefficient cases used in the FMS phase are used in order to facilitate comparison. Emphasis is on showing that the effect of plume interaction is substantial, and alters the results in the correct sense to account for differences between the AT and FMS torque models. The DSMC code is computationally intensive limiting the number of data points studied and further only permits static flow field interaction, therefore the effects upon the aerodynamic characteristics over time as an exhaust plume forms and dissipates could not be studied.

The appendix includes a section which compares Freemac to another free molecule simulation code called Freemol which uses the same geometry definitions as DSMC and has been used to analyze the Magellan geometry. Another section investigates the sensitivity of the free molecular simulation results to changes in the geometry and free stream models.

II. Magellan Spacecraft

II.1 Description

Magellan is a spacecraft measuring approximately ten meters from solar panel tip to tip with a mass of about 1100 kg. Major components from an aerodynamic view point are the High Gain Antenna (HGA), the Forward Equipment Module (FEM), the propulsion bus (BUS), the solid rocket motor shroud, the solar array panels and the reaction engine assemblies (REA) with their supporting trusswork. Other components are the altimeter, star tracker and the Medium Gain Antenna (MGA). Figure 2.1 illustrates the Magellan spacecraft.

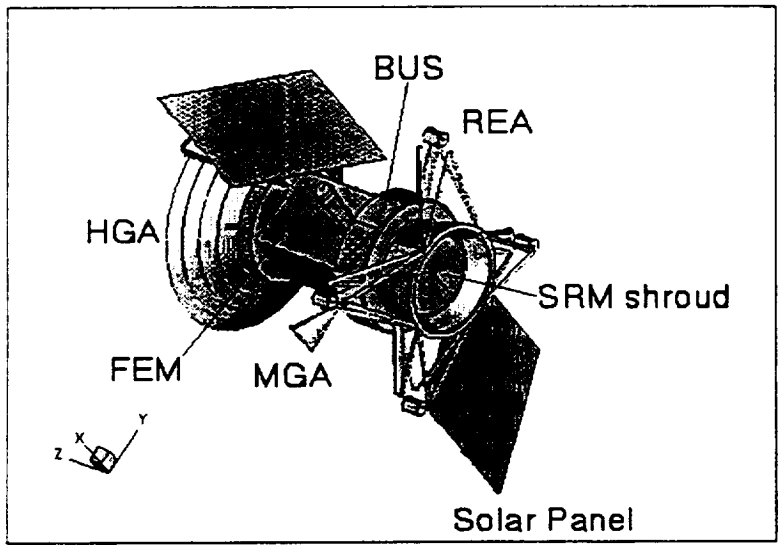

Figure 2.1: Magellan spacecraft.

II.2 Coordinate Systems

Two coordinate axis are defined fixed to the spacecraft[9]. The body axis is defined with the origin at the center of mass, the X axis parallel to the solar panels center line, the Y axis extends out the star tracker side, and the Z body axis extends along the length of the craft out the HGA as shown by the coordinate axis in the lower left hand corner of Figure 2.1. The control axis is the same as the body axis system except that it is rotated +45° about the Z axis.

The angles θ and ϕ are used in Freemac to describe the orientation of the free stream velocity U with respect to the body fixed axis. The component along each axis of the unit vector u is given by the equations.

$$u_X = \sin\phi\cos\theta \quad (1)$$
$$u_Y = \cos\phi\cos\theta \quad (2)$$
$$u_Z = -\sin\theta \quad (3)$$

Solar panel angles describe the orientation of the solar panels to the spacecraft. They represent the rotation about the X axis from an initial position lying in the X-Y plane with the photovoltaic cells facing in the -Z direction. The angle of incidence of the solar panels mentioned below is 180° minus the angle between the free stream and the solar panel surface normal, i.e. the angle of incidence is zero for flow normal to the active side of the solar panel.

II.3 Mission Description

The Termination Experiment was conducted on October 12, 1994, over orbits 15020 through 15032. Control constrains precluded the use of the High Gain Antenna for communication with its narrow ¼° beam[8]. Instead, the Medium Gain Antenna (MGA), located on the -Y side of the FEM at a 70° angle from the Z axis was used to transmit telemetry data back to Earth. The potential orientations for the windmill experiment were limited to rotations of the spacecraft about the MGA-Earth axis. Within this constrain and the demands of power generation, the Magellan spacecraft was flown in two different orientations to the free stream and solar panel configurations, the first over orbits 15020 to 15029 and the second from orbits 15030 to 15032. Nominal spacecraft orientation was to aim the MGA towards Earth while the X axis (the solar panel center line) was maintained perpendicular to the Magellan-Sun vector. For the Termination Experiment

the spacecraft was then rotated about the MGA-Earth vector and the solar panels rotated about the X axis to create the desired windmill effect.

Unforeseen at the time the Termination Experiment was designed was the potential interference of the attitude control engines with the free stream. The free flow disturbance caused by the engines as they fired to maintain Magellan's attitude proved to have a significant effect on the aerodynamic characteristics of the spacecraft. Discovery of this phenomena has already had an influence on the planning of the Mars Exploration program.

During orbits 15020 to 15029 the +X solar panel was rotated -60° about the X axis while the -X solar panel was set at 22° to create a windmill type aerodynamic torque. This configuration was designed so that at periapsis the angle of incidence of both panels to the wind vector would be 60°. The spacecraft orientation to the wind changed little from one orbit to the next. The angle θ, in equations (1-3), varied from about -53° at periapsis -10 minutes to -35° at periapsis to -7° degrees at periapsis +10 minutes, while ϕ varied from 20° to 75° to 103° respectively. The roll about the MGA-Earth axis for these orbits was -20°.

Figures 2.2, 2.3, and 2.4 show respectively the velocity, altitude, and relative wind orientation over orbits 15020 through 15029 with respect to the time of periapsis.

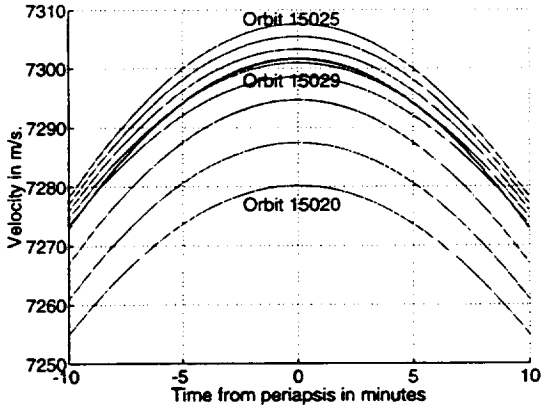

Figure 2.2: Velocity over Orbits 15020 to 15029

Figure 2.2 illustrates how the orbital velocity at periapsis increased from orbit 15020 to 15025 as the mean altitude was lowered. After orbit 15025 the velocity decreases as drag forces take effect. The velocity changes are small, less than ½%, over the orbits at periapsis.

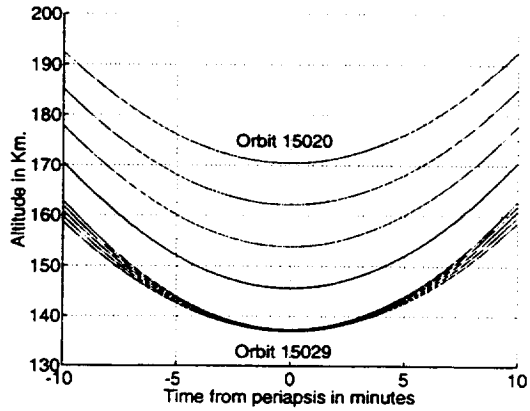

Figure 2.3: Altitude over Orbits 15020 to 15029

Orbital maneuvers lowered the altitude for each orbit from 15020 to 15023 by about 8 km. per orbit. The fourth orbit maneuver was performed after it was determined that the attitude control system had sufficient authority to control the attitude at an altitude of 138 km. The closely spaced lines showing the altitude for orbits 15025 to 15029 indicates the effect of drag in lowering the apoapsis.

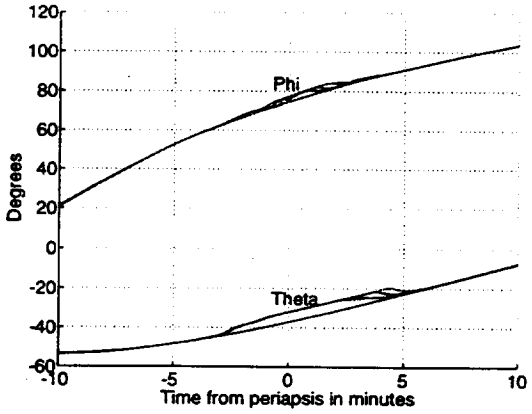

Figure 2.4: Attitude θ and ϕ over Orbits 15020 to 15029

Figure 2.4 shows the relative free stream orientation to the spacecraft in the θ and ϕ angles of equations (1-3). The θ and ϕ deviations in the vicinity of periapsis correspond to orbits with periapsis at 138 km altitude (orbits numbered 15025 to 15029). The deviations are approximately 4° and result from the relatively high torques experienced by the spacecraft at the lower altitudes higher atmospheric density. They indicate that the atmospheric torque at these times was high enough to require the full thrust of the reaction engines to maintain attitude. The next section gives a more detailed description of the Articulation and Attitude Control System.

Over orbits 15030 to 15032 the +X solar panel was rotated -4° about the X axis while the -X solar panel was set at -34°. This configuration was designed so that at periapsis the angle of incidence of both panels to the wind vector would be 15°. The spacecraft orientation to the wind changed little from one orbit to the next. The angle θ varied from about -40° at periapsis -10 minutes to -70° at periapsis to -55° degrees at periapsis +10 minutes, while ϕ varied from -50° to 10° to 90° respectively. The roll about the MGA-Earth axis for these orbits was -70°.

Figures 2.5, 2.6, and 2.7 repeat figures 2.2 to 2.4 for orbits 15030 to 15032.

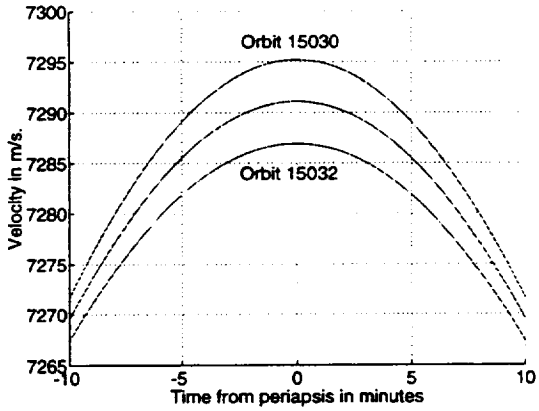

Figure 2.5: Velocity over Orbits 15030 to 15032

The orbital velocity for orbits 15030 to 15032 continues to decrease because of drag. Velocity change per orbit from 15025 to 15029 is about 3 m/s per orbit, while for orbits 15030 through 15032 the change is about 4 m/s per orbit.

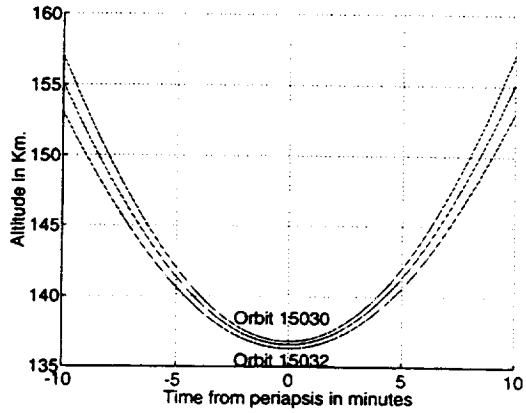

Figure 2.6: Altitude over Orbits 15030 to 15032

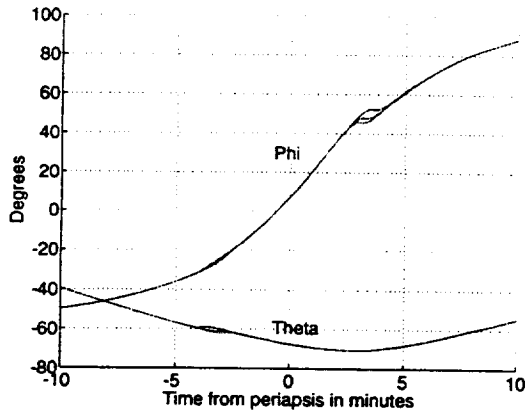

Figure 2.7: Attitude θ and ϕ over Orbits 15030 to 15032

In Figure 2.7 a clear change in the relative free stream angles due to the different orientation flown over the later orbits is visible. The cause of the slight divergences in θ at periapsis -3 minutes and ϕ at periapsis +3 minutes is unknown.

II.4 Articulation and Attitude Control System

The Articulation and Attitude Control System (AACS) performs two primary tasks. The first is to orient and maintain Magellan pointing in a commanded direction (Attitude Control). The second task is to control the positioning of the solar panels (Articulation Control).

Articulation control is most commonly used to aim the solar panels towards the sun to provide electrical power for the onboard systems. Another use is to orient the solar panels to induce a torque on the spacecraft during the Windmill and Termination experiments. Articulation control involves using the motors installed on the solar panel support struts to rotate the panels about Magellan's +X body axis.

Attitude adjustments are used to orient the spacecraft to satisfy mission requirements. These include: pointing communication antennas, aiming the radar mapper, star scanning, reaction wheel desaturation, and maintaining orientation during maneuvers. Magellan's attitude control was performed by a system operating at 7.5 Hz. The angular and angular rate errors from a commanded attitude are determined by gyroscopes within the Attitude Reference Unit (ARU). The gyroscopes were calibrated during previous orbits using the star tracker mounted on the +Y side of Magellan to the J2000 inertial reference frame[10]. Gyro drift was found to be less than 1° per day [M.Patterson, private comm.].

Corrective firings of the attitude engines are determined according to the spacecraft state and command law. The state is expressed in terms of φ and ω, the angular error and the angular rate error from the commanded attitude determined by the ARU for each control axis. The control law can best be explained with the help of the phase space graph shown in Figure 2.8.

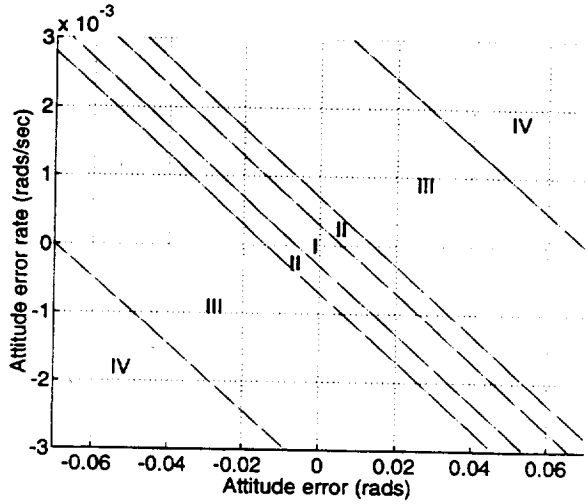

Figure 2.8: Control System Phase Space

The diagonal lines are the control system switching lines that divide the state space into seven control regions. Each control cycle (1/7.5 seconds or 133 ms), the spacecraft state (φ,ω) in each control axis is compared to the switching lines in this space. If the state lies in region I, no engine firing takes place. A state in region II triggers an 11 ms (1/12 full on) pulse from the proper corrective engine. In region III the control system would command a 33 ms pulse (1/4 full on). If the spacecraft becomes disturbed enough to place the craft in region IV the attitude engines will fire continuously for 133 ms.

While the control system cycled at 7.5 Hz, the timer for the thruster control cycled at 90 Hz, hence the multiples of 11 ms firing times. The longer pulses are a continuous burn and do not represent a series of 11 ms impulses. This distinction is necessary since the thrust counter telemetry data presents simply the number of thruster control cycles that

the respective thruster is on. Therefore, although three 11 ms pulses generate a different impulse than one 33 ms burst, both would be represented in the telemetry stream by a count of three. Additional analysis is needed to distinguish between the two cases.

II.5 Reaction Wheel and Reaction Engine Assemblies

Two means exist for effecting attitude control. The Reaction Wheel Assembly (RWA) can exert 0.18 N-m on the spacecraft to orient or resist the effect of external forces. The RWA consists of three reaction wheels, each mounted along one of the body fixed axis providing full 3 axis stability. The RWA system was not used during the Termination Experiment because of predictions that the torque's on the spacecraft during periapsis would be greater than 0.18 N-m. The RWA was used for aerodynamic studies at higher altitudes[4].

The Magellan mass expulsion system in turn uses twelve Reaction Engine Motors (REM) that are rated at 0.9N (0.2 lbf.) each. These engines are mounted in the four Reaction Engine Assembly (REA) pods at the rear of the craft, three to a pod. Fuel is fed from a central supply tank mounted in the spacecraft's bus. In each pod two REM's are mounted along the -Z axis, while the third is aligned in the X-Y plane to provide Z axis control. All engines are mounted with a moment arm of 1.95 meters. This arrangement provides stable 3-axis control of the Magellan spacecraft. Maximum controllable torque about any axis is therefore 0.9N x 2 x 1.95 or about 3.6 N-m. For convenience the locations of the REAs are shown in Figure 2.9.

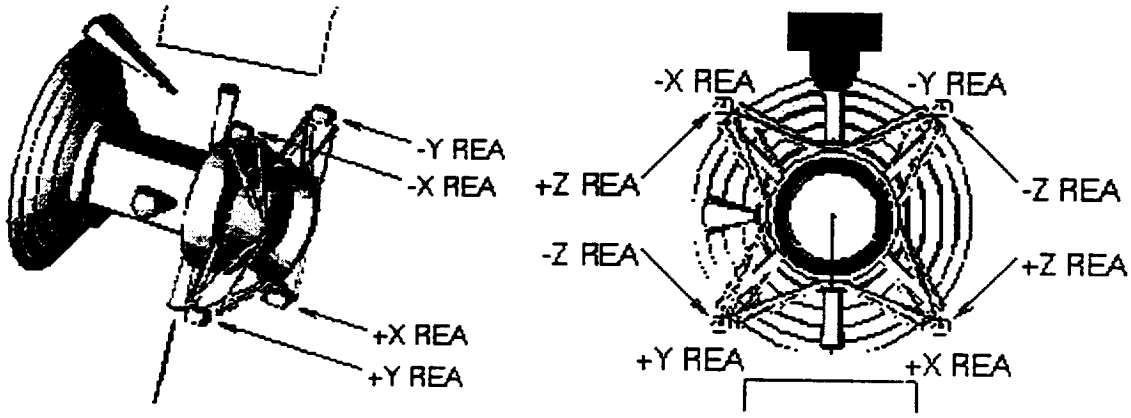

Figure 2.9: REA Thruster Locations

The REM's are model MR-103C/D/E engines which inject hydrazine into a platinum catalyst combustion chamber. As discussed above, thrust control time is in units of 11 ms pulses. Specific impulse is 230, nozzle radius is 2.92 mm with an expansion ratio of 100:1. Equivalent thrust is dependent on catalyst bed temperature, supply pressure, and pulse duration. Prior to the Termination Experiment, as much of the original fuel supply had been expended, thrust levels were anticipated to be lower than nominal. The REM's were calibrated at 0.5 N during the Termination Experiment orbit trim maneuvers [Kuen Wang, private comm.], which were essentially full-on maneuvers lasting about 10 minutes.

III. Data and Models

The telemetry data returned by Magellan and the various models used to represent the spacecraft characteristics and environment are presented in detail below.

III.1 Mission Telemetry Data

Telemetry was transmitted in real time to Earth every 2/3 second (every 5 control cycles). Each orbit generated from 4 to 5 thousand data points. Telemetry variables are presented in Table 3.1 with comments.

Variable	Name	Notes
t	Time	Universal time since start of day in seconds.
t1	Temperature of -X solar panel.	Resolution is 1.422 Celsius.
t2	Temperature of +X solar panel.	Resolution is 1.422 Celsius.
tx, ty, tz	Attitude errors in body coordinates.	Resolution is 6.1E-05 radians.
txd, tyd, tzd	Attitude time rate errors in body coordinates.	Resolution is 5.4E-05 rads/sec.
xpc, ypc, zpc	Cumulative thruster firing count of positive torque REAs.	1 count = 1 twin burst as REAs are mounted in pairs. Counters roll over at 65535.
xnc, ync, znc	Cumulative thruster firing count of negative torque REAs.	As positive counter above.

Table 3.1: Magellan Spacecraft Telemetry

The thruster firing count data only indicates how many 11ms counts the engines were commanded to be on during the 2/3 seconds of each telemetry frame. No information exists on when in those 2/3 of a second the actual firings take place.

III.2 Orbit and Orientation Analysis Model

Orbital parameters used in this analysis are from the Magellan Navigation Team. Spacecraft orbital path was determined in the J2000 reference frame for a time 600 seconds before and after periapsis in 10 second intervals. A nominal orientation was determined to which was added the attitude error from the telemetry. This correction is significant for the orbits 15025 to 15029 as the altitude drops to around 138 km. (see figure 2.4). Spacecraft data calculated from the orbit and orientation model includes altitude, velocity, solar panel angle of incidence, relative wind vector in θ and ϕ, and the gravity gradient torque.

III.3 Gravity Gradient Model

The gravity gradient torques are modeled using the orbital and attitude data presented above. These torques are small, on the order of 0.001 N-m, yet an order of magnitude greater than solar torques. The moments of inertia of the Magellan spacecraft as determined from reaction wheel analysis[11]:

$$I = \begin{bmatrix} 1106 & 4.0 & 21.0 \\ 4.0 & 2008 & -3.9 \\ 21.0 & -3.9 & 1556 \end{bmatrix}$$

in the body fixed coordinates. These values do not account for the rotation of the solar panels, but this effect on the moments of inertia is negligible during the Termination Experiment.

III.4 Solar Pressure Model

The effects of solar torques acting on Magellan over the course of the Termination Experiment are considered insignificant. The solar momentum flux at the orbit of Venus is 8.42E-6 kg/m s^2, the reference area and length are 23 m^2 and 3.66 m respectively, the maximum moment coefficient measured about any axis is 0.15, and time ranges from ten minutes before to ten minutes after periapsis, or 1200 seconds. The number of engine firings needed to correct for solar pressure during one orbit is therefore less than one 11 ms impulse per minute which is negligible.

III.5 Venus Atmospheric Model

The Venus International Reference Atmosphere model of the Venusian atmosphere was obtained from drag data gathered during the Pioneer mission to Venus[12]. The model is presented as a set of tables referenced by local solar time and altitude in 5 km increments and provides data on atmospheric density, composition, and temperature. Values for a typical altitude during the Termination Experiment of 140 km during local daytime are: atmospheric density of 0.613E-11 g/cm^3 of which 85.5% by mass is carbon dioxide. Other atmospheric components are atomic oxygen (3.96%), carbon monoxide (6.39%), and diatomic nitrogen (4.2%). Atmospheric temperature is given as 225 K.

III.6 Magellan Spacecraft Models

Two models of the Magellan spacecraft were developed for use with the Freemac code. With a third model created for the DSMC code these models are the starting points for the aerodynamic analysis. All models have a center of mass on the Z axis at a point

+6.529 inches with respect to the solar arrays centerline axis. All models have a reference area of 23.0 m^2 and a reference length of 3.66 m.

The model name convention used is to label each model according to the analysis code geometry conventions in which it is implemented (Freemac or Freemol/DSMC) followed by the source of the dimensions and geometries used.

The first model, referred to as the Freemac TRASYS model, is a high resolution depiction of the major components of the craft as built. In all, 72 components are defined and discretized into 112,874 flat elements. The dimensions and orientations used are taken from the TRASYS thermal code used by the Lockheed Martin Company [M.Patterson, private comm.]. This model is believed to be the most accurate measurements taken of the spacecraft as built. Differences between the components used by Freemac and TRASYS plus a desire to keep the number of shapes to a minimum led to six design compromises:

1) The High Gain Antenna is modeled in TRASYS as a paraboloid. This shape is not supported in Freemac, instead four cones are used.

2) The Altimeter is modeled with six triangular plates and one rectangular plate.

3) The thin support spars along the solar panels were omitted.

4) The Reaction Engine Assemblies are highly complicated box like structures mounting engine nozzles and support brackets. Each is simplified as a right cylinder with circular plate endcaps.

5) In the TRASYS model the SRM adapter endcap (the concave "cup" at the bottom of Magellan) as a concave spherical section. In Freemac this part is a circular flat plate.

6) Coaxial cables, wires, minor protrusions, and the like modeled in TRASYS were not included in the Freemac model.

The Freemac TRASYS model is used to determine the aerodynamic coefficient values in the FMS phase. Figure 3.1 presents the Freemac TRASYS model in both configurations during the Termination Experiment.

The second Magellan model, the Freemol/DSMC Didier model, was developed independently for the Freemol and DSMC codes[13]. This model uses 85 components discretized into approximately 132,000 cubics, each about 1 inch cube. The model is used for investigating the attitude engine plume exhaust interaction with the free stream using the DSMC method. Major differences between the models are listed below. Others exist, but are related to minor components such as the HGA secondary reflector, the star tracker, and the MGA.

	Freemac TRASYS	Freemol/DSMC Didier	Notes
High Gain Antenna	4 cones to imitate 70" max, 34.9" min radius x 20.7" high parabola	72"max, 34.7" min radius x 20.3" high spherical section	TRASYS HGA at Z+1.07" relative to Didier model.
Forward Equipment Module	65.5" L x 49.4" W x 38.6" D rectangular box. Centerline at X+0.9", Y+0.0	63.9" L x 49.4" W x 38.6" D rectangular box. Centerline on Z axis.	Bottom of TRASYS model mounted Z+2.88" relative to Didier model.
Altimeter	24.5" W x 11" D x 65" L triangular box.	10" radius x 75.9" cone	
Propulsion Bus	38.45" radius x 20" cylinder (bus). 33.5" max, 25.6" min radius x 30.1" cone (shroud)	36.6" radius x 16.8" cylinder (bus). 31.7" max, 28.4" min radius x 33.3" cone (shroud)	
REA and Trusswork	Simple REA geometry. 3.0" radius major spars, 1.25" radius minor spars.	Moderate REA geometry. 2.7" radius major spars, 1.1" radius minor spars.	
Solar Array Panels	98.3" L x 99.5" W. No central spar modeled.	98.3" L x 99.5" W. Central spar included.	Same locations. TRASYS model mounted 0.2" further

Table 3.2: Freemac TRASYS and Freemol/DSMC Didier Models

The coordinate system used to describe the Freemol/DSMC Didier model differs from that described in chapter 2. The Freemol/DSMC X axis corresponds to the Z body axis while the Y axis corresponds to the -X body and the Freemol/DSMC Didier Z axis is the same as the -Y body axis.

The second Freemac model developed, called the Freemac Didier model, is a translation of the Freemol/DSMC Didier model into Freemac conventions. The only differences between the two are: the High Gain Antenna in the Freemac Didier model is created with four cones instead of a spherical section, and the SRM adapter end cap is a circular flat plate versus another spherical section. The axis system used is the same as the Freemac TRASYS model. Figure 3.2 shows both the Freemac Didier and Freemol/DSMC Didier geometries in the solar panel -60°/22° configuration. Freemac Didier and Freemol/DSMC Didier models in the -4°/-34° configuration were not developed.

Freemac TRASYS Magellan Geometry
Solar Array Angles: +X= -60°, -X= 22°
Orbits 15020-15029

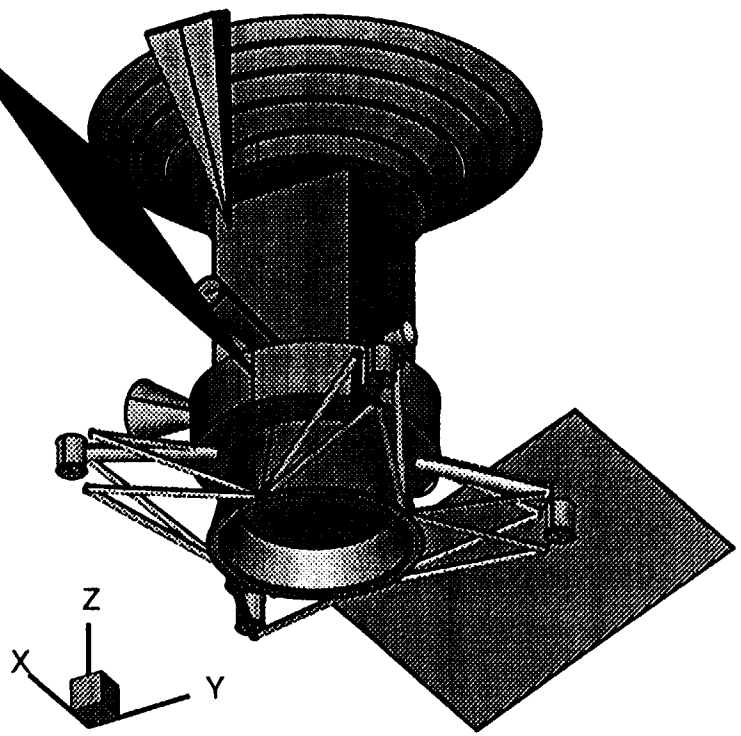

72 element model

Freemac TRASYS Magellan Geometry
Solar Array Angles: +X=-4°, -X=-34°
Orbits 15030-15032

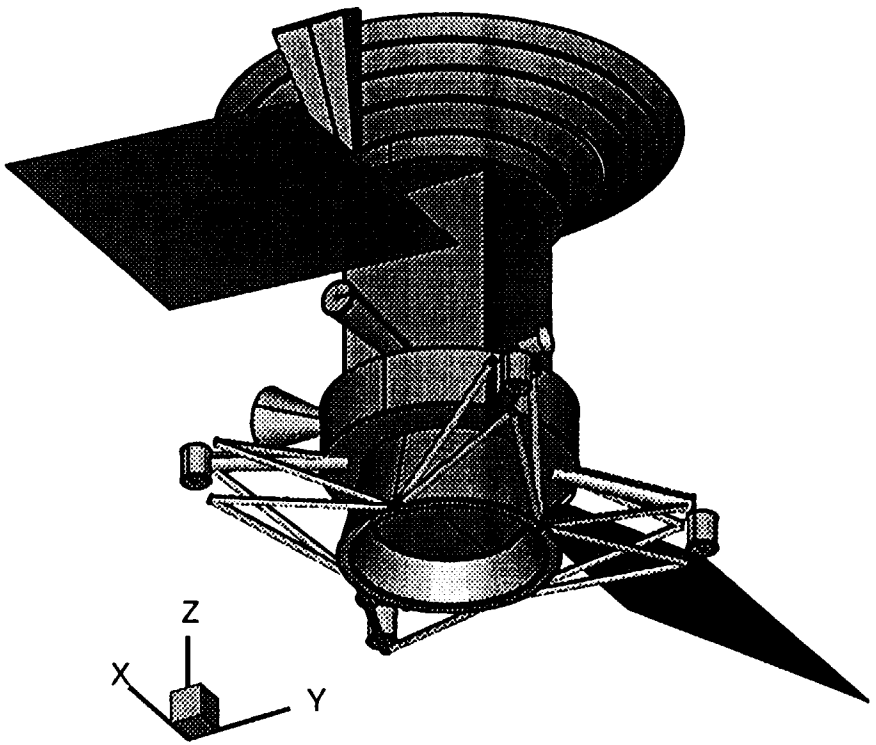

72 element model

Figure 3.1: Freemac TRASYS Magellan Model

Figure 3.2: Freemac Didier and Freemol/DSMC Didier Magellan Models

IV. Reaction Engine Calibration

Outside the Venusian atmosphere the predominant torques acting upon Magellan are caused by the gravity gradient torques. Under these conditions, the control system operates almost exclusively in region I, figure 2.8, occasionally firing 11 ms pulses as the spacecraft state crosses the first switching line. The thruster count data reflects this by having clusters of 11 ms bursts scattered over the time frame outside the atmosphere. The time isolated nature of the clusters allow their individual effects on the spacecraft to be analyzed.

The intent is to model each cluster as an impulse and determine the corresponding change in angular rate from the telemetry data. Clusters separated by at least five seconds are used to fit a third order polynomial in time to the attitude error data points before and after the cluster firing. An example is shown below in Figure 4.1.

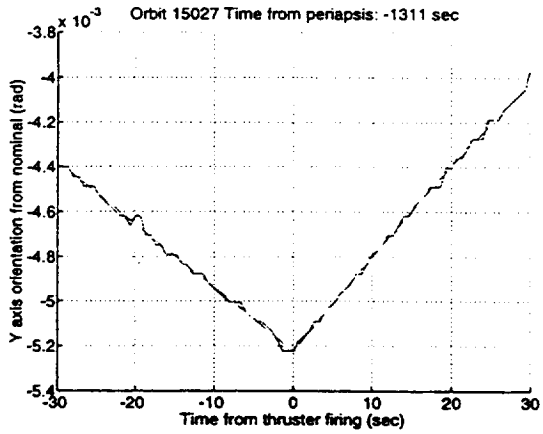

Figure 4.1: Attitude Error Polynomial Fit

Attitude rate errors are not used because of poor resolution. The first degree terms are compared at the firing time and the $\Delta\omega$, the change in the attitude rate errors, is calculated. This value is used in the Euler equations of motion for a rigid body.

$$\{N\} = [I]\left\{\dot{\omega}\right\} + \{\omega\} \times [I]\omega \qquad (4)$$

Where N is the impulse torque acting on the body. For small ω the second term is negligible, and for an impulse equation (4) becomes:

$$\{\bar{N}\} = [I]\{\Delta\omega\} \tag{5}$$

The thrust is then determined for a known moment arm of 1.95m and normalized to its full on condition by multiplying by 90/n, where n is the number of pulse counts recorded by the telemetry.

The thrust solutions determined in this manner correspond to very low duty cycle points as only 11 ms impulses are isolated in the data. Engine calibration performed during the orbit trim maneuvers indicated thrust of about 0.5 N per engine at full on conditions.

V. Free Molecular Flow Aerodynamics

The aerodynamic forces acting upon Magellan as treated by Freemol and Freemac are those of a free molecular stream in Maxwellian equilibrium and constant accommodation coefficients.

The Knudsen number is:

$$Kn = \frac{1}{\sqrt{2}\,\pi d^2 nL} \tag{6}$$

where d is the diameter of the molecule (CO_2: 3.8 angstroms), n is the number density of the particles and L is the characteristic length of the Magellan spacecraft. The Knudsen number is used to indicate if the carbon dioxide molecules are in free molecular conditions (Kn >> 1).

The molecular speed ratio S is defined as ratio of the free stream velocity to the mean thermal molecular velocity, or:

$$S = \frac{U}{\sqrt{2\frac{k}{m}T_\infty}} \tag{7}$$

The Venusian atmosphere consists of several species of molecules, each specie having a different speed ratio. As Freemac assumes a homogenous free stream, the weighted mean of the speed ratios must be determined. The weighted average of the individual specie is modeled as:

$$m_{av} = \sum_{i=1}^{M} m_i N_i \tag{8}$$

Where M is the number of species and m_i and N_i are respectively the mass and molar fraction of specie i.

The forces and torques acting on an object in a fluid flow are given by:

$$F_x = \tfrac{1}{2}\rho C_x A_{ref} U^2 \tag{9}$$
$$F_y = \tfrac{1}{2}\rho C_y A_{ref} U^2 \tag{10}$$
$$F_z = \tfrac{1}{2}\rho C_z A_{ref} U^2 \tag{11}$$
$$T_x = \rho C_{mx} L_{ref} A_{ref} U^2 \tag{12}$$
$$T_y = \rho C_{my} L_{ref} A_{ref} U^2 \tag{13}$$
$$T_z = \rho C_{mz} L_{ref} A_{ref} U^2 \tag{14}$$

The forces acting on an exposed surface element, where x is considered normal to the elemental surface[5] A are given by:

$$F_x = \frac{\rho A U^2}{2S^2}\left[\left(\frac{2-\sigma_n}{\sqrt{\pi}}(S\varepsilon_x) + \left(\frac{\sigma_n}{2}\right)\sqrt{\frac{T}{T_\infty}}\right)\exp\left(-(S\varepsilon_x)^2\right) + \left((2-\sigma_n)\left(\frac{1}{2}+(S\varepsilon_x)^2\right) + \frac{\sigma_n}{2}\sqrt{\pi\frac{T}{T_\infty}}\,S\varepsilon_x\right)(1+erf(S\varepsilon_x))\right] \tag{15}$$

$$F_y = \frac{\rho A U^2 \sigma_t}{2S^2\sqrt{\pi}}\left[\left(S\varepsilon_y \exp\left(-(S\varepsilon_y)^2\right)\right) + \sqrt{\pi}\,S^2\varepsilon_x\varepsilon_y(1+erf(S\varepsilon_x))\right] \tag{16}$$

$$F_z = \frac{\rho A U^2 \sigma_t}{2S^2\sqrt{\pi}}\left[\left(S\varepsilon_z \exp\left(-(S\varepsilon_z)^2\right)\right) + \sqrt{\pi}\,S^2\varepsilon_x\varepsilon_z(1+erf(S\varepsilon_x))\right] \tag{17}$$

where σ_n and σ_t are the normal and tangential accommodation coefficients, T an T_∞ are the surface and ambient temperatures, U is the free stream velocity, and ε_x ,ε_y , and ε_z are the direction cosines of the free stream with respect to the local surface normal.

The overall force coefficients over the body axis are determined by summing the area weighted elemental coefficients and dividing by the reference area. In turn the overall moment coefficients are determined by summing the cross product of the area weighted elemental force vectors with the elements position vector and dividing by the reference area times the reference length.

Analysis of the aerodynamic characteristic focuses on the moment coefficients as there is no data to compare with the force coefficients model. The results are expressed as a ratio of two moment coefficients in order to eliminate the requirement to know the atmospheric density.

VI. Aerodynamic Simulation Codes

Two free molecular codes and one DSMC simulation code were used to study the aerodynamic characteristics of the Magellan spacecraft models presented in section III.6. Freemac is easier to use and modify and was used to perform most of the analysis. The DSMC code was used to model the effect of the engine plumes and interparticle collisions. Freemol performs free molecular flow analysis while using the same discretization methods as the DSMC code, and forms a bridge between Freemac and DSMC.

VI.1 Freemac

Freemac is a computer simulation software program, written in FORTRAN 77, which numerically determines the aerodynamic coefficients of a modeled spacecraft in a free molecular flow environment[5,6]. The spacecraft model uses a set of basic components (rectangles, cones, spheres, etc...) that are discretized into m x n small flat plate elements. For each element visible to the flow field, the free molecule flow equations (15-17) are evaluated, applied to the element's area, and the aerodynamic coefficients determined. These coefficients are then summed to obtain the total aerodynamic coefficients of the spacecraft. The forces act on an element only on the side facing the incoming flow, a surface with its normal vector turned away from the free stream will generate a zero result although the surface will shadow other elements as viewed along the incoming wind vector. In the Freemac code the flow is modeled as a homogenous, constant speed ratio free stream, with particles undergoing a single collision with the spacecraft surface.

Currently there are six component types, as well as four component macros, that can be used to model an object in Freemac. The component types are circular flat plate, rectangular flat plate, triangular flat plate, right cylinder, right cone, and sphere. The four component macros are thin rectangular plate (two rectangles facing in opposite directions), rectangular box (six rectangles forming a right parallelepipe), thin triangular plate (two triangles facing in opposite directions), and triangular box (two triangles and three rectangles forming a box).

Three sets of coordinate systems are used in Freemac to describe a model. The body axes are the primary axis fixed to the spacecraft (the object) and are used to describe the relative positions and orientations of each of the components and free stream direction. Each component in turn has an axis system which is fixed to the component. Component

dimensions are expressed in this system. Finally, each discretized element on a component has a defined element axis oriented such that the x-axis is always normal to the surface, which defines the active side.

VI.2 Enhancement of Freemac

Over the course of this research a number of problems with the Freemac program were found and more code was added to expand capability and flexibility. This section describes the problems found and details the changes made to the original source code.

Several of the basic components and macros were found to have computational errors in the initialization and shadowing subroutines. The loose coding standards also contributed to potential hidden errors that the user would find difficult to detect and trace. The testing and error checking performed during the course of this thesis identified the following four problems which were corrected. Frequent testing and comparison with known cases provide confidence in the results.

The initialization routines for the thin rectangular and rectangular box macros contained simple errors in their orientation and position logic. In addition, flag variables that had been left "hanging" in the previous code are set to zero.

The thin triangle and triangular box contained errors similar to those of the rectangular macros in their initialization routines. Flag variables were also left in the component data list. Poor coding standards in tandem with the logic used for calculating the surface elements gave erroneous results if the number of elements along each axis were unequal (that is $m \neq n$).

The shadowing subroutine for the sphere, which determines whether the sphere blocks the free stream in front of any element, was found to return a positive result in all

cases, even if the sphere was positioned behind the element in question. A new algorithm was developed , put in place and tested.

In addition to the errors found, several new analytic capabilities were added to Freemac. These had the effect of making the output easier to understand, increasing the users confidence in the output, and providing more insight into the results.

Originally in Freemac the relative wind vector could only vary over a rectangular grid of angles in θ and ϕ. For example, θ and ϕ could be programmed to vary from 0° to 180° in 10° increments. Interpolation was necessary for intermediate values of θ and ϕ. With complex geometries the variation of the aerodynamic coefficients with attitude angles is generally non-linear and 2-D bi-linear interpolation introduced errors. Though this can be solved by using smaller angle increments this solution proved to computationally intensive. Instead, the main loop of Freemac was changed to accept an attitude trajectory, i.e. a set of θ and ϕ angles.

An important new feature of Freemac is the ability, in conjunction with Tecplot[13], to view the output in a graphic format. For a pair of θ and ϕ, the coordinate of each elemental centroid, the calculated pressure, and shear forces are placed in an ASCII data file which can be plotted and viewed. These plots show which components are visible and which are shadowed as well as color coding the elements according to the pressure and shear coefficients making output analysis much more efficient.

The last analysis tool added to Freemac outputs the force and moment coefficients of each individual component used to model a given spacecraft. This allows the user to quickly determine which components are the major contributors to the overall coefficients from a given perspective.

In Freemac each component has a defined active side over which free molecular forces are calculated. The inactive side is always treated as being shaded from view, the result of using the dot product of the surface normal vector with the wind vector as a test of visibility. Having only one sided objects places a great restriction on the type of geometry that can be accurately modeled with the six basic shapes available with Freemac. In particular concave shapes like antennas dishes and engine nozzles must be modeled as cones plus flat endcaps instead of their true shapes. Note that Freemac does not account for multiple impacts of a single particle. This together with concave components can provide results that differ from the coefficients of a real concave component.

In light of the above, logic that would treat both sides of circular flat plates and cones as active was implemented and tested. This was accomplished by the simple expedient of adding code that would reverse the surface normal unit vector and place the new logic within an IF-THEN statement keyed to a flag variable input from the Freedat.dat file (Appendix F). The shadowing routine also needed to be altered so that a component could shade itself and a small (0.0001) shift in the centroid position was implemented to numerically differentiate the two sides.

Other enhancements include a flag variable that allows the users to specify the gas-surface interaction model for each component on an individual basis instead of on a global basis as previously implemented.

Finally, measures were taken to verify the force calculating logic and equations for all the basic components as well as the shadowing routines for same. The maximum number of basic components was increased from 40 to 120 and the maximum number of trajectory points was set to 600.

VI.3 Direct Simulation Monte Carlo Method

Freemol/DSMC is a set of two simulation programs written in FORTRAN 77[6]. Both use the same modeling conventions to describe an object and are intended to operate in tandem.

Freemol is similar in function to Freemac, a code which numerically determines the aerodynamic coefficients of a model geometry in a free molecular flow conditions. The major difference in the codes is that Freemac integrates the forces generated over a discretized surface area, while Freemol discretizes an object over a volume into cubical cells (cubics) arranged in a 3-D mesh aligned with a body fixed coordinate system. Creation of an object from primitive components in Freemol can be accomplished with a CAD like preprocessor. The CAD program then discretizes the volume of the object. The set of cubics that encompasses a part of the mathematical description of an object as well as the surface normal and surface area encompassed are recorded and considered active. These active cubics are then analyzed to determine which are exposed to the free stream.

Freemol supports the use of sixteen primitive components to define objects. Any number of gas species can be specified and two gas-surface interaction models are provided. Accommodation coefficients are global values to all primitive shapes. As with Freemac, single molecule-wall collisions are modeled.

Extra features added to Freemol parallel those added to Freemac. Small changes were made to make the relative wind velocity angle conventions compatible with Freemac. The ability to track the wind vector along a trajectory of angles, as well as a component by component breakdown of the overall aerodynamic coefficients were also added.

DSMC is a Direct Simulation Monte Carlo software package used herein to study the flow field interaction with the attitude engine exhaust plumes, the effect of multiple

particle collisions with the spacecraft, and the effect of intermolecular collisions. The flow field is not modeled with continuum fluid mechanics, but rather the aerodynamic characteristics are calculated from the aggregate effect of several individual particles acting as molecules. Individual particles are introduced into a discretized volume where the interactions of the particles are resolved over computational cycles which mimic the passage of time in the environment. As particles disappear into the far field, new particles are introduced into the system. The system does not calculate a solution, rather it converges towards one over several computation cycles as the particle interactions reach a steady state. By accounting for intermolecular collisions and using statistical analysis the macroscopic flow field characteristics are determined. In order to preserve computational resources the work environment is divided into a high resolution near field and a low resolution far field.

Engine plumes are modeled by injecting particles into the environment from locations corresponding to the engine nozzles. Each particle is given an initial position at the REA motor exit plane and a velocity vector equal to the mean flow velocity superimposed on a Maxwellian distribution.

VII. Results

The results of the various research phases conducted are presented in order. Each set of results builds on the results of previous stages. The Reaction Engine Calibration (REC) results are presented first. Then the Atmospheric Torques (AT) are introduced and compared to the results achieved from the Free Molecular Simulation (FMS) phase. Differences between the AT and FMS results are discussed and the DSMC simulation results are introduced to partially explain the differences observed during orbit 15027.

VII.1 Reaction Engine Calibration

Thrust calibration data was gathered for orbits 15020 through 15032 resulting in 546 data points. These points represent the thrust calculated by using a third order polynomial fit to the attitude error data and solving Euler's equations of motion for an impulse. Only 11 ms pulses could be isolated. The thrust value generated in this manner is multiplied by 90/n, where n is the number of 11 ms pulses fired, to normalize the value to a full-on condition for purposes of comparison. Each REA pair is calibrated independently from the other five with statistical analysis used to determine an overall value that can be incorporated into a function that characterizes the thrust level. In order to save space, as each REA pair has a counter part on the other side of the spacecraft, the positive side of the axis in each figure refers to the REA that creates a positive torque about the corresponding control axis. Similariy, the negative side presents the results of the negative torque REA's.

Figures 7.1, 7.2, and 7.3 present the normalized thrust levels as a function of the number of 11 ms impulses fired during a given 2/3 second telemetry frame for each of the control axis. Error bars were calculated (20% typical value) but are not shown for

clarity. The REA's are relatively simple mechanical devices built for reliability and fed from a common fuel tank. Therefore the scatter in the results is believed to arise primarily from the ability to recover thrust values from the telemetry rather than thruster performance variation. The graphs more properly illustrate the comparative strengths of the engines than a trend in the data that can be modeled as a function other than a constant value.

The mean of the data points in Figure 7.1 for each number of pulses per telemetry frame gives a flat trend at different thrust levels below 2 Newtons for the +X and -X thrusters. That is, the normalized thrust is roughly constant for any number of 11 ms impulses. Figure 7.2 shows a downward trend in the -Y engines as the thrust count increases while the +Y engines seem to indicate constant normalized thrust. Again, the normalized thrust is approximately 2 Newtons. The trend in the Z engine data shown in figure 7.3 also seem to indicate a constant normalized thrust level for both thruster pairs, with the normalized thrust being slightly greater than 2 Newtons. An overall trend in the three data sets is that as the number of thruster counts increases, the scattering of the data at that count level decreases.

The 2 Newton (per engine pair) figure arrived at is in contrast to the 0.5 Newton (per engine) , mentioned in section IV, expected from the results of the OTM. One possible cause of this is the residual fuel inside a REA engine after a thruster impulse. For isolated impulses the effect of this residual fuel escaping through the engine nozzle could be comparatively large, whereas the thrust levels of the orbital trim maneuvers, being essentially continuous firings, would be relatively unaffected.

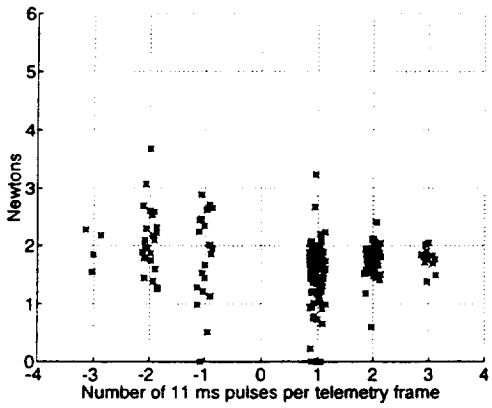

Figure 7.1: X REA Thrust vs. Counts

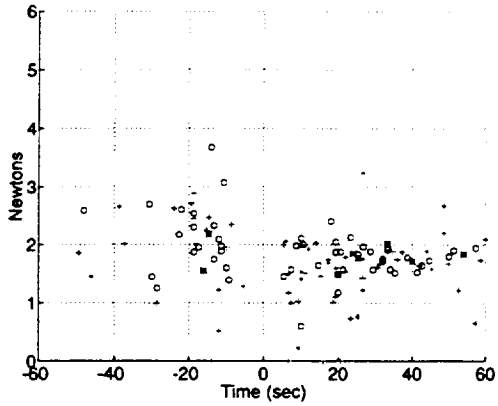

Figure 7.4: X REA Thrust vs. Time

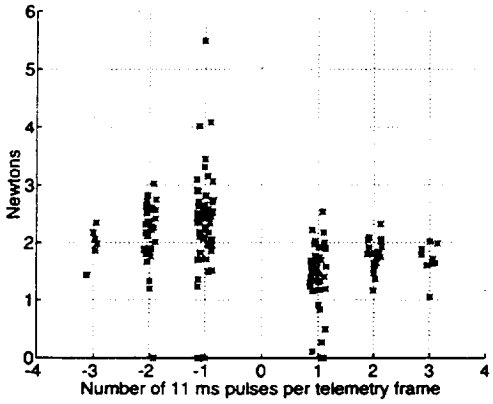

Figure 7.2: Y REA Thrust vs. Counts

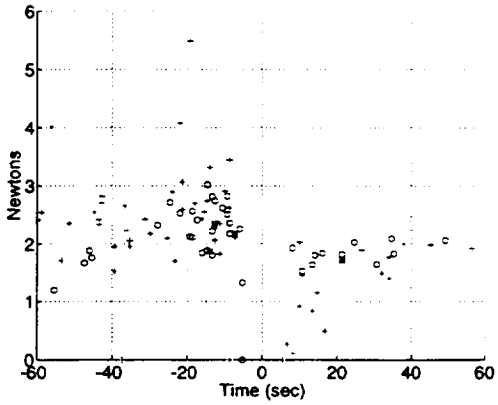

Figure 7.5: Y REA Thrust vs. Time

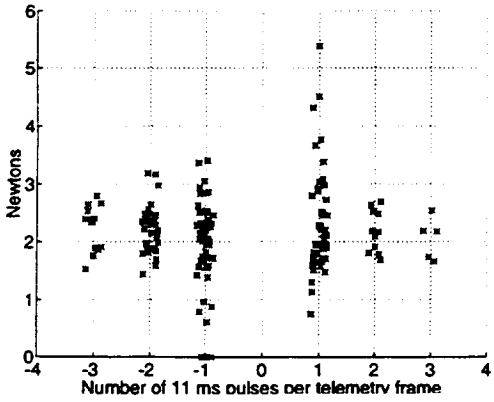

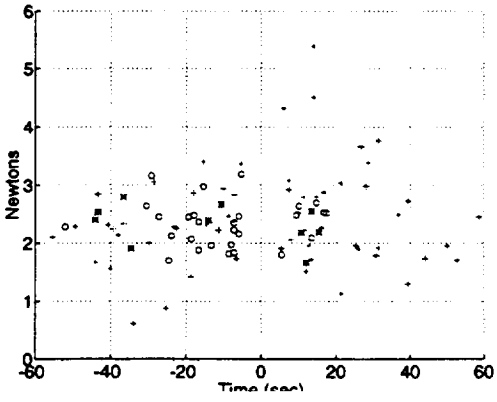

ıst vs. Time

To study the potential effects of having the catalyst bed heated by previous firings, figures 7.4, 7.5, and 7.6 display the same data points, but as a function of the time since last firing. Data points are coded to distinguish between single (+), double (o), and triple (x) impulses. In these plots, any trend in the data is difficult to identify. As most of the data trends in figures 7.1 to 7.3 indicate constant thrust levels and as the thrust levels as a function of time from last firing are indiscernible, a solution based on these results is to model the thrust levels as a constant for each REA.

Calibrated thrust levels approximate 2 N for all engine pairs. Discarding data points below 0.5 N and above 4.0 N and using statistical analysis gives the mean and standard deviation of the results.

The relatively large differences between the thrust derived for each engine pair, as shown in table 7.1, were unexpected. Solar thermal effects on REA thrust were investigated using the orbit parameter data. The solar direction in the spacecraft coordinate system was a constant θ angle of approximately -60° and a ϕ angle of 30° for orbits 15020 to 15029. The angles θ and ϕ are those described in section II.2. For orbits 15030 to 15032 the solar θ and ϕ were about -30° and 45° respectively. At these angles all REA's are equally exposed to the sun.

The mean values for each REA presented in the next to last column are the thrust levels used in the AT phase.

REA	No. of pulses	Data Points	Mean Newtons	Std. Dev., Newtons	Std. Dev. as % of Mean	Mean all data, N	Std.Dev. all data, N
Positive X	1	90	1.61	0.41	25	1.67	0.36
	2	52	1.75	0.27	15		
	3	13	1.78	0.18	10		
Negative X	1	20	1.9	0.66	35	2.01	0.6
	2	23	2.11	0.58	27		
	3	4	1.97	0.33	17		
Positive Y	1	32	1.58	0.39	25	1.67	0.34
	2	21	1.78	0.27	15		
	3	9	1.7	0.29	17		
Negative Y	1	53	2.35	0.48	20	2.29	0.46
	2	34	2.24	0.43	19		
	3	6	1.98	0.31	16		
Positive Z	1	48	2.16	0.63	29	2.16	0.57
	2	12	2.21	0.36	16		
	3	5	2.06	0.36	16		
Negative Z	1	56	2.09	0.57	27	2.15	0.5
	2	35	2.22	0.4	18		
	3	14	2.25	0.39	17		

Table 7.1: Statistical Analysis of REC Results.

VII.2 Atmospheric Torques and Free Molecular Simulation

In this section the results of the AT and FMS research into the atmospheric torques affecting the Magellan spacecraft are presented. First, the thrust levels used to generate the AT results are presented. Then, preliminary results that characterize the free molecule environment are presented, and the effective speed ratio to be used in the FMS stage is determined. The results of the AT and the FMS are then presented together for comparison. A discussion of the results then follows.

VII.2.1 Atmospheric Torques

The results of the REC phase are used to calculate the total torque acting on the Magellan spacecraft at a given time in each body axis. These are expressed as a ratio of moment coefficients so that atmospheric density is not a knowledge requirement. As there exists a margin of error in the REC results, three solutions are determined: the first atmospheric torque solution uses the mean thrust values from table 7.1, while the minimum and maximum solutions are determined by varying the thrust values of the REA's by one standard deviation. The intent is to define a range in which the actual moment coefficient ratios can confidently be said to exist.

As noted in the REC phase description (section IV), only 11 ms pulses were investigated. As coefficient ratios are the data presented, the value of the AT data points are determined by the ratio of the thrust of each engine to the others, rather than the absolute values. Accordingly, data from the orbital trim maneuvers (OTM) suggest the REA thrust levels vary at most by 8% at the higher duty cycle rates compared to the 20% generally found for the 11 ms pulses. Therefore it is expected that the region bounded by the AT lines for each moment ratio account for the thrust levels at high duty cycles.

The REA thrust values used to determine the nominal, maximum, and minimum solutions are presented below in tables 7.2 and 7.3. During orbits 15023 and 15027 the -X, -Y, and -Z REA's performed at least 98% of all the attitude engine firings each orbit. Table 7.2 shows the thrust values used for each REA for each of the torque solutions (max., nominal, and min.) for each of the moment coefficient ratios (CMX/CMY, CMZ/CMY, CMX/CMZ) for orbits 15023 and 15027. The REA's are listed across the top row, while the torque ratio solutions are listed on the left hand side. Note that for the CMX/CMY ratio the -X and -Y thruster values vary by one standard deviation. In turn the CMZ/CMY ratio varies the -Y and -Z thrusters while the CMX/CMZ varies the -X and the -Z thruster values. These atmospheric torque solutions are later compared graphically to the FMS solutions in section VII.2.3.

	+X	-X	+Y	-Y	+Z	-Z
max	1.67	2.61	1.67	1.83	2.16	2.15
CMX/CMY	1.67	2.01	1.67	2.29	2.16	2.15
min	1.67	1.41	1.67	2.75	2.16	2.15
max	1.67	2.01	1.67	1.83	2.16	2.65
CMZ/CMY	1.67	2.01	1.67	2.29	2.16	2.15
min	1.67	2.01	1.67	2.75	2.16	1.65
max	1.67	2.61	1.67	2.29	2.16	1.65
CMX/CMZ	1.67	2.01	1.67	2.29	2.16	2.15
min	1.67	1.41	1.67	2.29	2.16	2.65

Table 7.2: REA Thrust Levels used for Orbit 15020 to 15029 AT Data.

Table 7.3 presents the same data as table 7.2 for orbit 15031. The difference is that during orbit 15031 the engines most commonly used are the +X, -Y, and +Z REA's.

	+X	-X	+Y	-Y	+Z	-Z
high	2.03	2.01	1.67	1.83	2.16	2.15
CMY/CMX	1.67	2.01	1.67	2.29	2.16	2.15
low	1.31	2.01	1.67	2.75	2.16	2.15
high	1.67	2.01	1.67	1.83	2.73	2.15
CMY/CMZ	1.67	2.01	1.67	2.29	2.16	2.15
low	1.67	2.01	1.67	2.75	1.59	2.15
high	2.03	2.01	1.67	2.29	1.59	2.15
CMZ/CMX	1.67	2.01	1.67	2.29	2.16	2.15
low	1.31	2.01	1.67	2.29	2.73	2.15

Table 7.3: REA Thrust Levels used for Orbit 15030 to 15032 AT Data.

VII.2.2 Free Molecule Simulation

The Knudsen number that characterizes the Magellan spacecraft during the Termination Experiment is obtained using equation (6) and the VIRA model. The effective diameter of a carbon dioxide molecule is 3.8 angstroms, atomic oxygen is 2.6 angstroms, CO is 3.1 angstroms, and N_2 is 3.0 angstroms. Using the particle density given by the VIRA model and the characteristic length of the Magellan spacecraft as the distance between the two solar panel tips (10.0 meters) gives the results in table 7.4.

Orbit Number	Altitude at periapsis	Knudsen number
15023	146.7 km.	6.83
15027	138.2 km.	1.32
15031	137.6 km.	1.17

Table 7.4: Knudsen Number of Termination Experiment Orbits.

The rapid increase in the Knudsen number at higher altitudes results both from the particle density decreasing exponentially from 1.52E+17 particles/m^3 at 137.6 km. to 2.95E+16 particles/m^3 at 146.7 km, as well as the change in the atmospheric composition from the large carbon dioxide molecules to the smaller atomic oxygen particles. These

result indicate that after orbit 15024 the free stream is characterized by a Knudsen number around 1. It is clear that the Termination Experiment places the Magellan spacecraft in a region that can not be considered a strictly free molecular environment for these orbits and the results of the Free Molecular Simulation should be taken in that light.

The ratio of the Magellan spacecraft velocity to the ambient particle velocities does not vary greatly from one orbit to the next (figures 2.2 and 2.5). The orbital velocity is virtually a constant, and though the density varies greatly, the average particle mass does not (from an atomic weight of 39.5 at 137.6 km. to 35.8 at 146.7 km.). Equations (15), (16), and (17) are relatively insensitive to changes in the speed ratio at high values so a constant value for this parameter can be determined for use in all orbit simulations. Using the VIRA model densities for CO_2, N_2, CO, and O at an altitude of 140 km with an orbital velocity of 7300 m/s in equations (7) and (8) gives:

Specie	Speed Ratio	Molar Fraction
CO_2	25.03	0.76
CO	19.97	0.09
N_2	19.97	0.06
O	15.1	0.1

Table 7.5: Speed Ratios of the Venus Atmospheric Species

The aerodynamic coefficients of the Freemac TRASYS Magellan model were determined using the Freemac code over the attitude trajectory as determined by the orbital analysis. Constant accommodation coefficients of 1.0 for both normal and tangential coefficients were used in one case, the other case represents the 0.8 normal and tangential accommodation coefficient case.

VII.2.3 Atmospheric Torque and Free Molecule Simulation Comparison

The thirteen orbits of the Termination Experiment can be divided into roughly three groups on the basis of altitude (and hence atmospheric density) at periapsis and angle of incidence. Orbits 15020 through 15024 can be categorized as high altitude with a 60° solar panel angle of incidence at periapsis, while orbits 15025 through 15029 are at low altitude with a 60° angle of incidence. Finally the orbits 15030 to 15032 which are at low altitude in the second panel configuration with an angle of incidence at periapsis of 15° degrees. While the atmospheric torques determined for all orbits are presented in the appendix, the results are presented here for orbits 15023, 15027, and 15031, which are representative of all orbits.

The relative wind vector and the orientation of the attitude engines for these orbits can be illustrated graphically by imaging the Magellan model from the known relative wind attitude data and indicating the active REA thruster. These are pictured in Figure 7.7 for orbit 15027 and in Figure 7.8 for orbit 15031. The orientation during orbit 15023 is essentially the same as orbit 15027. The red highlighted cones illustrate the exhaust plumes of the attitude engines that are on at the time given below each illustration. The cones are used for illustration purposes and do not indicate the size of the plume. For orbit 15023 and 15027 these plumes block major aerodynamic components up to periapsis and cease to shadow the spacecraft afterwards. The -Y REA blocks the +X solar panel from periapsis -4 minutes until periapsis, while the -Z REA plume passes in front of the HGA, FEM, and MGA during the same period. For orbit 15031 the REA plumes shadow major components in all the time instances imaged, though shadowing of the spacecraft seems to decrease with time. The +Z REA blocks the HGA, an obstruction which appears

to decrease over time. At periapsis +2 minutes the -Y REA plume begins to shadow the +X solar panel, this will have a pronounced effect on the moment torques acting on the spacecraft since the solar panel presents such a large area to the free stream at the end of a long moment arm. The effects of the plume-free stream interaction is the subject of the chapter VII.3.

Orbit 15027

Magellan Space Craft with cones representing active attitude control engine exhausts at points along orbital path.

Active engines are -X -Y -Z Reaction Engine Assemblies

Cones are used for illustration purposes only.

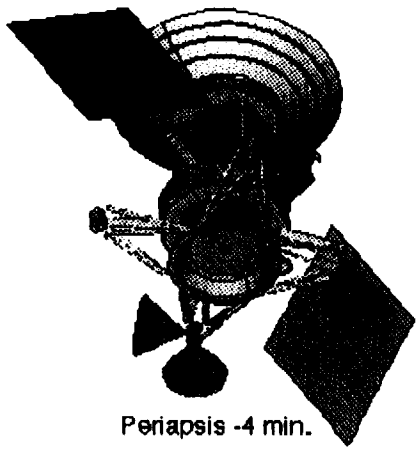

Periapsis -4 min.

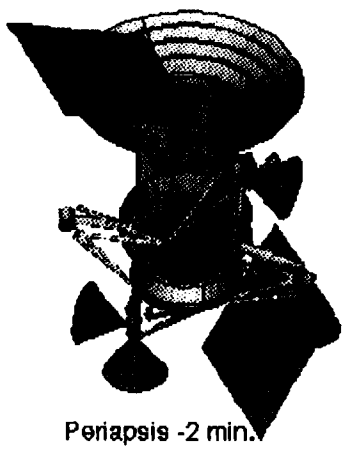

Periapsis -2 min.

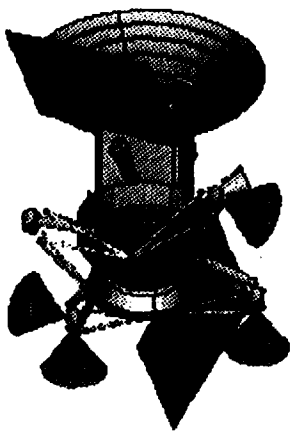

Periapsis

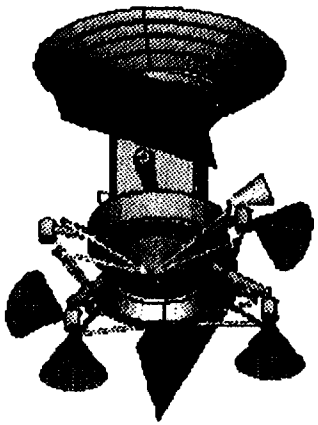

Periapsis +2 min.

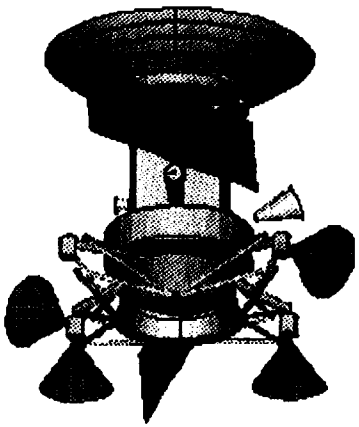

Periapsis +4 min.

Orbit 15031

Magellan Space Craft with cones representing active attitude control engine exhausts at points along orbital path.

Active engines are +X -Y +Z Reaction Engine Assemblies

Cones are used for illustration purposes only.

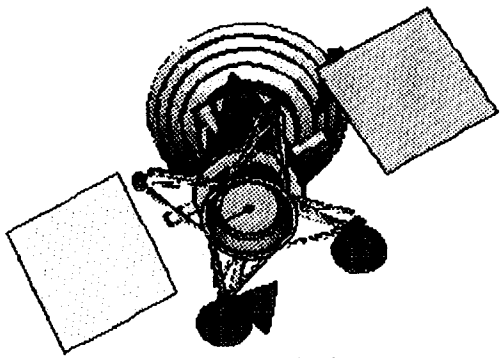

Periapsis -4 min.

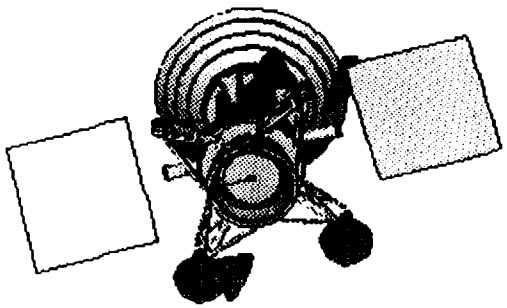

Periapsis -2 min.

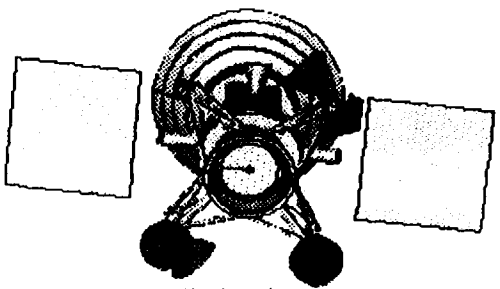

Periapsis

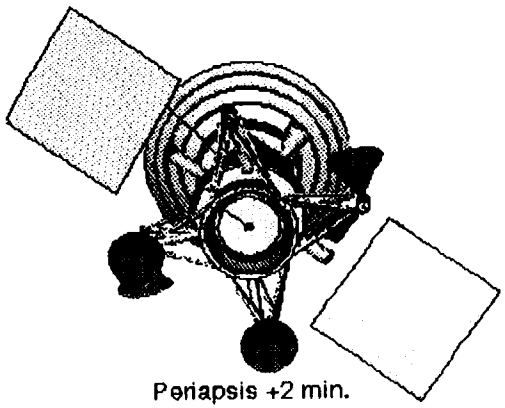

Periapsis +2 min.

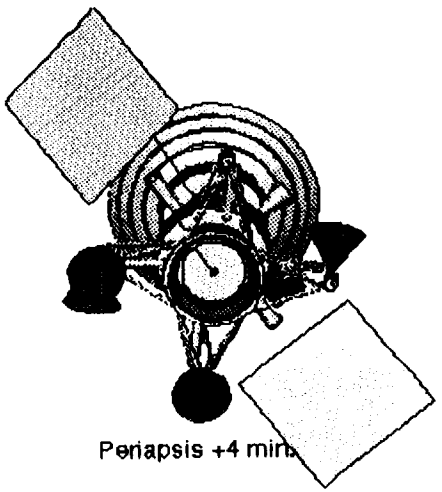

Periapsis +4 min.

The final results of the AT and FMS phases are presented graphically over the next three pages. The first three graphs presented for each orbit present the Cmx/Cmy, Cmz/Cmy and Cmx/Cmz coefficient ratios with respect to the time of periapsis. The three gray lines are the results of the AT phase while the FMS results are determined for accommodation coefficients of 1.0 and 0.8. The fourth graph is a plot of the duty cycles of the significant REA systems during the orbit. The duty cycle varies from 0 for an REA that is turned off, to 1.0 when the REA is at maximum commanded thrust (full on).

Comparison of the AT and FMS results are most meaningful when the duty cycles for the attitude engines are low. The reason is two fold: the lower the duty cycle the more the duty cycle is generated by 11 ms pulses, the only type directly calibrated in the REC phase. Secondly, the lower duty cycle implies less interference of the REA exhaust plumes with the free stream but this needs to be correlated with the spacecraft orientation to the free stream to determine which exhaust plumes may be shading parts of the spacecraft. Also necessary for analysis is that there be a reasonable difference between the FMS 0.8 and FMS 1.0 cases for interpolation purposes.

The original intent of the Termination Experiment was to use the Y and Z moments to determine the accommodation coefficients of the Magellan spacecraft during orbits 15020 to 15029 and the X and Z moments during orbits 15030 to 15032.

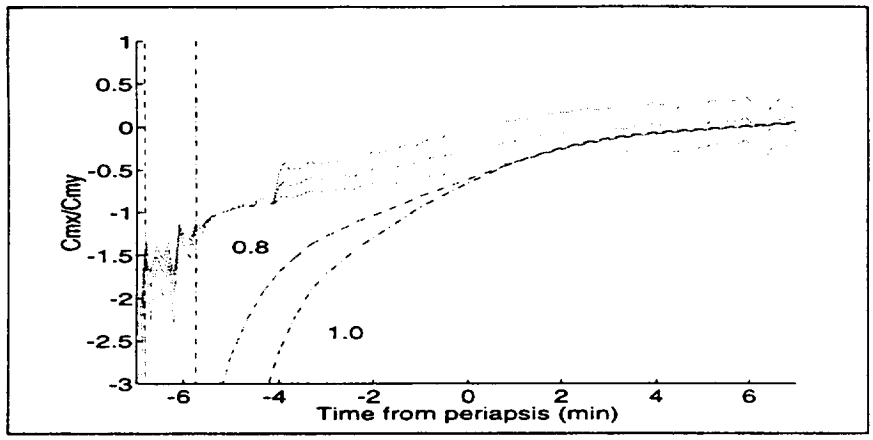

Figure 7.9: Cmx/Cmy over Orbit 15023

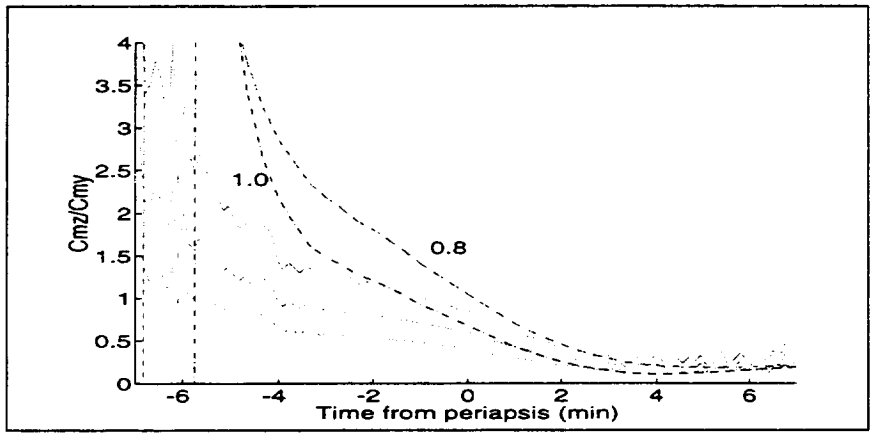

Figure 7.10: Cmz/Cmy over Orbit 15023

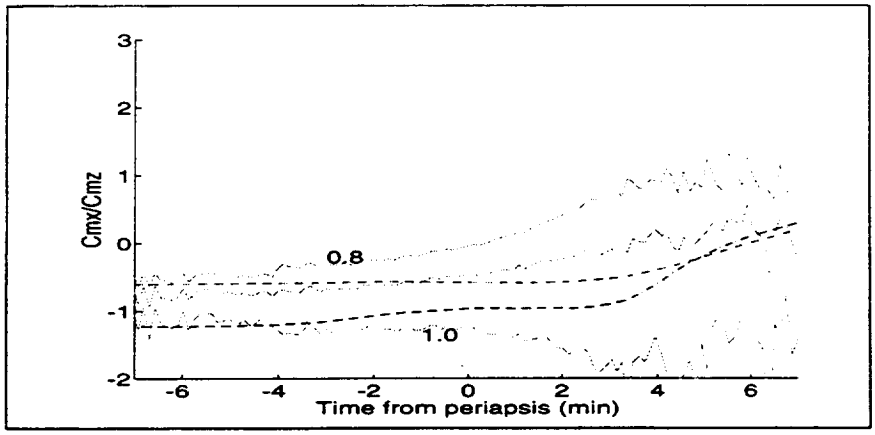

Figure 7.11: Cmx/Cmz over Orbit 15023

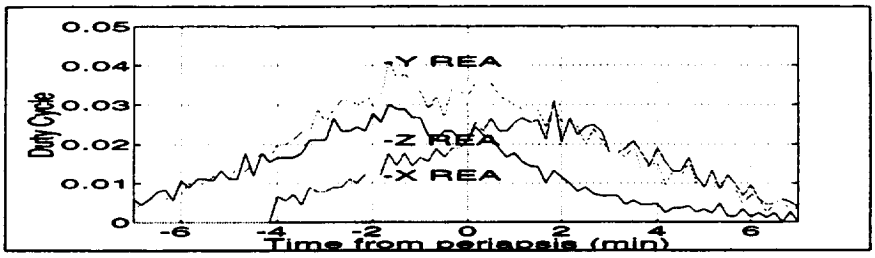

Figure 7.12: Orbit 15023 REA Duty Cycle

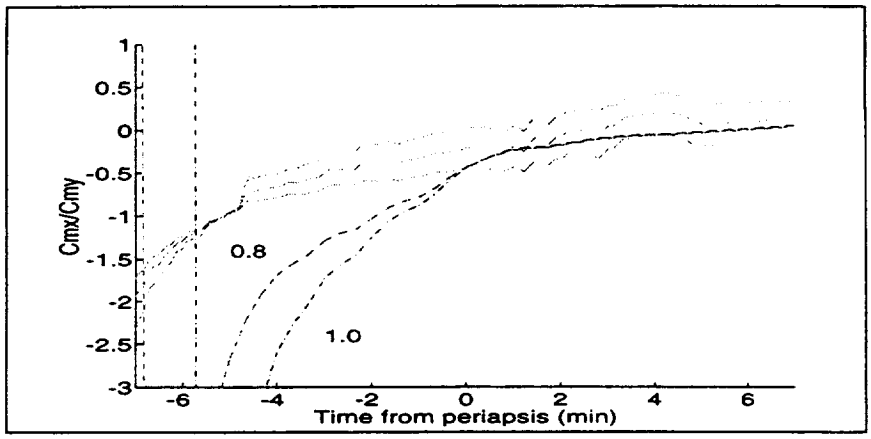

Figure 7.13: Cmx/Cmy over Orbit 15027

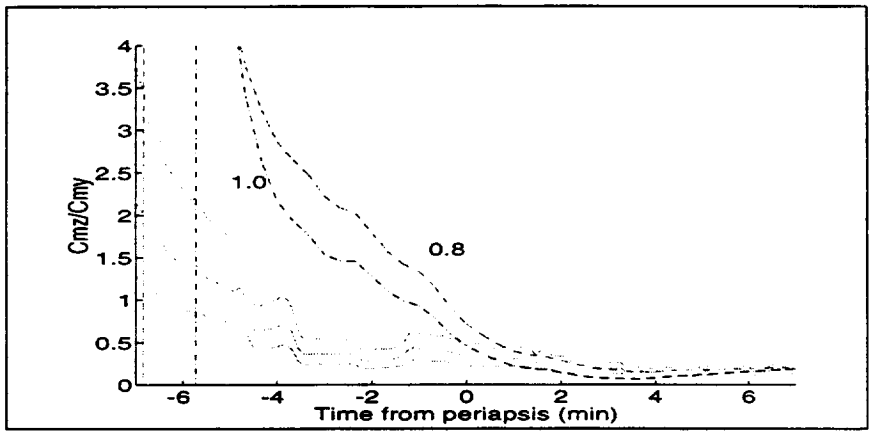

Figure 7.14: Cmz/Cmy over Orbit 15027

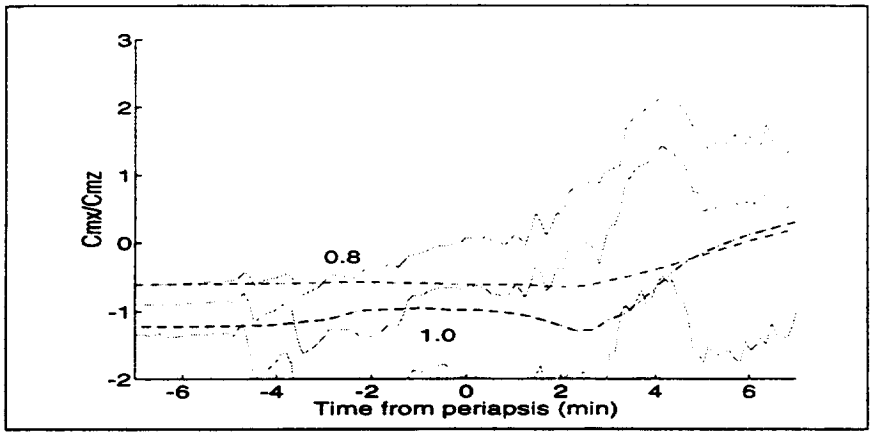

Figure 7.15: Cmx/Cmz over Orbit 15027

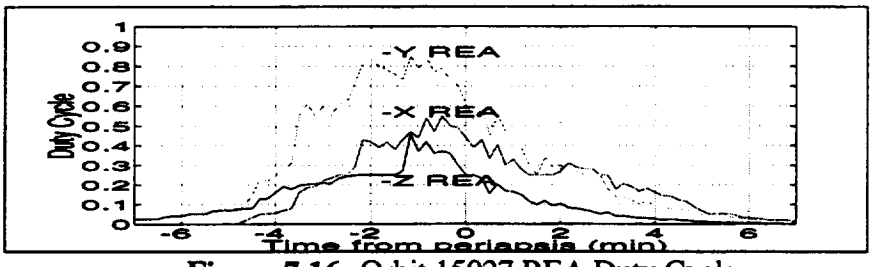

Figure 7.16: Orbit 15027 REA Duty Cycle

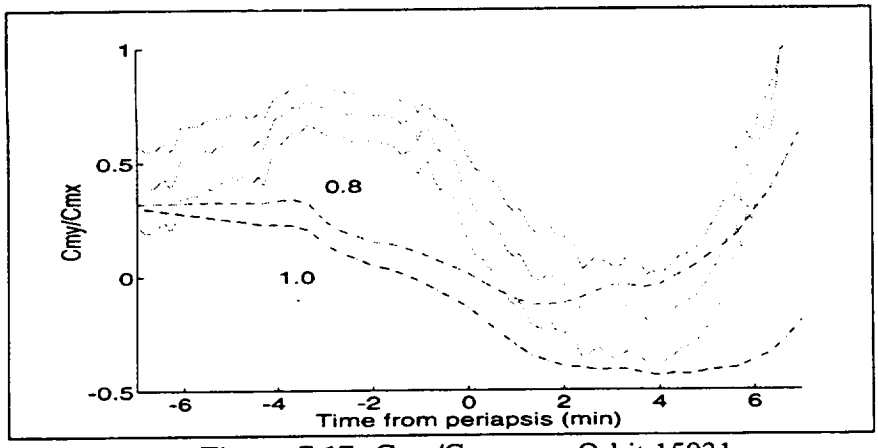

Figure 7.17: Cmy/Cmx over Orbit 15031

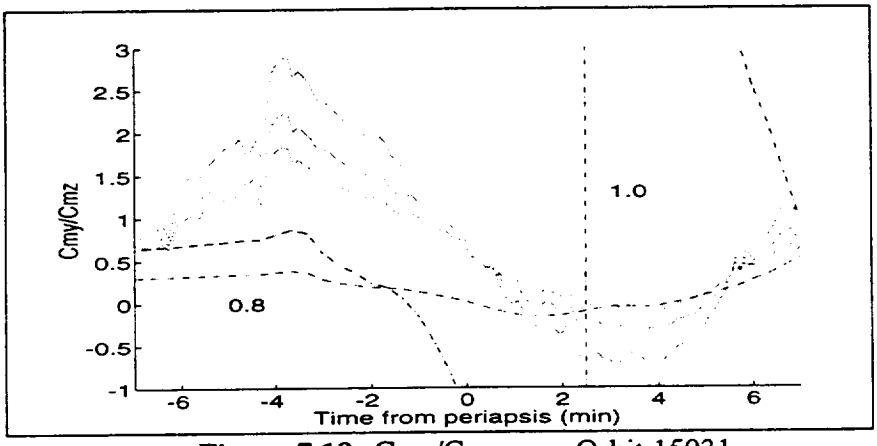

Figure 7.18: Cmy/Cmz over Orbit 15031

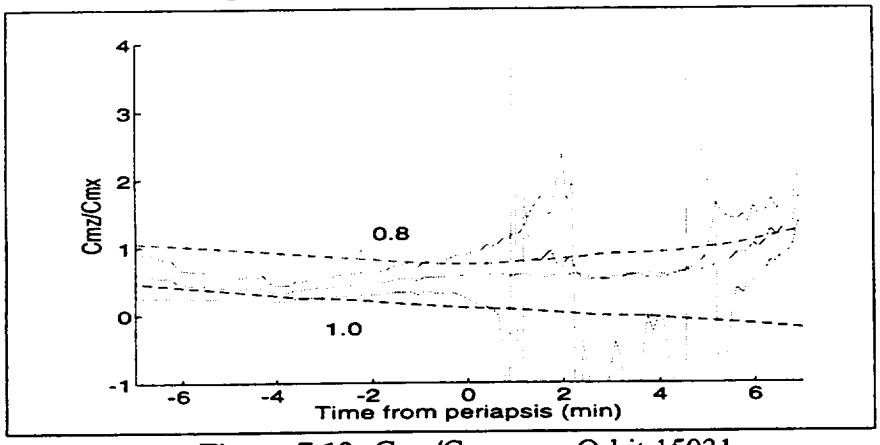

Figure 7.19: Cmz/Cmx over Orbit 15031

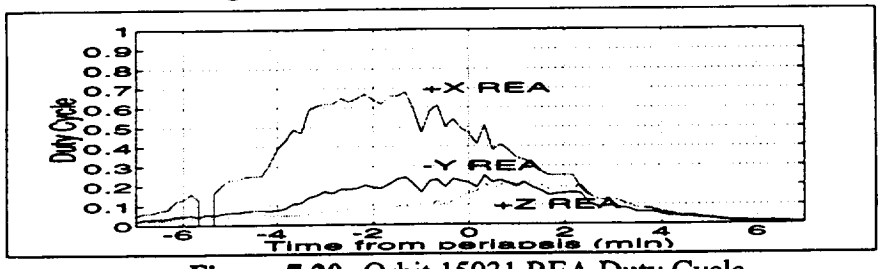

Figure 7.20: Orbit 15031 REA Duty Cycle

Orbit 15023 is a high altitude pass with low attitude engine duty cycles. In fact the control system never enters regions III and IV (Figure 2.8) during this orbit. While the general shapes of the AT and FMS curves are similar, it is difficult to estimate an accommodation coefficient from this data First consider the Cmx/Cmy and Cmz/Cmy graphs. From periapsis -7 minutes to periapsis -1 minute there is a clear difference in the FMS 1.0 and 0.8 cases but these are outside the region bounded by the AT data. After periapsis -1 minute the two data sets begin to merge but at that point the differences between an accommodation coefficient of 1.0 and 0.8 are negligible.

Determining an effective accommodation coefficient from the two graphs gives conflicting results. The Cmx/Cmy plot suggests a value less than 0.8 while from the Cmz/Cmy plot a solution greater than one is inferred, a physical impossibility and a clear indication that there are other effects not accounted for in the analysis.

The results of orbit 15027 are similar to those of orbit 15023 and the conclusion derived from the graphs of orbit 15027 are essentially the same as those derived above. This is to be expected as the spacecraft attitude is inertially fixed and the orbital paths are alike. The principal difference between the two is that orbit 15027 penetrates deeper into the atmosphere and therefore the duty cycle of the attitude control engines are higher, often reaching the full on (control region IV) state.

Comparison of Figure 7.10 of orbit 15023 and 7.14 of orbit 15027 clearly shows a decrease in the AT Cmz/Cmy ratio of orbit 15027 relative to orbit 15023 from periapsis -4 minutes to periapsis -2 minutes. As the only significant difference between the two orbits is the duty cycles of the attitude engines, it is proposed that the attitude jet plumes are the cause of this decrease.

The large differences between the AT and FMS results correspond to times in which Figure 7.7 indicates that surface areas of the spacecraft could be shadowed from the free stream by the exhaust plumes. As the spacecraft's orientation changes to unmask these surfaces, the simulation results converge towards the middle (nominal) AT result. These tends to confirm not only that the exhaust plumes have a marked effect on the atmospheric torques acting on the spacecraft, but also that the geometry model simulated and the thruster calibration method used are sound, as well as suggesting that there have been no major unforeseen alterations in Magellan's geometry during its four years in space.

The results of orbit 15031 differs from the other orbits presented. For clarity the coefficient ratios shown are the inverse of those used for the previous orbits. The Cmz/Cmx plot is of interest since the free stream attitude during this orbit was in a nearly optimal orientation for the solar panels to produce torque about the z axis at periapsis (see Figure 7.8). Analysis results have the same shape and there is separation between the FMS 0.8 and 1.0 cases which bracket the AT data. The duty cycle rates reach the control region III, but do not seem to affect the AT results as they do for orbit 15027. Unfortunately, Figure 7.8 indicates that exhaust plumes mask large portions of the spacecraft up to around periapsis +2 minutes.

In summary, there are significant differences in the atmospheric torques as determined by each analysis technique. The results of orbits 15023 and 15027 that indicate an accommodation coefficient greater than 1.0 show this. Unfortunately the regions before and about periapsis during which the Termination Experiment was designed to produce the best data correspond to those times when the attitude control engines were most used and pointed into the free stream. Still, in those regions (generally after

periapsis) where the plume effects appear to be minimized, the TA and FMS results converge suggesting the soundness of the models used.

Besides the REA calibrations, other factors could account for the differences between the TA and FMS results, some of which are:

1) Variation in the accommodation coefficient as a function of the free stream incident angle to the surface.

2) Different values for the normal and tangential accommodation coefficients.

3) The low Knudsen number and the implications on the validity of a free molecular analysis.

4) Multiple collisions of free stream particles with the spacecraft and the effect of concave surfaces in the geometry. Concave surfaces could also be brought about by the orientation of Magellan to the free stream.

5) Free stream particles intercollisions and the effect this would have on the areas shadowed by thin components in the Magellan geometry.

6) The flow field disturbance around the craft caused by the attitude control engines exhaust.

The first two factors are addressed in Appendix B, when the effects of uncertainties in the simulation and the potential effects on the results are presented. The other factors cannot be modeled using Freemac and the next section presents the results of the Plume Analysis (PA) phase that uses the Direct Simulation Monte Carlo method to address these factors.

VII.3 DSMC Plume Analysis

The Direct Simulation Monte Carlo method was used to model (1) the effects of the attitude control system reaction engine exhaust upon the Magellan spacecraft aerodynamic moment coefficient ratios, (2) the effect of multiple particle collisions with the spacecraft, and (3) the effects of interparticle collisions. Two instances were modeled, both during orbit 15027, at 4 and 2 minutes before periapsis. The free stream, surface, and thruster properties are listed in table 7.6.

Free Stream Properties:		Surface Properties:	
Density	5.26E+16 mols / m^3	Temperature	300 K
Composition:	85.5 % CO_2	Accommodation	0.8 and 1.0
	4.1 % N_2	REA Properties:	
	6.4 % CO	Mass Flux at Full On	3.16E+23 mols/s
	4.0 % O	Composition	48.0% H_2
Temperature	225 K		30.0% N_2
Velocity	7294 m/s		22.0% NH_3
Attitude Angles:P-4 min	θ =-44.590,ϕ=60.390	Temperature	1000 K
P-2 min	θ =-38.950,ϕ=67.990	Exhaust Velocity	2329 m/s

Table 7.6: DSMC Free Stream, Surface, and Thruster Properties.

The REA mass flow rate in table 7.6 is multiplied by the duty cycle for each engine. The duty cycle rates used for each instance are given in table 7.7.

Active REA Thruster Duty Cycles	Periapsis -4 minutes	Periapsis -2 minutes
+X REA (-X, +Y)	0 %	0 %
-X REA(+X, -Y)	16 %	42 %
+Y REA (-X, -Y)	0 %	0 %
-Y REA (+X,+Y)	56 %	83 %
+Z REA(-X+Yand +X-Y)	20 %	25 %
-Z REA(-X-Yand +X+Y)	20 %	25 %

Table 7.7: DSMC REA Duty Cycles.

Four DSMC simulations were performed for each time instance. For the accommodation values, both normal and tangential of 0.8 and 1.0, DSMC was first used without modeling the REA systems to determine the effect of multiple particle collisions. The purpose being to compare free molecular flow results with DSMC. A second simulation was performed with both accommodation coefficient values with the REAs modeled as shown in tables 7.6 and 7.7. The DSMC results are presented in two formats, the numerical aerodynamic values are plotted for comparison with the AT and FMS results, and graphically, showing the pressure and shear coefficient distribution over the spacecraft models for the periapsis -2 minutes orientation.

Figure 7.21 shows the Cmx/Cmy ratio data for orbit 15027 presented previously in Figure 7.13. In addition, the results achieved by Freemol, as well as both DSMC results are presented.

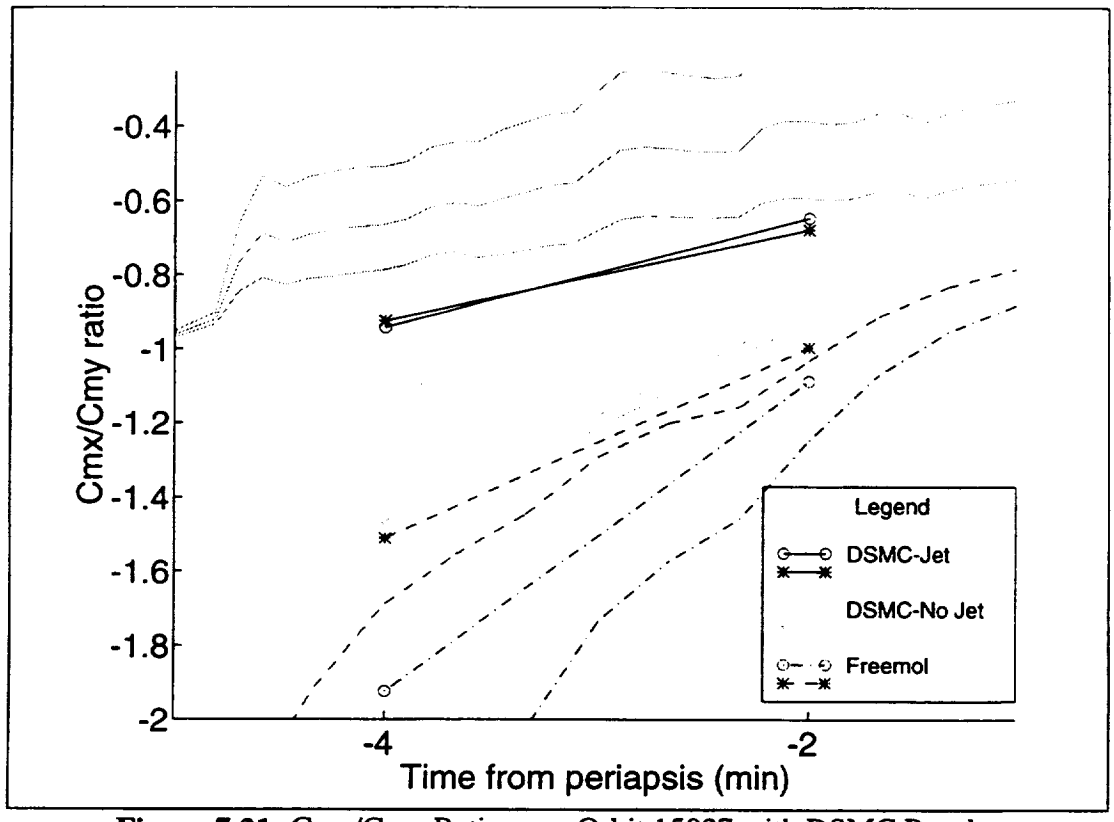

Figure 7.21: Cmx/Cmy Ratio over Orbit 15027 with DSMC Results.

The set of three lines at the top are the AT results. Below these are two solid lines that almost overlap. These are the DSMC "with jets" results determined at -4 and -2 minutes from periapsis. The accommodation 1.0 case data is marked using circles, the asterisks denote the accommodation 0.8 case. The next pair of near parallel lines plot the results of the DSMC "no jets" case. Beneath these are a final pair of line segments from -4 to -2 minutes which are the Freemol simulation results. The two continuous dashed lines are the FMS results (dashed 0.8 case on top, dot-dashed 1.0 case below).

Freemac and Freemol show very similar trends, with Freemac slightly below Freemol. The differences between Freemac and Freemol are caused by the use of slightly different geometric models and the effects of the different discretization methods as discussed in the appendix A. The DSMC "no jets" results shows that when multiple particle collisions are included, the simulation data is closer to the AT data and that the results are less sensitive to the accommodation coefficient value.

The DSMC "with jets" cases show a marked change in the Cmx/Cmy ratio towards the AT data indicating that the effects of the plumes are pronounced and affect the aerodynamics in the correct direction to nearly account for the differences between the AT data and the free molecular simulations. The slope of the DSMC results is also more consistent with the AT results.

Figure 7.22 presents similar information as 7.21. Note that the instances analyzed with DSMC correspond to the depression in the AT data visible in Figure 7.14 and discussed in section VII.2.3. Several observations can be made. The Cmz/Cmy ratio is more dependent upon the accommodation value and remains so when particle collisions and plume effects are modeled. Judging from the small differences between the Freemol

and "no jets" cases the effects of interparticle collisions and multiple collisions on the aerodynamic coefficient ratio is small. The effect of the exhaust plume on the Cmz/Cmy ratio is clear and, again the change is in the correct direction to account for the differences between the flight data derived AT results and the simulation.

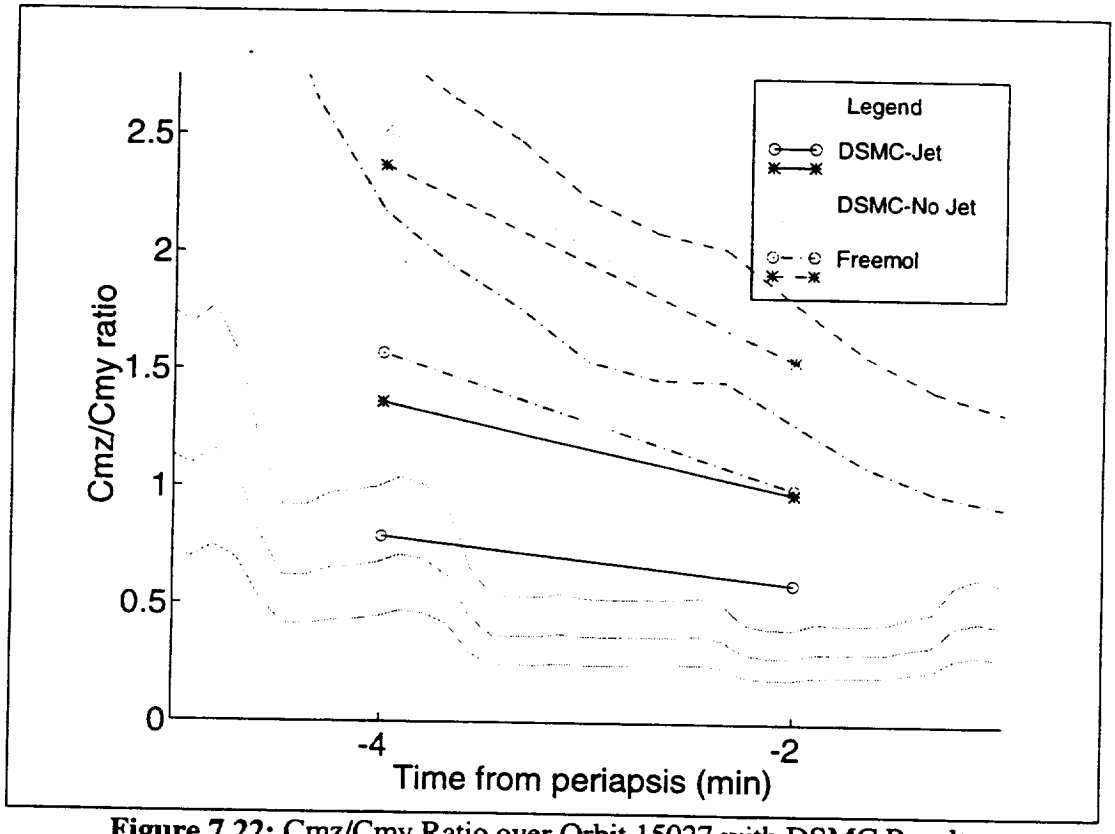

Figure 7.22: Cmz/Cmy Ratio over Orbit 15027 with DSMC Results.

The graphic presentation of information is often useful as it allows for a more intuitive grasp of the data presented. Figure 7.23 illustrates the pressure and shear coefficient distribution over the Freemac Didier Magellan geometry as determined using Freemac for the instance at periapsis -2 minutes with an accommodation value of 1.0. This can be compared with Figure 7.24 which presents the same analysis as performed using Freemol with the Freemol Didier Geometry. The different effect caused by modeling the HGA as a spherical section in Freemol and as a series of cones in Freemac

can be clearly seen. The pressure and shear coefficients vary continuously over the surface of the Freemol model forming clear isometric bands along cross sections of the HGA. In the Freemac analysis these bands are discontinuous from one cone to the next. This effect is also apparent in the SRM shroud where the circular flat plate used in the Freemac geometry presents a constant angle of incidence to the free stream. Still, it can be seen that the conical approximation of a spherical section yield similar results.

Figure 7.25 presents the pressure and shear distribution over the Freemol Didier model determined using the DSMC code with the REA exhaust plume models. The Freemol and Freemac analysis show a sharp shading boundary where the -X solar panel shades the HGA. When particle collisions are modeled the solar panel creates a scattering which shields a larger area of the HGA producing a region over which the pressure and shear decrease gradually. Also visible are small areas of high pressure and shear on the BUS ring just below the -X solar panel and on the lip of the SRM shroud below this. This could be caused by the extra flux of particles striking these areas after colliding with the solar panel. Another area of note is the +X solar panel where the outline of the +X, -Y REA exhaust plume can be clearly seen. As expected both the pressure and shear in these areas are reduced. Such a reduction has a significant effect on the moment about both the y and z axis. The shadowing on the solar panel caused by the REA trusswork is also more considerable in the DSMC simulation than the free molecular, this suggests the importance even relatively small components can have on the aerodynamic properties of a craft.

Freemac Didier Geometry

Freemac free molecule code

Pressure and Shear Coefficients, Orbit 15027 at Periapsis minus 2 minutes

θ=-38.946°, ϕ=67.994°

Free Stream is perpendicular to page.

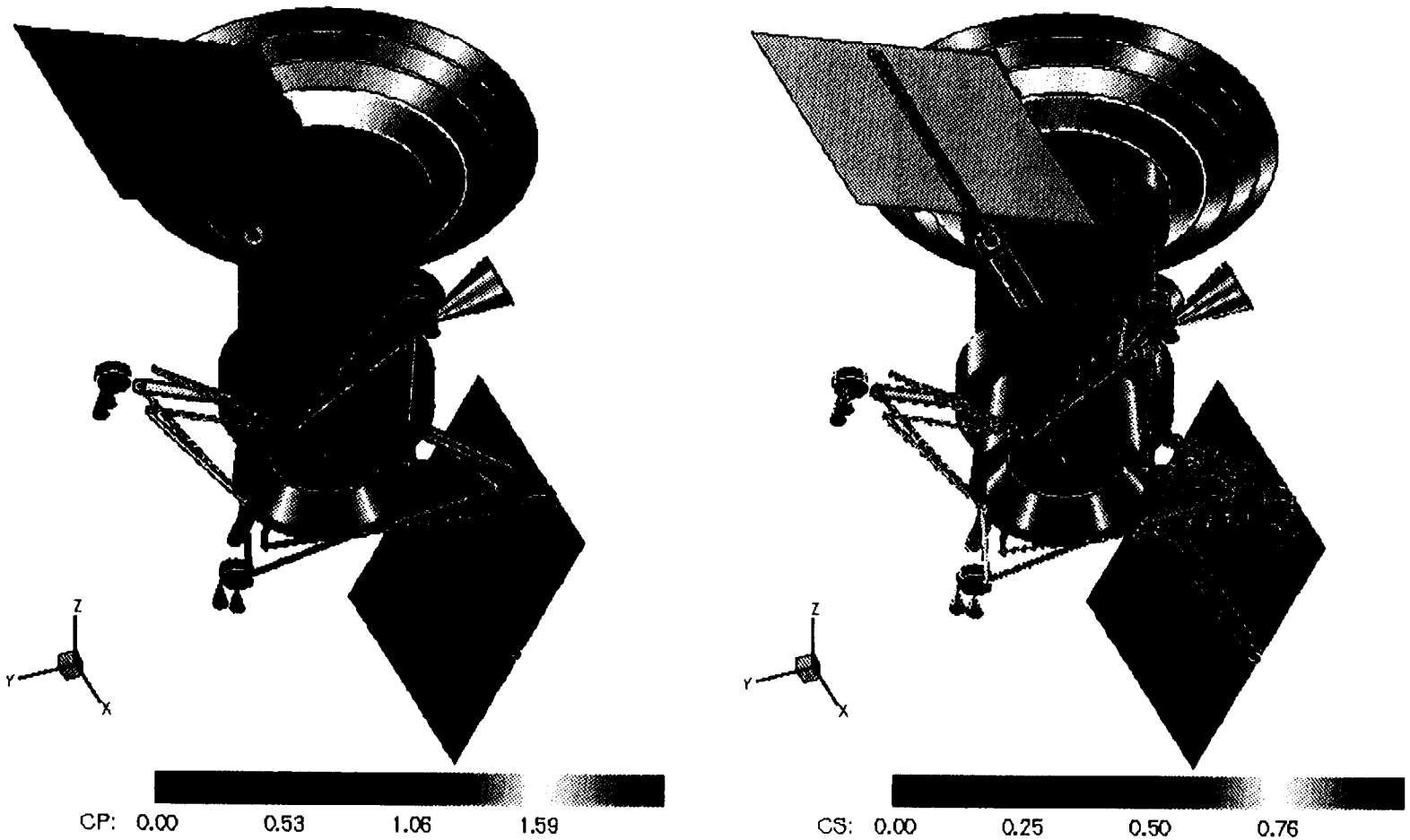

Freemol/DSMC Didier Geometry

Freemol free molecule code

Pressure and Shear Coefficients, Orbit 15027 at Periapsis minus 2 minutes

θ=-38.946°, ϕ=67.994°

Free Stream is perpendicular to page.

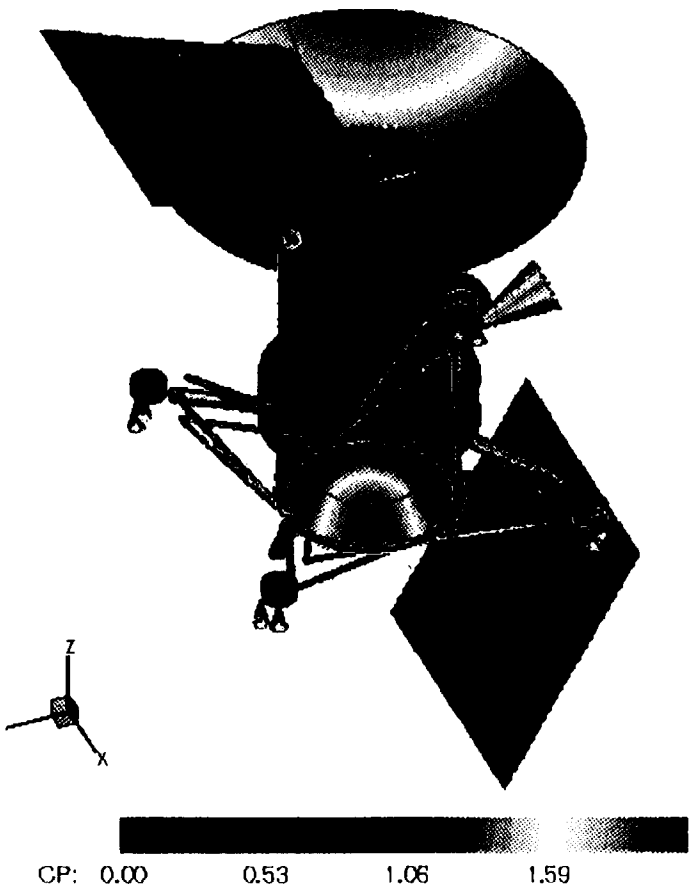

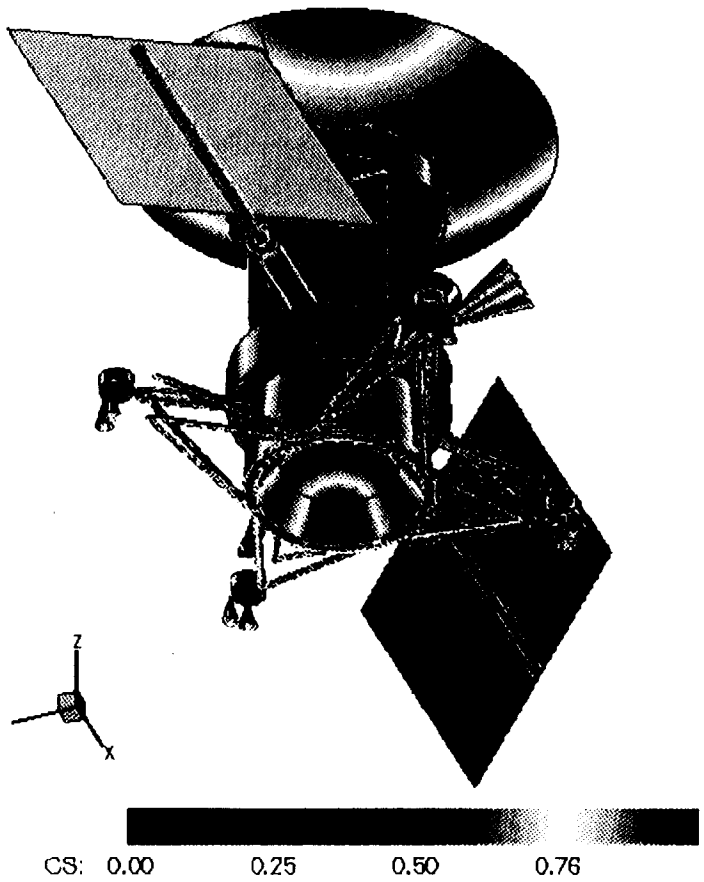

DSMC Freemol Didier Geometry

DSMC analysis code

Pressure and Shear Coefficients, Orbit 15027 at Periapsis minus 2 minutes

θ=-38.946°, ϕ=67.994°

Free Stream is perpendicular to page.

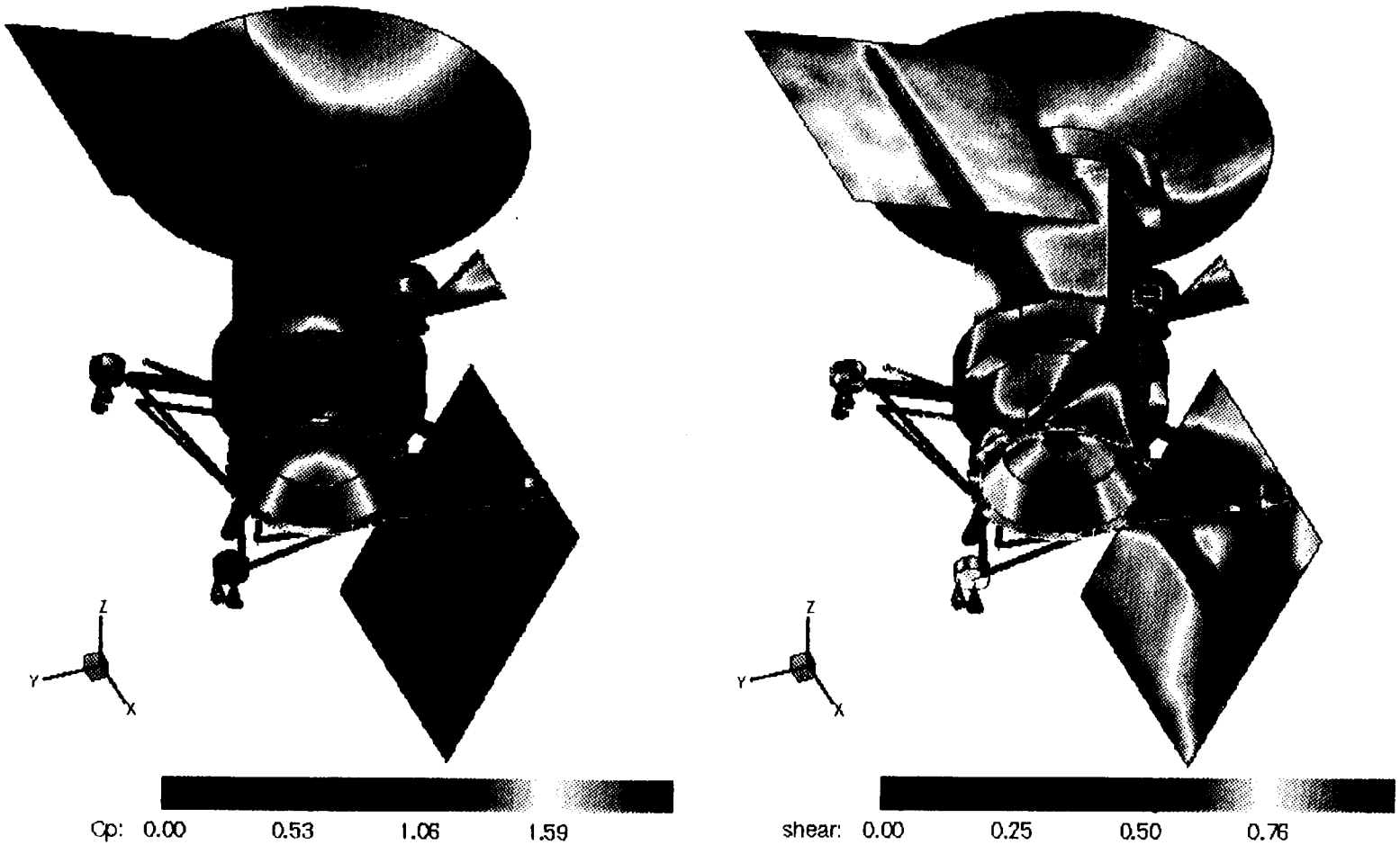

VIII. Summary and Conclusions

Comparison of free molecular analysis with Direct Simulation Monte Carlo analysis indicated the importance of intra-particle collisions and multiple particle collisions with the spacecraft surface. The DSMC method was used to model the reaction engine exhaust plumes and particle collisions under condition established for the Magellan spacecraft at periapsis -4 minutes and periapsis -2 minutes during orbit 15027. The DSMC moment coefficient ratios, which included modeling the exhaust plume and particle collision effects, accounted for nearly all of the differences noted between the atmospheric torque measurements and the free molecular simulations. In the two instances investigated, exhaust plume interference and particle collision effects reduced the Cmx/Cmy and Cmz/Cmy moment ratios by a factor of two. Graphic presentation of the DSMC data clearly indicates the shadowing of spacecraft components by simulated engine plumes. The effects of modeling particle collisions can also be observed.

Thrust levels for the attitude control engines are determined from flight telemetry data provided by the spacecraft control system. Calibration of 11 ms pulses using a third order polynomial fit and solving Euler's equations of motion for a torque impulse gave solutions of approximately 1 Newton per thruster. This is greater than the 0.5 N determined from the orbit trim maneuvers for 133 ms burns. Large variations in the mean thrust and 20% standard deviations achieved in the reaction engine calibration phase confirmed the difficulty in calibrating the engine thrust from flight data. These variations were accounted for by determining the atmospheric torque ratios for different thrust levels, defining a minimum, a nominal, and a maximum torque ratio.

Free molecular simulations were performed on geometric models of the Magellan spacecraft assuming constant accommodation values of 0.8 and 1.0 for equal values for both normal and tangential accommodation at a speed ratio of 23.5. The free stream orientation to the models was the same as those experienced by the Magellan spacecraft during orbit 15020 to 15032 around the time of periapsis. The Knudsen number of the flow field during these orbits was found to vary between 1 and 8. Free molecular torque ratios followed the same general trend as the atmospheric torque ratios but were not consistently inside the region bounded by the minimum and maximum atmospheric torque ratios. Although no precise accommodation coefficients were determined, generally the atmospheric torque ratios seem to indicate a high accommodation level.

In conclusion, this study seems to indicate that the reaction engine exhaust plumes can have a large effect on the aerodynamic moments experienced by spacecraft at high altitudes. Therefore these effects need to be studied and taken into consideration when planning missions of such a nature.

IX. Future Work

This study raised more questions than it answered. A study into free molecular aerodynamics and accommodation coefficients took on the added dimension of a study of engine plume effects upon the free stream at low Knudsen numbers. This is because the times during which the atmospheric torque acting on the Magellan spacecraft was expected to be most sensitive to the accommodation value of the surface were found to coincide with the times when the attitude control engines were most in use. The effects of the flow field upon the spacecraft are therefore masked by the effects of the exhaust plumes on the flow field. In order to accurately remove this mask and develop a gas surface model for carbon dioxide the following suggestions for future work on this subject are made:

1) Development of better Reaction Engine Assemblies models to permit more precise determination of thrust levels at all duty cycles. As these calibrations form the basis for determining the atmospheric torques acting on the spacecraft, this step is the basis for the data against which aerodynamic simulations will be compared.

2) Further investigate the effects of exhaust plumes disturbance and particle collisions upon the flow field around a spacecraft.

3) The need to develop a better understanding of the flow field characteristics at Knudsen numbers of 1 to 10, the transition region between continuum and free molecular flows.

Appendices

A. Free Molecular Code Comparison
B. Magellan Model Analysis
C. Free Molecular Simulation of Termination Experiment Orbits
D. Software Description
E. Freemac Magellan Models
F. Freemac File Formats

Appendix A: Free Molecule Code Comparison

As Freemac and Freemol/DSMC use different methods of discretization, comparison of two identical geometries and free streams is necessary to evaluate the codes physics and insure that both programs generate the same output from the same input.

The straight forward comparison of results from Freemac and Freemol for the Freemac Didier model and the Freemol/DSMC Didier model are given in Figures A.1 through A.6. Each plot presents one of the force or moment aerodynamic coefficients for each program during orbit 15027 in which the Freemol results are rotated into Freemac coordinates for comparison.

Freemol was run with the Freemol/DSMC Didier Geometry (see Figure 3.2) with the atmospheric composition predicted by the VIRA model for 140 km. altitude. An orbital velocity of 7300 m/s and an ambient temperature of 225 °K.

Freemac was run with the Freemac Didier Geometry (see Figure 3.2) with a speed ratio of 23.5. In both cases the accommodation coefficients, both normal and tangential, were set to 1.0 and the surface temperature of the craft components were set at 300 °K.

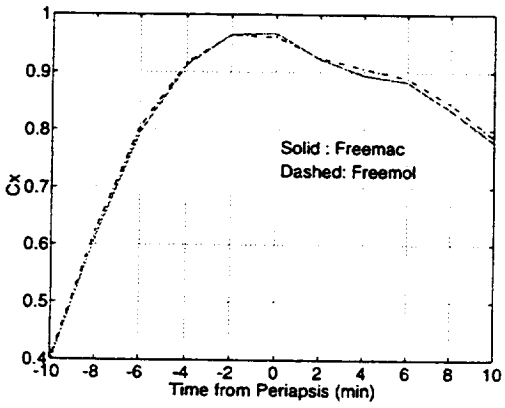

Figure A.1: Freemac and Freemol Cx

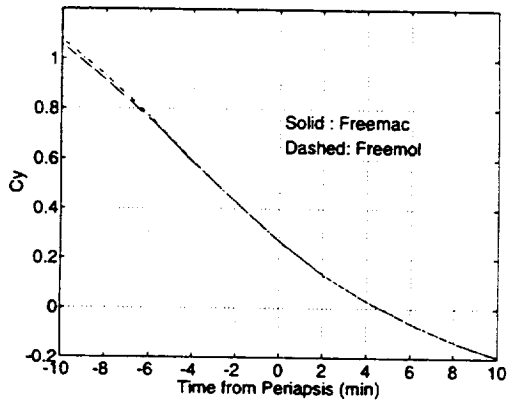

Figure A.2: Freemac and Freemol Cy

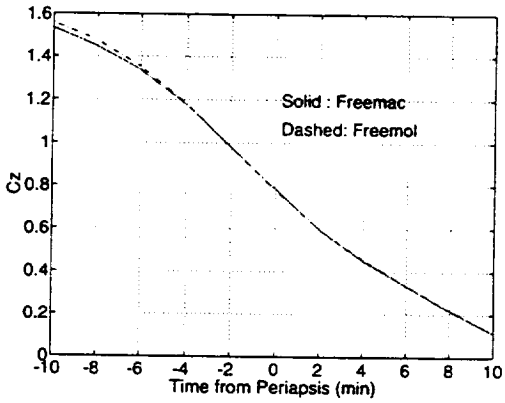

Figure A.3: Freemac and Freemol Cz

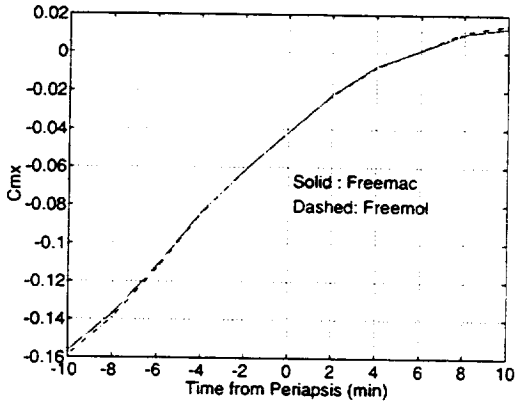

Figure A.4: Freemac and Freemol Cmx

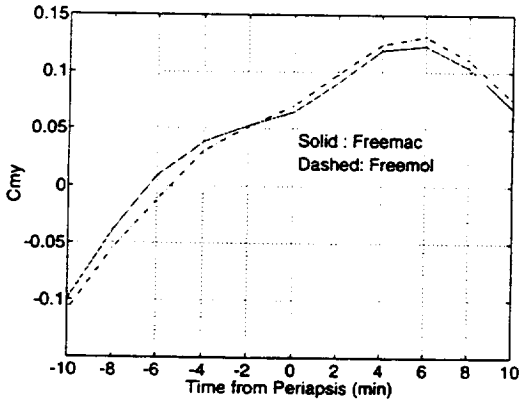

Figure A.5: Freemac and Freemol Cmy

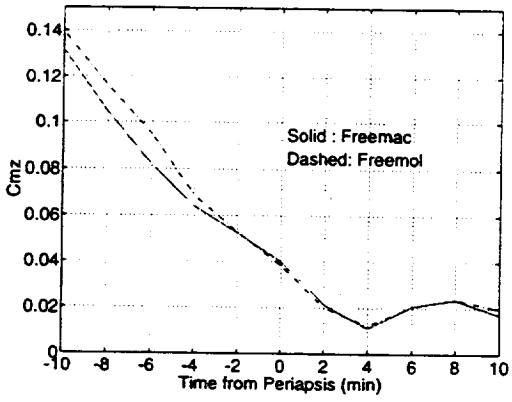

Figure A.6: Freemac and Freemol Cmz

The results of Freemol and Freemac are in close agreement for the force coefficients Cx, Cy, and Cz. Even the worst correlation of Cx at about periapsis is less

than 2%. This would seem to confirm that both codes are generating consistent data. The relatively large differences in the Cmy and Cmz values in spite of the nearly identical forces implies that the moment arms of those forces in each model about the center of mass are different, in effect that the forces are being applied at different points on each model. This could stem from two sources: 1) the minor differences in the two models (as described in Chapter 3) not having a significant effect on the area exposed to the free stream but having a significant effect on the moments, or 2) that the differences stem from the different methods the two codes use to discretize an object, as well as subsequent differences in shading effects.

The orientation at periapsis -6 minutes (θ = -49.976°, ϕ = 46.886°), is chosen for further analysis. Table A.1 presents the results and the difference between each code.

	Cx	Cy	Cz	Cmx	Cmy	Cmz
Freemac	0.7942	0.7599	1.3356	-0.1190	0.0082	0.0819
Freemol	0.8083	0.7698	1.3509	-0.1134	-0.0128	0.0950
Difference	-0.0096	-0.0099	-0.0153	0.0015	0.0210	-0.0131

Table A.1: Results of Freemol and Freemac for Didier Magellan Models

The coefficient contribution of some components of each model at this point are listed in tables A.2 and A.3.

Component	Freemac			Freemol		
Name	Cx	Cy	Cz	Cx	Cy	Cz
High Gain Antenna	0.1752	0.1666	0.2985	0.1772	0.1687	0.3016
+X Solar Array	0.1762	0.1802	0.2972	0.1877	0.1917	0.3164
+X Array Spar	0.0095	0.0093	0.0162	0.0096	0.0093	0.0164
-X Solar Array	0.1307	0.1180	0.2259	0.1319	0.1191	0.2278
-X Array Spar	0.0101	0.0098	0.0171	0.0095	0.0092	0.0161
SRM Shroud	0.0482	0.0453	0.0814	0.0490	0.0460	0.0820
REA truss element	0.0004	0.00033	0.00062	0.00064	0.00056	0.00107

Table A.2: Freemol and Freemac Force Coefficients by Component

Component Name	Freemac			Freemol		
	Cmx	Cmy	Cmz	Cmx	Cmy	Cmz
High Gain Antenna	-0.1372	0.1139	0.017	-0.143	0.1165	0.0189
+X Solar Array	0.0102	-0.2769	0.1618	0.0115	-0.296	0.1725
+X Array Spar	0.0005	-0.0146	0.008	0.0005	-0.0148	0.0081
-X Solar Array	0.0053	0.1958	-0.1053	0.0055	0.1974	-0.1064
-X Array Spar	0.0006	0.0139	-0.0083	0.0006	0.013	-0.0078
SRM Shroud	0.0205	-0.0218	0	0.0208	-0.0222	0
REA truss element	0.00024	-0.00032	0.00002	0.00032	-0.00052	0.00008

Table A.3: Freemol and Freemac Moment Coefficients by Component

The results for the HGA and SRM shroud components agree well between the two programs, showing that the approximation of cones and circular plates used in the Freemac Didier to model the circular sections in the Freemol Didier model are not the cause of the differences in the moment coefficients.

Instead, the answer is found in the 7% difference in the force coefficients for the +X Solar Panel (rotated at -60°) given by the two codes. The 7% is not large in comparison to the other components listed but as the array is a large surface at the end of a long moment arm a difference between the two models will clearly show in the results.

The next table presents the difference in the results of each model for the +X solar panel compared to the overall differences, the third line of table A.1, reproduced here. This table shows that indeed the main differences are due to the +X solar panel.

	Cx	Cy	Cz	Cmx	Cmy	Cmz
Freemac	0.7942	0.7599	1.3356	-0.1119	0.0082	0.0819
Freemol	0.8038	0.7698	1.3509	-0.1134	-0.0128	0.095
Difference in Models	-0.0096	-0.0099	-0.0153	0.0015	0.021	-0.0131
Difference in +X Solar	-0.0116	-0.0115	-0.0192	-0.0013	0.0191	-0.0107

Table A.4: Freemol and Freemac +X Solar Panel Comparison : Periapsis -6 min

The different values determined by each free molecular code for the +X solar panel are approximately 120% of the difference in the overall force coefficients. The +X solar panel exacerbates the Cmx differences between the two codes but overall this effect is minimal (about 3% of the Freemac and Freemol values). The different moments of the +X solar panel around the Y and Z axis indicate that the +X solar panel also accounts for upwards of 80% of the total difference for these two values. The +X solar panel difference is the single largest contributor to the overall difference. No other component has such different results: it is not the case that the +X solar panel is one set of large differences amongst many others that more or less cancel out.

The magnitude of the differences in the moment coefficients changes over time in Figures A.4, A.5, and A.6. When the relative wind vector is accounted for, this variation agrees with the conclusion that the difference between the models is caused by the +X solar panel. Indicating that the difference is persistent from one orientation to the next. When the spacecraft is about 10 minutes before periapsis the relative wind vector is 20° from the Y-Z plane and 50° below the craft, an orientation which is nearly perpendicular to the solar panel center line (the x axis) which would tend to maximize any moment differences calculated by Freemol and Freemac. As the orbit progresses the orientation shifts to one closely aligned with the X-Z plane and 7 degrees below the craft. As this is effectively along the x axis, the solar panels are virtually edge on to the free stream and any differences in the computations would be minimized. This effect is seen in the graphs as the two solutions converge after periapsis.

Eighty percent of the total error between the two simulations can therefore be traced to a 7% difference in the force coefficients of the +X solar panel, for the most part,

when it is shaded from the free stream by the +X, -Y REA. The solar panel is a simple rectangular plate identical in both models. This strongly suggests that the cause of the difference lies in the manner in which each program discretizes its respective model and in the manner in which they resolve shading. Recall that Freemac discretizes the surface area of a primitive into small rectangular plate elements, while Freemol discretizes each primitive component into small cubes ("cubics", in this case about 1 inch on a side) with all cubics of all primitives oriented with a fixed set of axis.

Supporting evidence for this conclusion can be gained by comparing model components with dimensions approaching the limits of each models resolution. The truss work that connects the REA systems to the craft and the solar panel spar which extends underneath a solar panel are good examples. Twenty of the twenty-four truss elements are cylinders 1.1" radius (the other four have 3" radii), while the solar panel spar has a 2" radius (the truss element listed in Tables A.2 and A.3 has a length of 54.1" and connects to the +X,+Y REA). The solar panel spar extends along the X axis (Y Freemol axis) while the truss cylinders have a more general orientation (see Figure 3.2). The Freemac Didier Model each of these primitive cylinders is discretized into sixteen elements radially and along each inch of length. When comparison between Freemol and Freemac is made for the 1.1" radius truss components the difference percentage is large, typically around 30% but with a very high variability: from less than 1%, to more than 100%. The solar array spars with a larger radius show only a 4-5% difference. The 3" radius truss elements in turn showed percent difference of about 10 to 20%. In short, as component size approaches the limits of resolution, the variance in results between the two free molecular codes increases.

As Freemol defines a set of cubics that just envelops a component in question, all components are effectively discretized into slightly larger forms. The larger solar panel area shadowed will affect the moment coefficients determined for that component. Furthermore, the degree to which a component aligns with the discretization grid can affect the results of the discretization. The results for large objects would generally be less sensitive overall but smaller objects, those with dimensions approaching the size of a cubic can, as shown, vary more.

Therefore Freemac and Freemol compute a 7% difference in the moment coefficients for the +X solar panel (large area, long moment arm, -60 rotation may not align with discretization grid) when it is shadowed by the REA truss (dimension approach the resolution of models, may not align with discretization grid). The next step can be phrased as a simple question: "How much of the 7% difference in the solar panel results is due to the cubic alignment effects on the +X solar panel, and how much is due to the different shadowing effects from the REA truss?".

At periapsis -6 minutes the +X solar panel is partially shadowed by the +X,-Y REA system and the supporting trusswork. Comparison with the results from a time when the solar panel is not shadowed (periapsis -10 minutes, θ = -53.418°, ϕ = 21.356°) yields the results summarized in table A.5

	Cx	Cy	Cz	Cx	Cmy	Cmz
Freemac +X Solar	0.09789	0.2756	0.3795	0.01230	-0.3433	0.2461
Freemol +X Solar	0.10287	0.2894	0.3985	0.01313	-0.3604	0.2583
Percent Difference %	5.08	5.01	5.01	6.71	4.99	4.97

Table A.5: Freemol and Freemac +X Solar Panel Comparison: Periapsis - 10 min.

Eliminating the effects of the REA shadowing upon the solar panel reduces the difference margin to 5%. This would seem to imply that the lattice alignment effects discussed above account for the bulk of the differences in the moment coefficient determined for each model. However a 1" worst case increase in the effective dimensions of the solar panel (due to cubic discretization) should only account for approximately 2% of the difference. The probable cause of the remaining 3% difference in the models remains unknown.

This analysis accounts for the computational results. The large percent difference for the 1.1" truss elements is due to the radius approximating the size of the discretizing cubics. The high variability is also explained. The errors observed for the 2" panel spars are indeed smaller than for the 1.1" as predicted. And though the 3" truss elements have greater difference percentages than the 2" panel spars, the panel spars are aligned along the Freemol cubic lattice axis.

Appendix B: Magellan Model Analysis

In any research of this nature there are always questions as to how well the models used to simulate the events represent the actual systems. The geometries used to simulate the Magellan spacecraft in this research are complex models constructed from dozens of component shapes. Differences between the models and the Magellan spacecraft could stem either from errors in the measured dimensions that characterized the model, from the necessary simplification of the actual geometry, or from changes in the actual spacecraft due to wear and tear during the mission. As fuel is consumed the center of mass may shift as well. The Magellan normal momentum accommodation coefficient may differ from the tangential. Also, the modeling of the gas-surface interaction can affect the results achieved.

The VIRA model along with the orbit analysis provide critical data used to model the free stream. Differences in the modeled and actual free streams would have an effect on the effective speed and temperature ratios used. The sensitivity of the results to these differences are unknown.

The purpose of this Magellan Model Analysis chapter is to address some of these issues. The investigation is not exhaustive. Rather it is intended to illustrate the sensitivity of the results computed to variations in the input of the model.

In this section Freemac was used to study variations in the factors mentioned above and compare these to a baseline aerodynamic characteristic model. The baseline is defined as the results achieved when the Freemac TRASYS model is analyzed over orbit 15027 with a speed ratio of 23.5, a component to free stream temperature ratio of 1.33, both normal and tangential accommodation coefficients modeled at a constant value of

1.0, with the center of mass 6.529" above the solar panel axis along Magellan's center line. This baseline is the FMS 1.0 case presented in VII.2.2 and VII.2.3.

From the equations for the free molecular forces (15), (16), and (17) it is expected that the forces and moments are insensitive to changes in the temperature ratio and speed ratio if the speed ratio is greater than fifteen. Simulation confirms this to be the case. Therefore uncertainties regarding the speed ratio and temperatures of the spacecraft and the ambient temperature predicted by VIRA are not critical.

The location of the center of mass affects the moment arms of the forces acting on the craft. The effect of any difference between the simulation center of mass and the actual center on the moment ratios is modeled here by shifting the simulation center of mass from the nominal modeled position two inches along each positive axis. These four simulations, D, X, Y, and Z, are presented in figures B.1, B.2, and B.3 where,

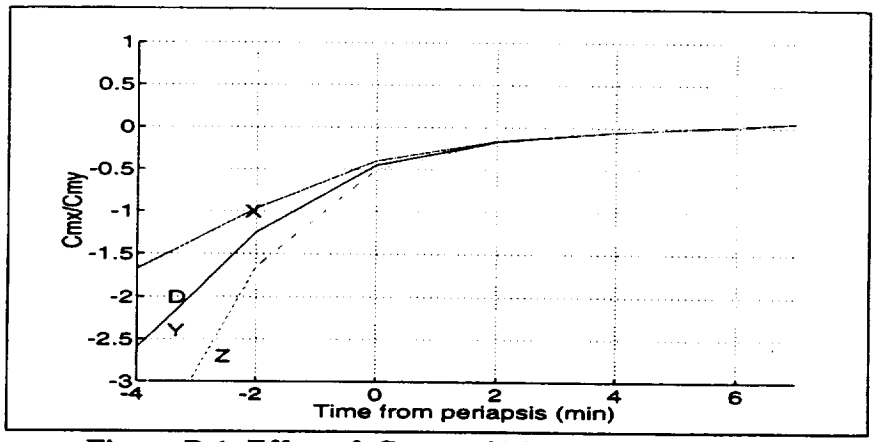

Figure B.1: Effect of Center of Mass on Cmx/Cmy

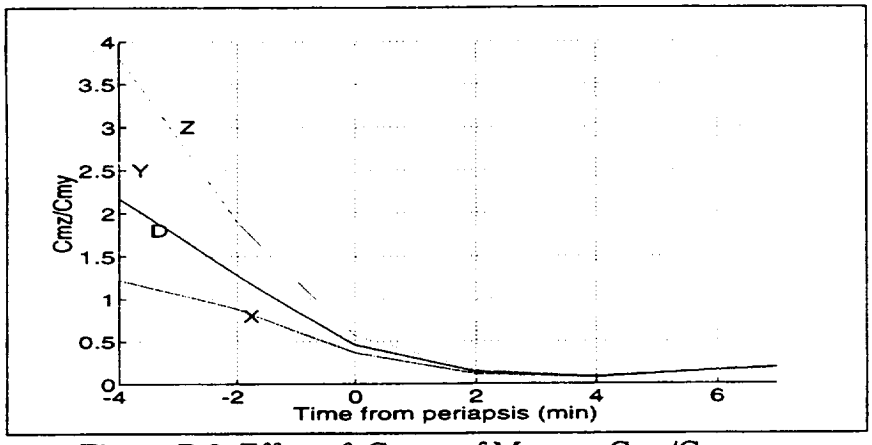

Figure B.2: Effect of Center of Mass on Cmz/Cmy.

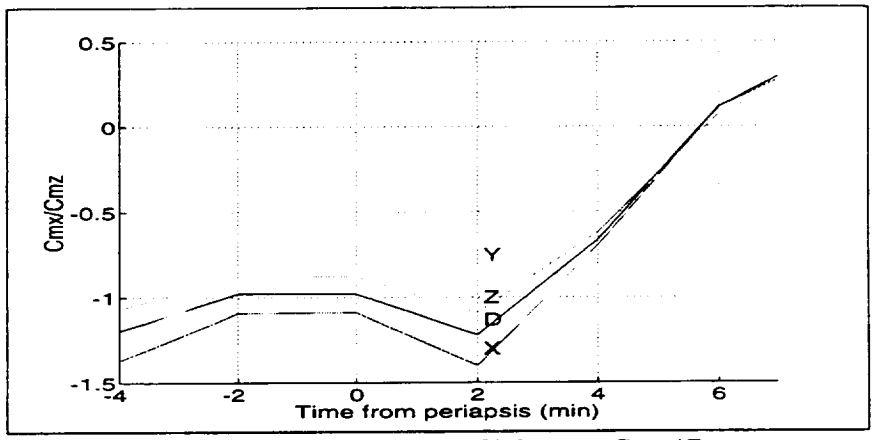

Figure B.3: Effect of Center of Mass on Cmx/Cmz.

the D case is the nominal center of mass location, the X, Y, and Z cases each represent the case where the center of mass is shifted two inches along the respective positive axis. These figures indicate that the location of the center of mass has a significant effect on the moment ratios determined before periapsis. After periapsis the orientation of the craft is such that the moment coefficients are less dependent on center of mass location. A shift of the center of mass along the positive X axis moves the simulation results towards the AT data in the cases of the Cmx/Cmy and Cmz/Cmy ratios (AT data shown in figures 7.13 and 7.14). The same could be said for shifting the center of mass along the negative Y and Z axis. These results could indicate that the center of mass of the actual Magellan

spacecraft was in the +X, -Y, -Z octant relative to the baseline model center of mass location. This effect could help to account for the small differences remaining between the AT and DSMC moment coefficient ratios, but no evidence to confirm a shift in the center of mass position has appeared in other analysis.

In Appendix A the aerodynamic characteristics of the Freemac Didier model were compared to the Freemol/DSMC Didier model. This was done to compare the physics of Freemac and Freemol. In this section the results of a comparison between the Freemac TRASYS model and the Freemac Didier model are presented. This comparison will relate the Magellan models to one another, allowing the Freemac TRASYS model to be compared to the Freemol/DSMC Didier model. By comparing two slightly different model geometries one can also begin to judge the potential errors small geometric differences between the Magellan spacecraft and the geometric models might introduce into the analysis of the aerodynamic characteristics. In the figures, the results are labeled "T" and "D" for the Freemac TRASYS and Freemac Didier model results respectively. Figures B.4, B.5, and B.6 show the force coefficients while figures B.7, B.8, and B.9 show the moment coefficient ratios that can be compared to figures 7.9 to 7.20.

These figures indicate that the results are relatively sensitive to the geometry modeled, yet less sensitive than to the accommodation coefficient. While the force coefficients of the Freemac TRASYS and Didier models are in very good agreement, the moment ratios vary by about 5%. This indicates that for the Magellan geometry, small differences can have a disproportionately large effect on the moment coefficient ratios.

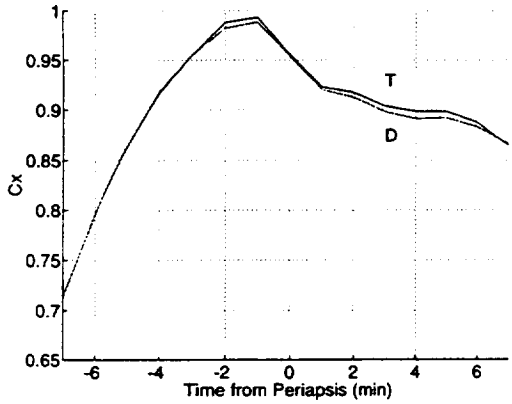

Figure B.4: Cx for Geometry Models

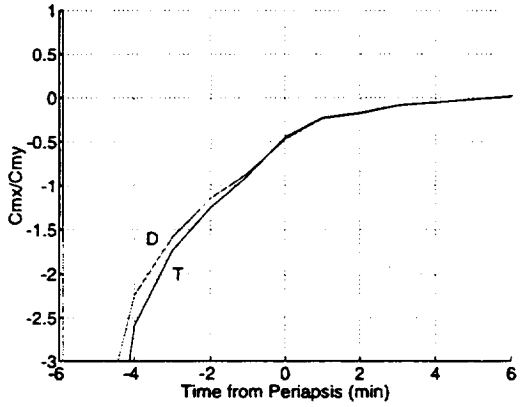

Figure B.7: Cmx/Cmy for Geometry Models

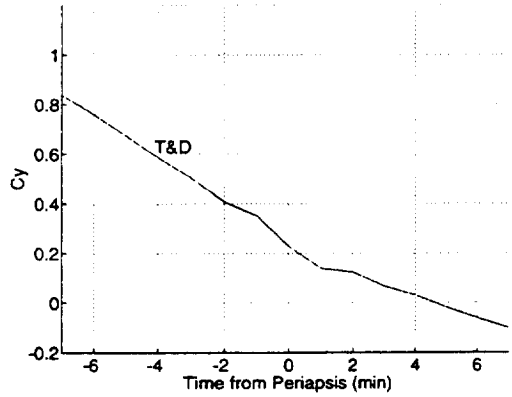

Figure B.5: Cy for Geometry Models

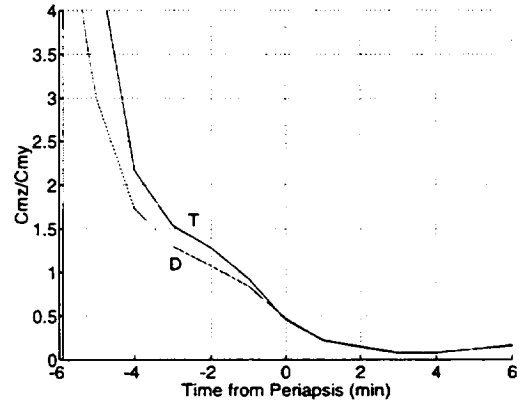

Figure B.8: Cmz/Cmy for Geometry Models

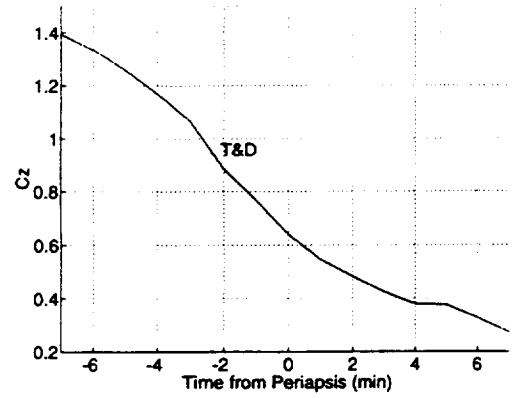

Figure B.6: Cz for Geometry Models

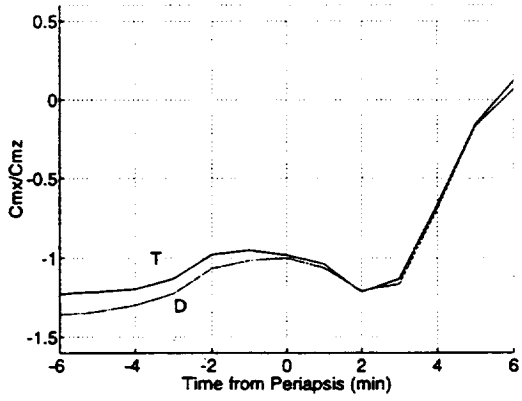

Figure B.9: Cmx/Cmz for Geometry Models

It has been assumed to this point that the normal and tangential accommodation coefficients are of equal value. This assumption was made since the symmetry of the

spacecraft main body suggests that the moments are determined by the solar panels and at high speed ratios (>15), the forces acting on the solar arrays are dependent on the sum of σ_n and σ_t. Still the question of the sensitivity of the moment ratio to different values of the normal and tangential accommodation numbers remains. Two cases in which the coefficients differed were analyzed. In the first case the normal coefficient was set at 1.0 while the tangential was set to 0.8. In the second case the normal was set to 0.8 while the tangential was set at 1.0. These cases are called the normal case (labeled "N") and the tangential case (labeled "T") respectively. Figures B.10 to B.12 present the results plotted against the baseline case.

The small separation between the N and T cases would seem to indicate that it would be difficult to distinguish between one case or the other, or between either case and a case where $\sigma_n = \sigma_t = 0.9$.

One goal of the Termination Experiment was to define a gas surface interaction model for free molecular carbon dioxide by determining the accommodation coefficient at different angles of incidence to the solar panels. The exhaust plume effects were unforeseen and resulted in complicating the analysis. In order to illustrate the effects a gas-surface model on the moment ratios the Freemac TRASYS model was analyzed under baseline conditions except that the approximate Knechtels and Pitts (KP) surface model implemented in Freemac was used instead of constant accommodation coefficients. The KP model was developed for nitrogen (N2) acting on an aluminum surface at velocities from 7.4 to 8.3 km/sec. The moment ratios are presented in figures B.13 to B.15 and the KP accommodation coefficients as a function of the angle of incidence are presented in figures B.16 and B.17 on the next pages. The constant accommodation cases is labeled "C" while the Knechtels and Pitts surface model case is labeled "KP".

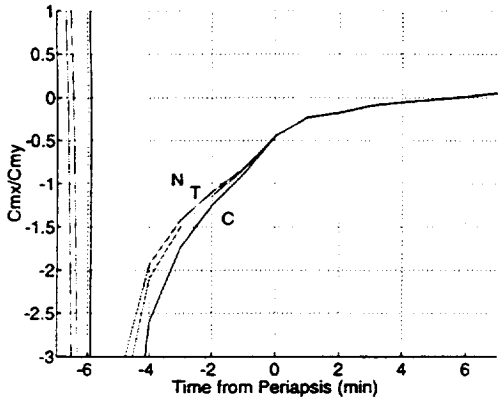

Figure B.10: Cmx/Cmy results of $\sigma_n \neq \sigma_t$

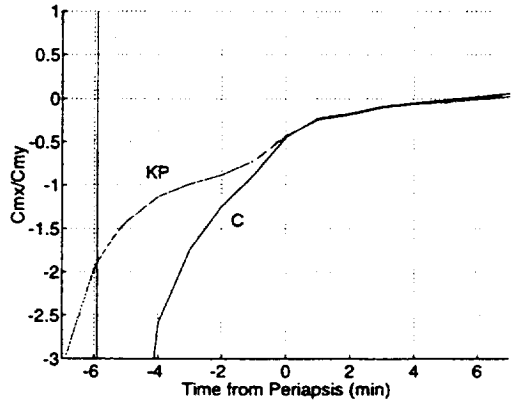

Figure B.13: Cmx/Cmy with KP surface model

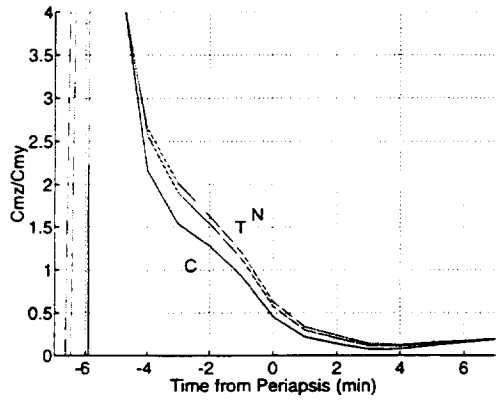

Figure B.11: Cmz/Cmy results of $\sigma_n \neq \sigma_t$

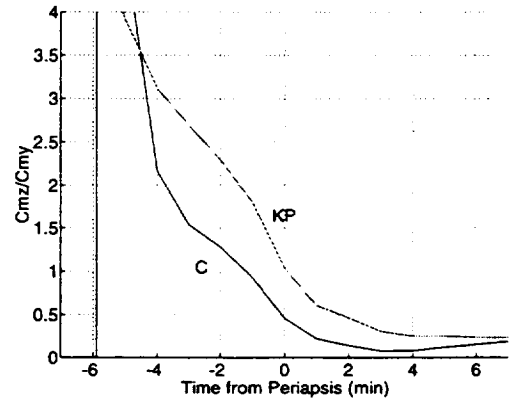

Figure B.14: Cmz/Cmy with KP surface model

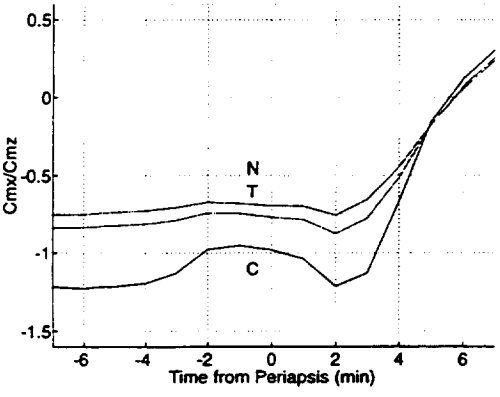

Figure B.12: Cmx/Cmz results of $\sigma_n \neq \sigma_t$

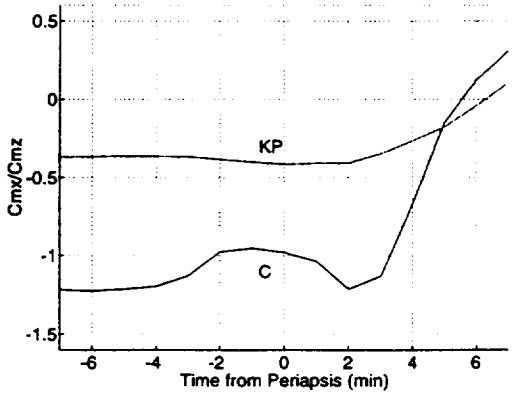

Figure B.15: Cmx/Cmz with KP surface model

The large differences between the C and KP cases in figures B.13, B.14, and B.15 indicate the importance of developing an accurate gas-surface momentum accommodation coefficient model in order to determine through simulation, the moments acting upon a craft in a free molecular flow field.

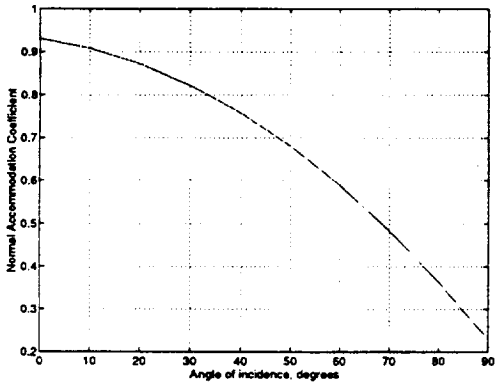

Figure B.16: KP Normal Accommodation

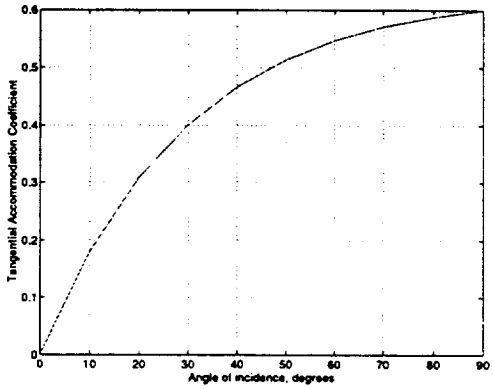

Figure B.17:KP Tangential Accommodation

These five factors then: the accommodation coefficient values, the position of the center of mass, the accuracy of the geometry model, and the gas-surface interaction model are the most critical knowledge requirements when performing free molecular simulations on complex geometries.

Appendix C: Free Molecular Simulation of Termination Experiment Orbits

The results of the Atmospheric Torque analysis and Free Molecular Simulation phases for the remaining orbits of the Termination Experiment are included here. They include orbits 15020 to 15032 exclusive of orbits 15023, 15027 and 15032 already presented in the text.

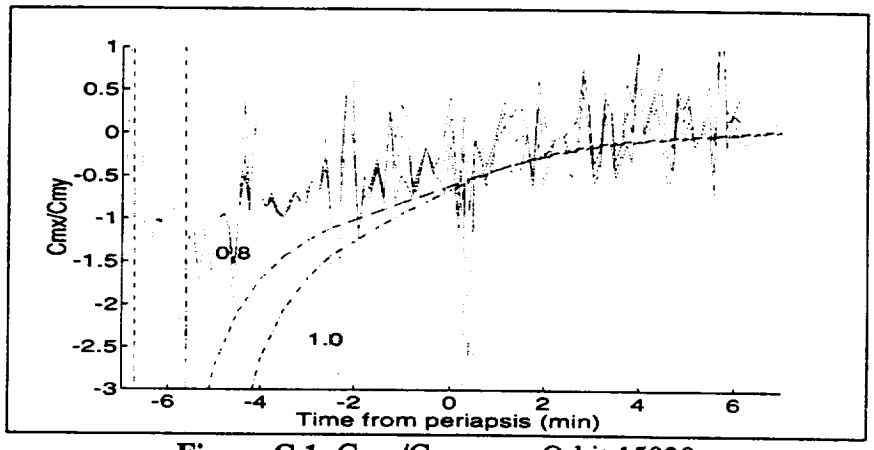

Figure C.1: Cmx/Cmy over Orbit 15020

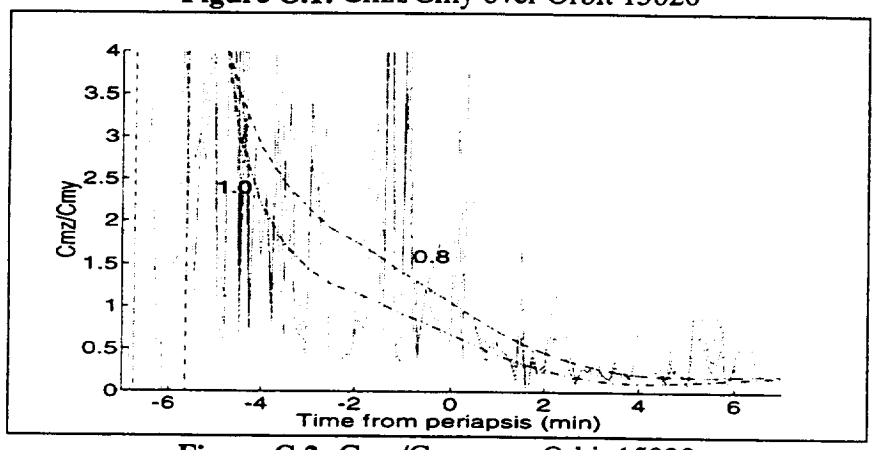

Figure C.2: Cmz/Cmy over Orbit 15020

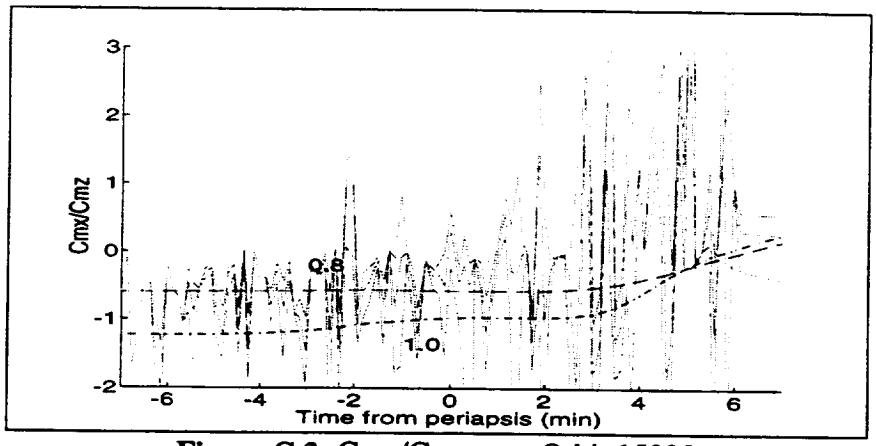

Figure C.3: Cmx/Cmz over Orbit 15020

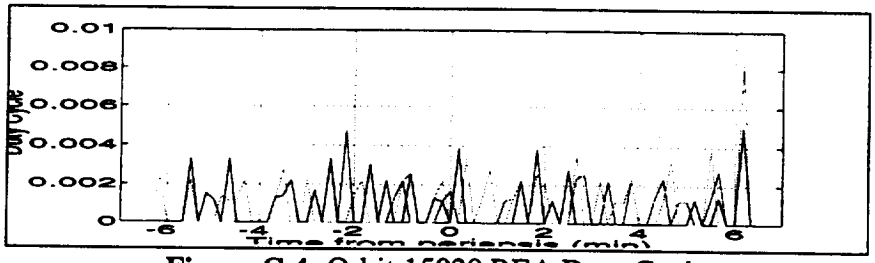

Figure C.4: Orbit 15020 REA Duty Cycle

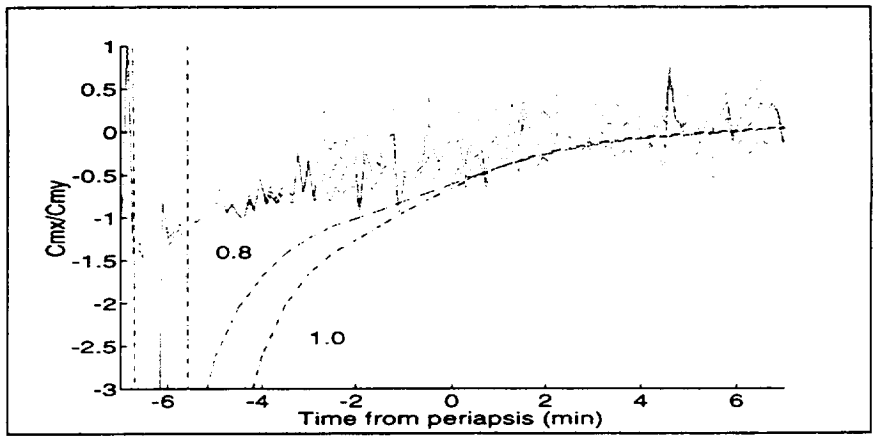

Figure C.5: Cmx/Cmy over Orbit 15021

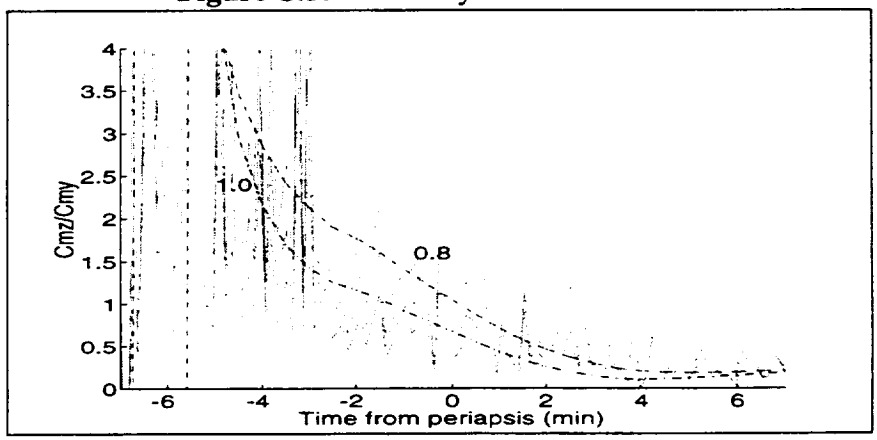

Figure C.6: Cmz/Cmy over Orbit 15021

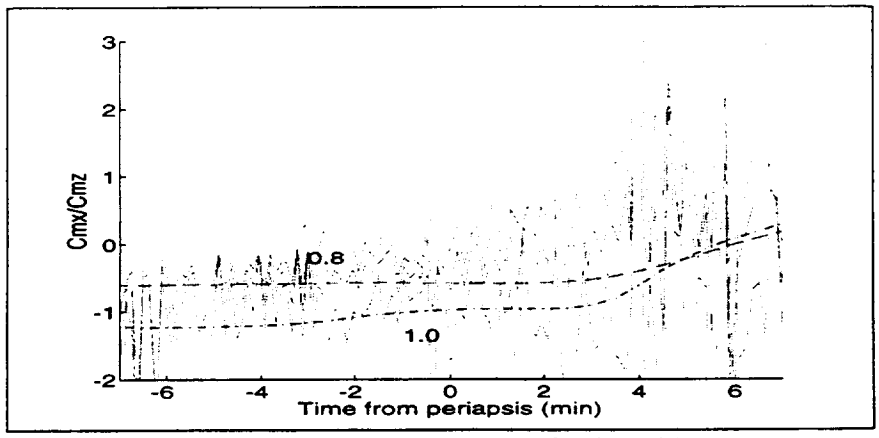

Figure C.7: Cmx/Cmz over Orbit 15021

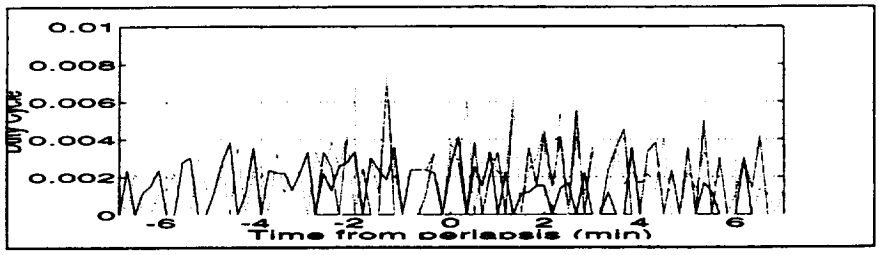

Figure C.8: Orbit 15021 REA Duty Cycle

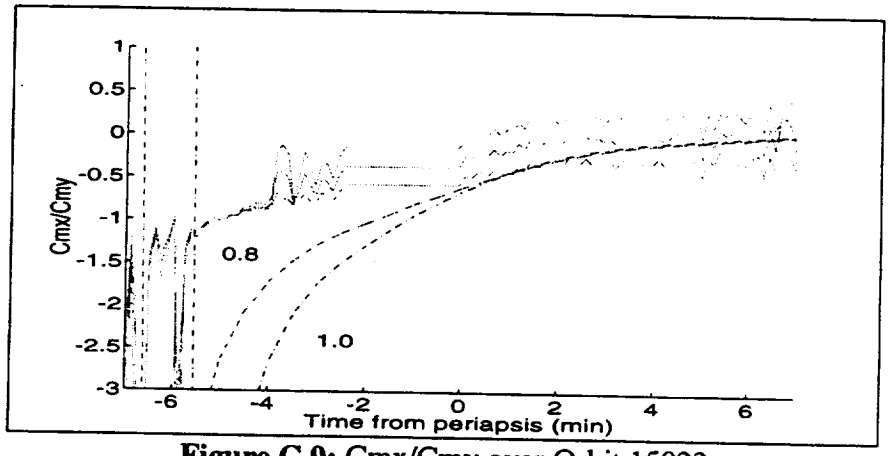

Figure C.9: Cmx/Cmy over Orbit 15022

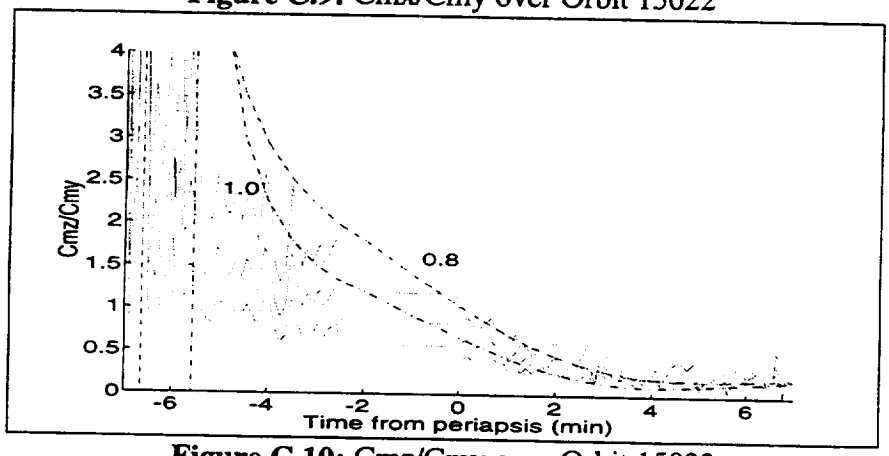

Figure C.10: Cmz/Cmy over Orbit 15022

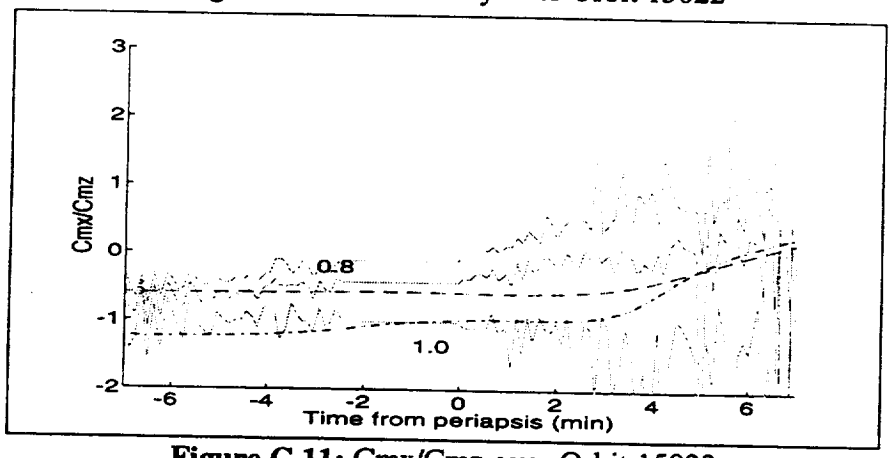

Figure C.11: Cmx/Cmz over Orbit 15022

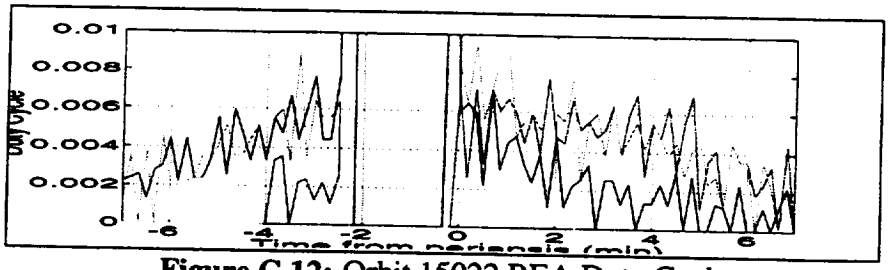

Figure C.12: Orbit 15022 REA Duty Cycle

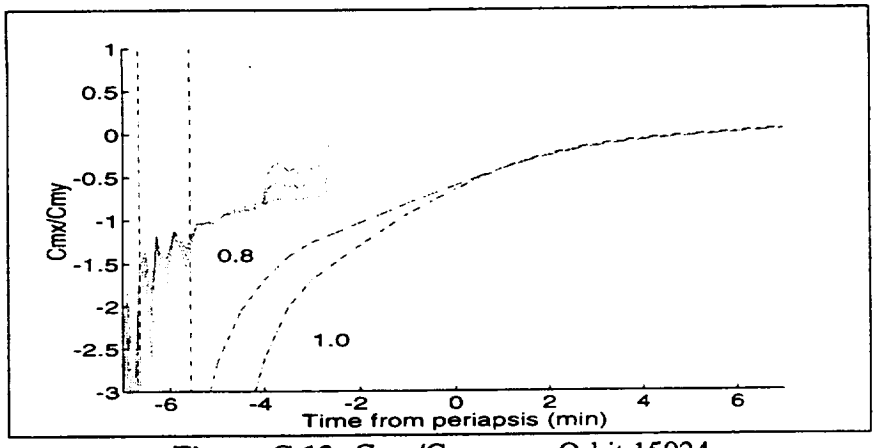

Figure C.13: Cmx/Cmy over Orbit 15024

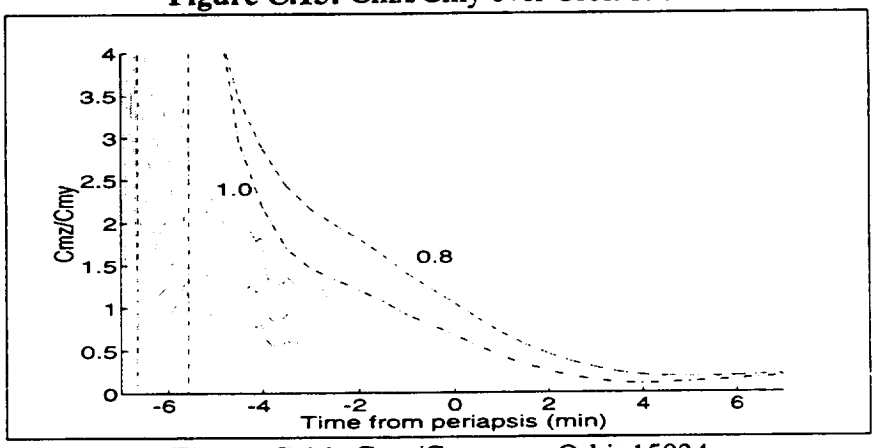

Figure C.14: Cmz/Cmy over Orbit 15024

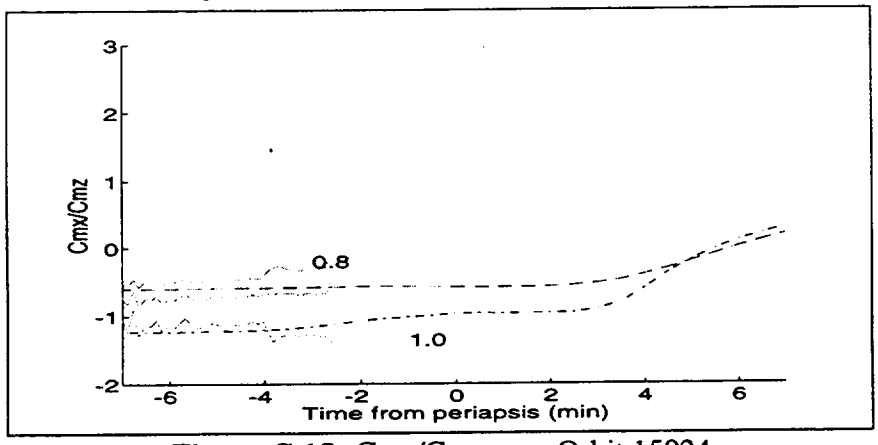

Figure C.15: Cmx/Cmz over Orbit 15024

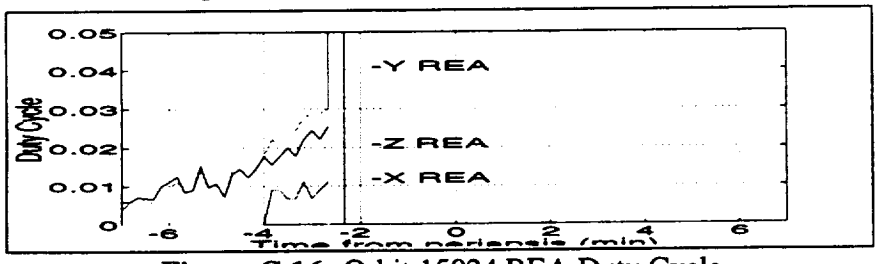

Figure C.16: Orbit 15024 REA Duty Cycle

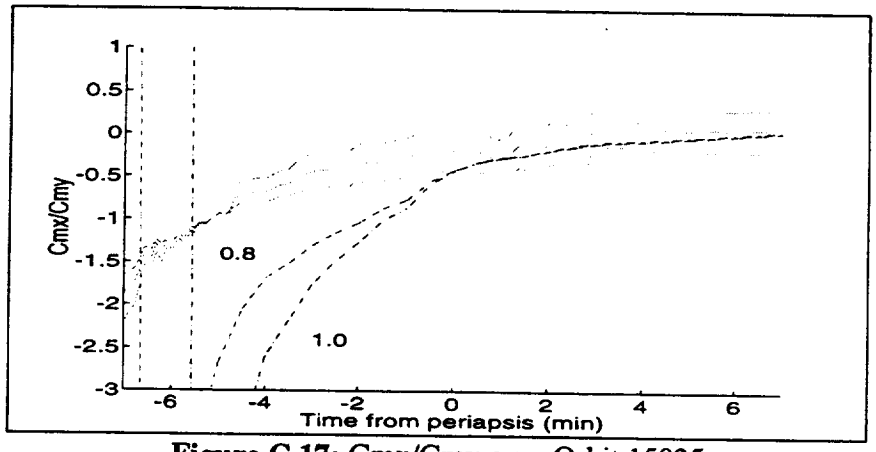

Figure C.17: Cmx/Cmy over Orbit 15025

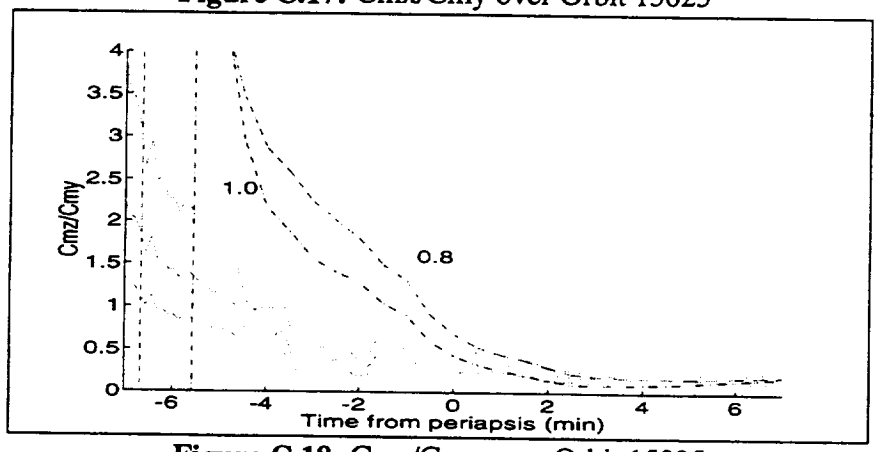

Figure C.18: Cmz/Cmy over Orbit 15025

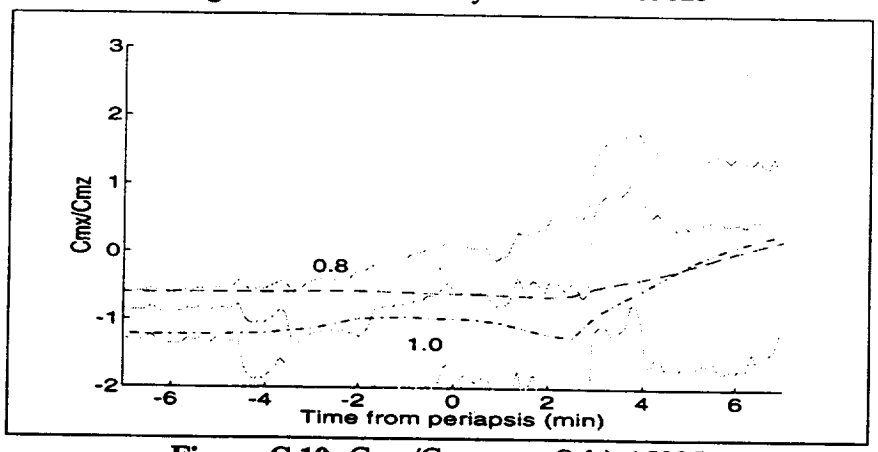

Figure C.19: Cmx/Cmz over Orbit 15025

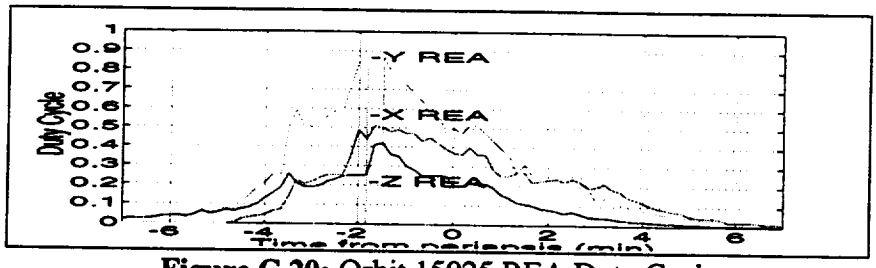

Figure C.20: Orbit 15025 REA Duty Cycle

86

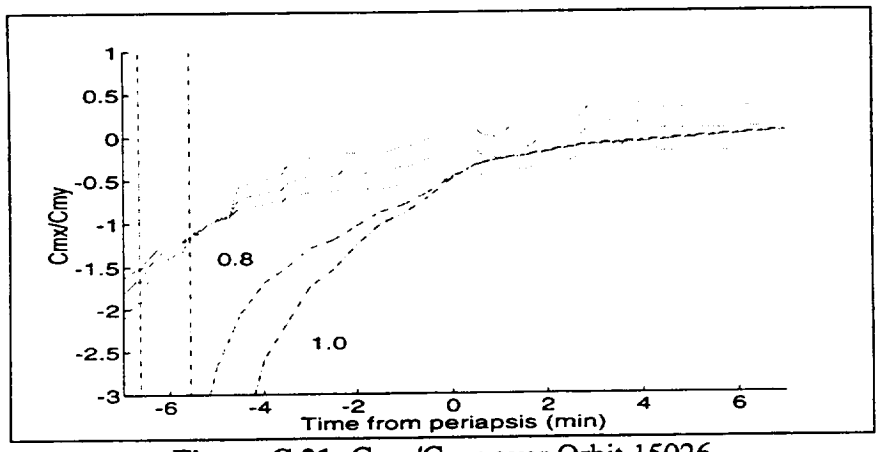

Figure C.21: Cmx/Cmy over Orbit 15026

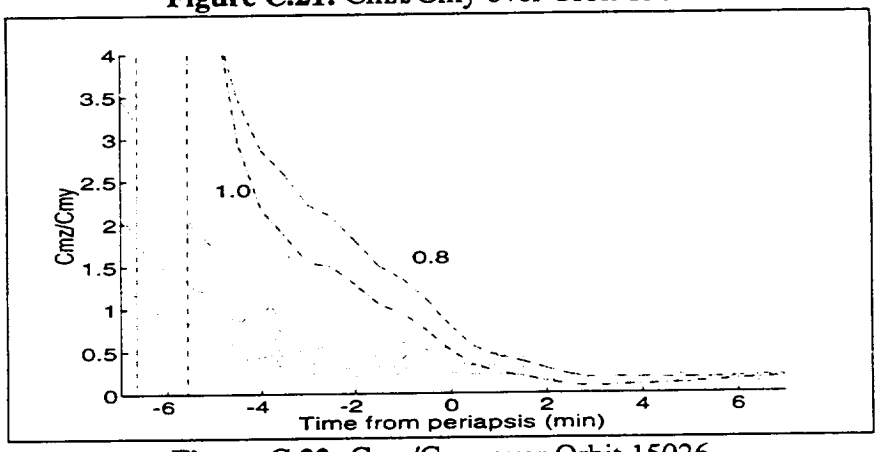

Figure C.22: Cmz/Cmy over Orbit 15026

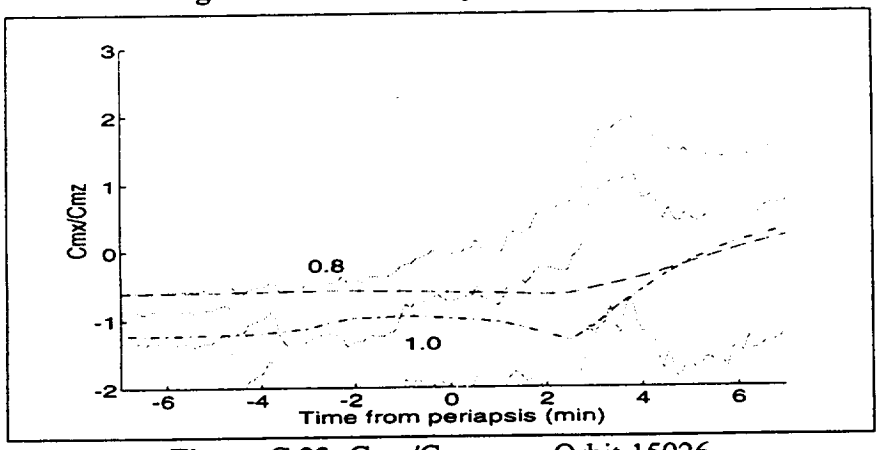

Figure C.23: Cmx/Cmz over Orbit 15026

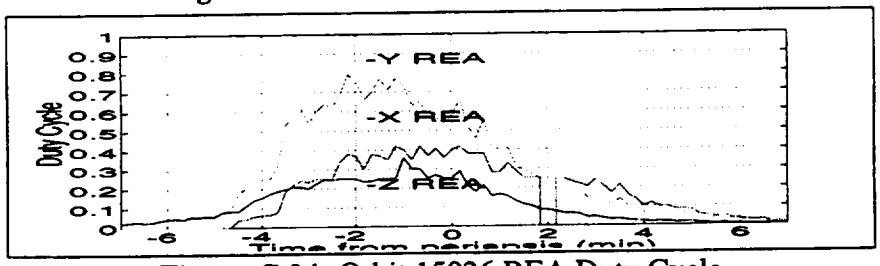

Figure C.24: Orbit 15026 REA Duty Cycle

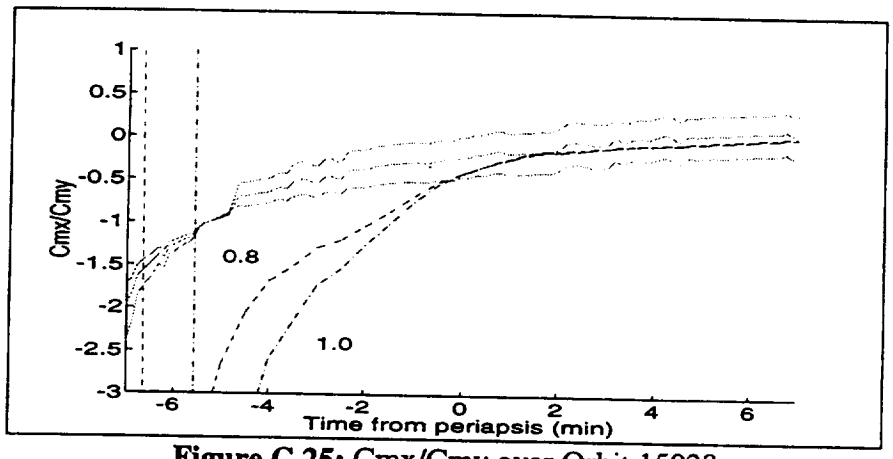

Figure C.25: Cmx/Cmy over Orbit 15028

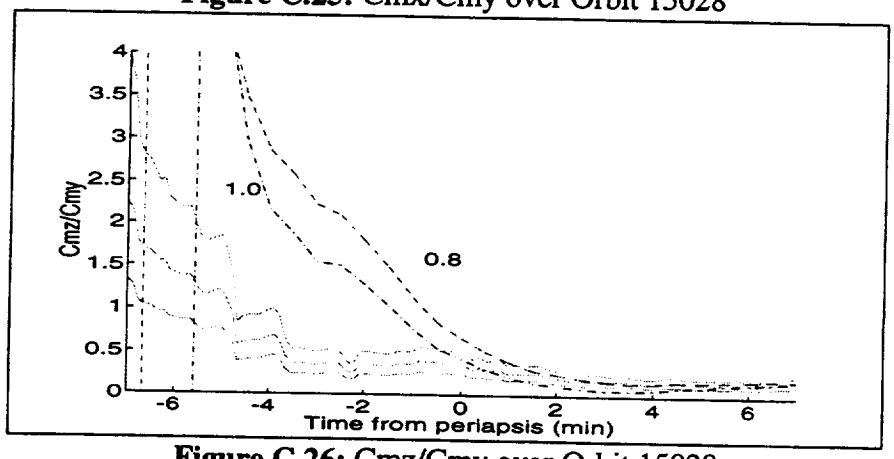

Figure C.26: Cmz/Cmy over Orbit 15028

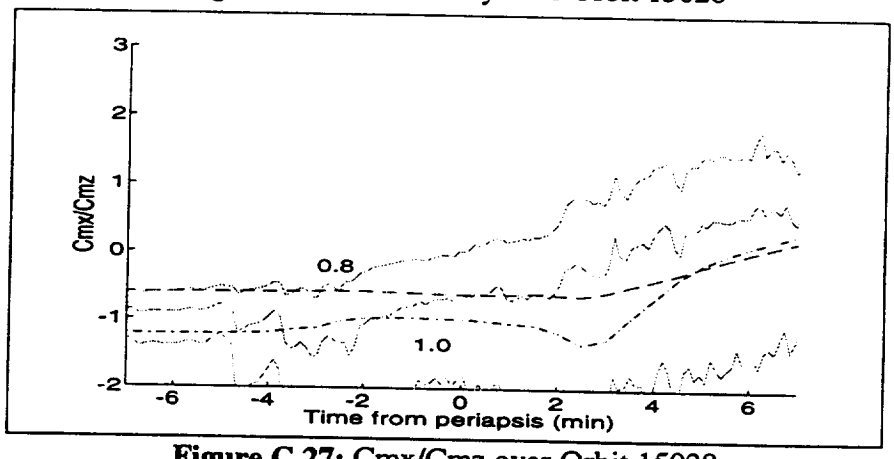

Figure C.27: Cmx/Cmz over Orbit 15028

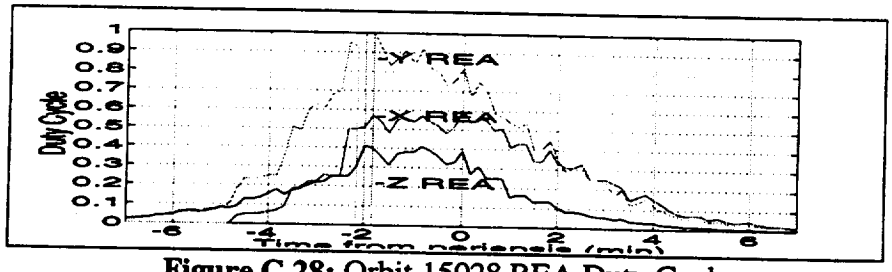

Figure C.28: Orbit 15028 REA Duty Cycle

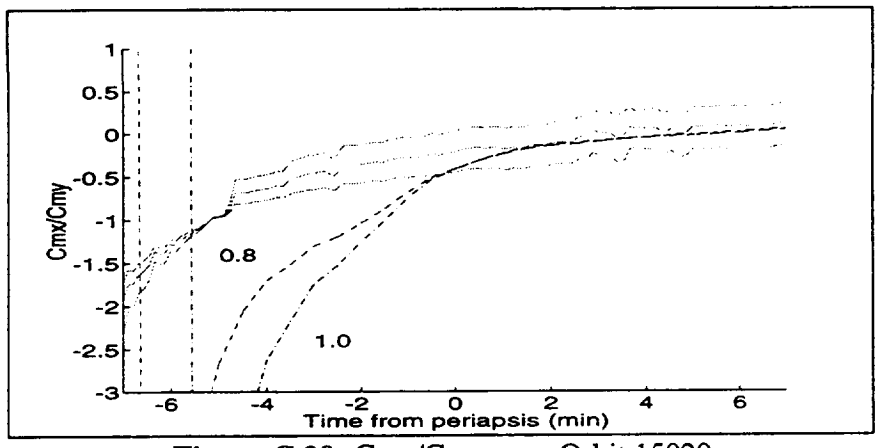

Figure C.29: Cmx/Cmy over Orbit 15029

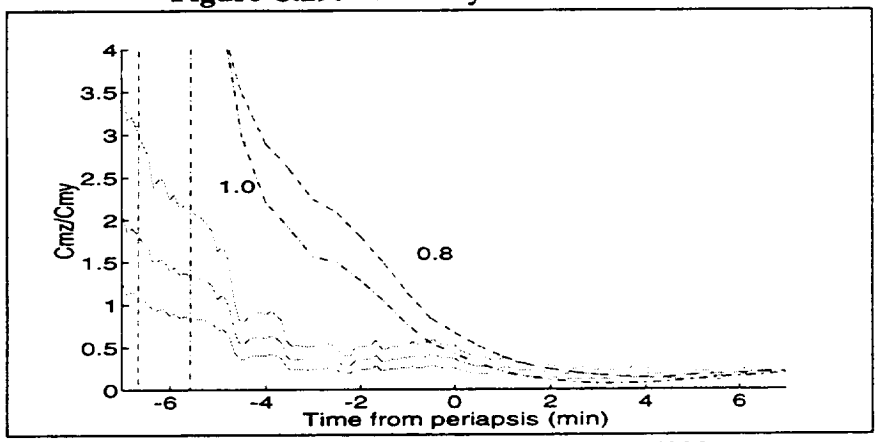

Figure C.30: Cmz/Cmy over Orbit 15029

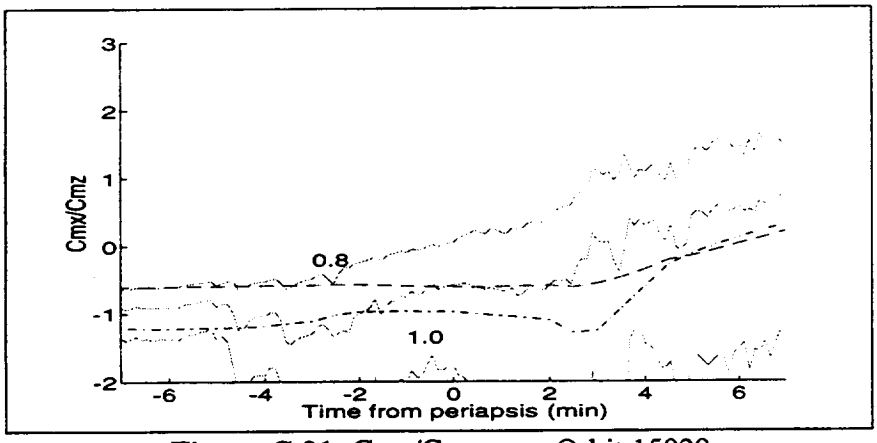

Figure C.31: Cmx/Cmz over Orbit 15029

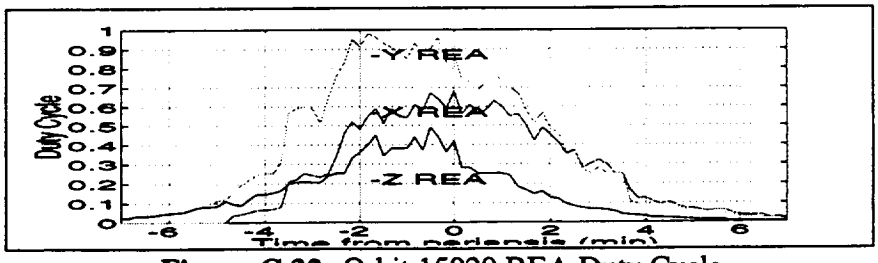

Figure C.32: Orbit 15029 REA Duty Cycle

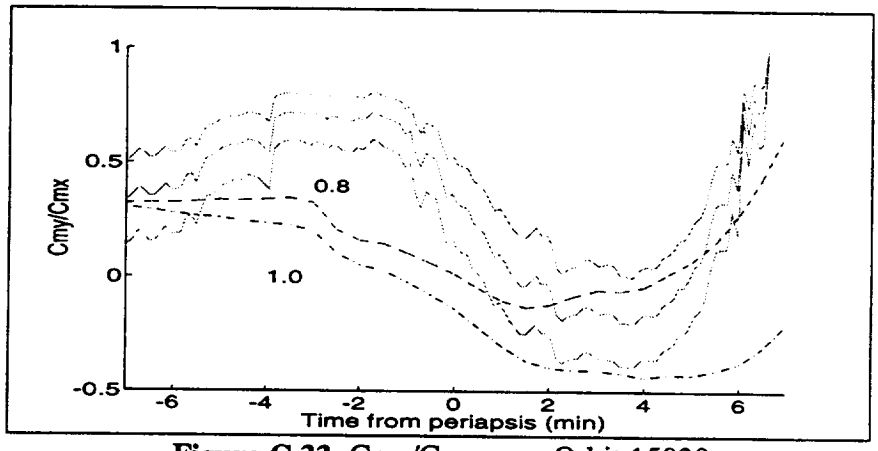

Figure C.33: Cmy/Cmx over Orbit 15030

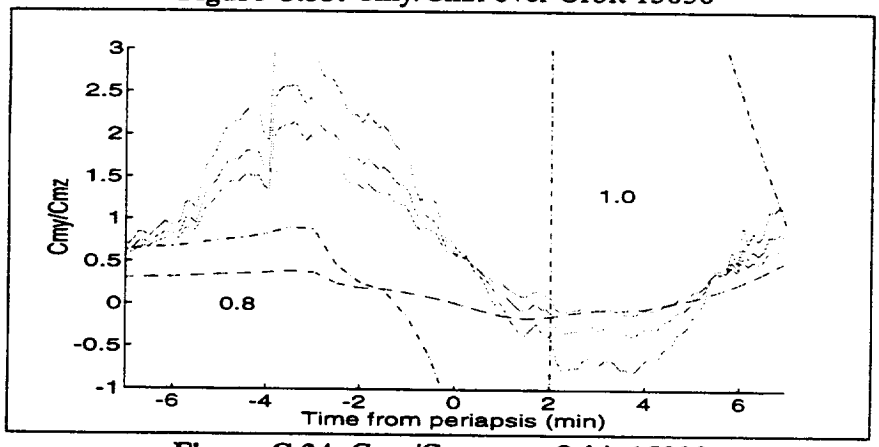

Figure C.34: Cmy/Cmz over Orbit 15030

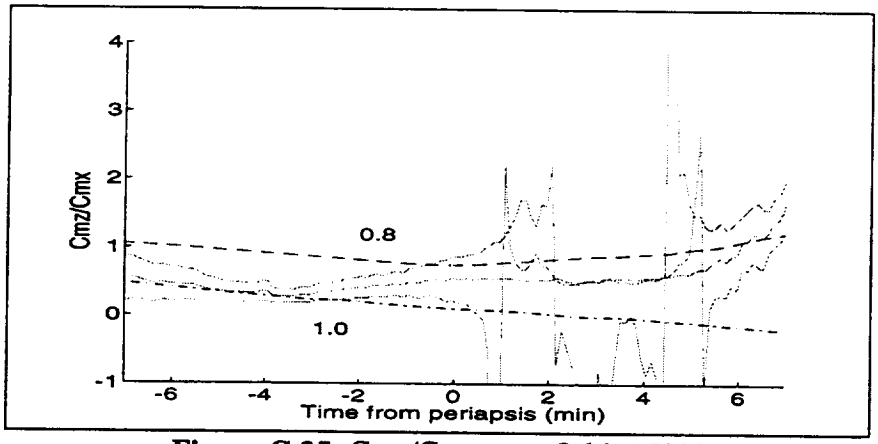

Figure C.35: Cmz/Cmx over Orbit 15030

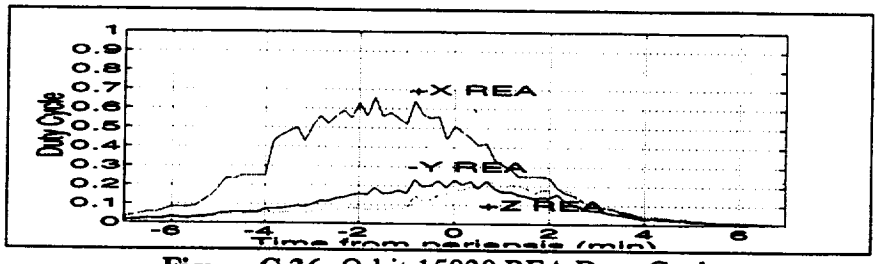

Figure C.36: Orbit 15030 REA Duty Cycle

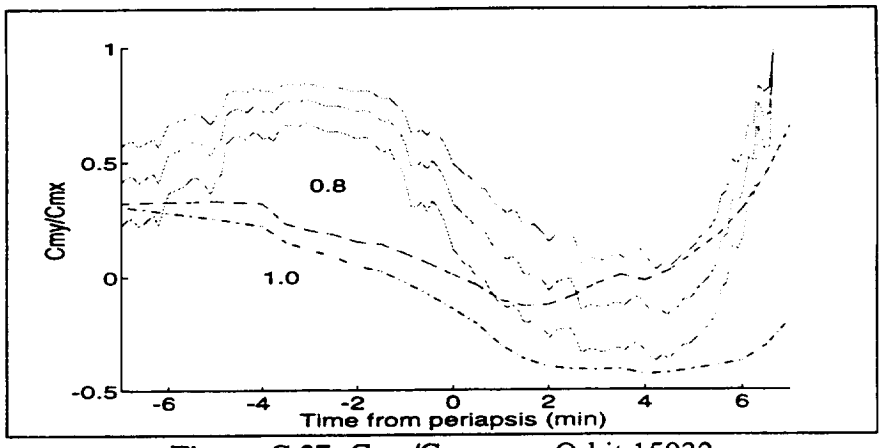

Figure C.37: Cmy/Cmx over Orbit 15032

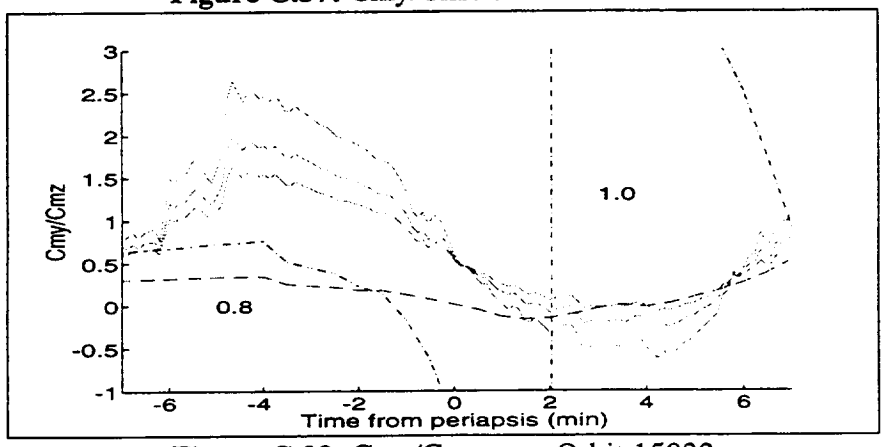

Figure C.38: Cmy/Cmz over Orbit 15032

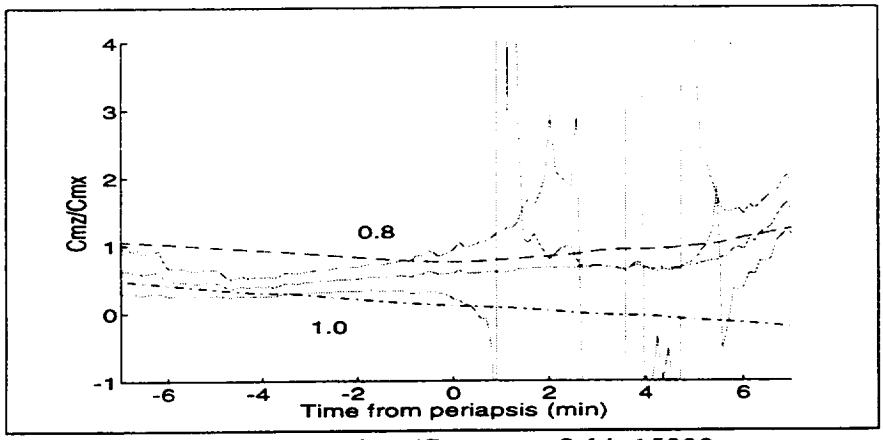

Figure C.39: Cmz/Cmx over Orbit 15032

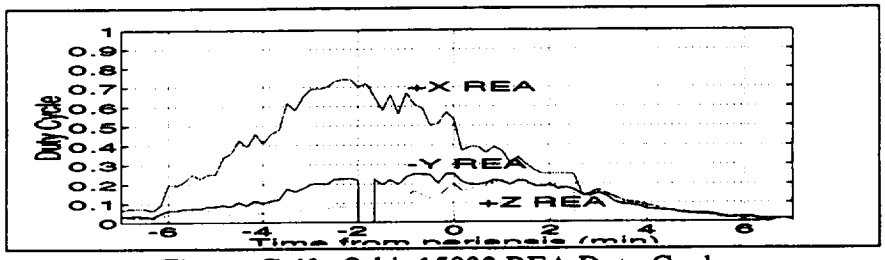

Figure C.40: Orbit 15032 REA Duty Cycle

Appendix D: Software Description

Data and Model Files

orbXXXXX.mat	Contains telemetry data for orbit XXXXX
magterm.m	Contains orbit parameters for all orbits

Magellan Model Files

All the Magellan models for use with freemac are called freedat.XXX where the extension indicates any variation of the model. The geometry model is indicated by the directory containing the file. The directories are:

TRASYS1	Freemac TRASYS models: solar panels at -60°/22°
TRASYS2	Freemac TRASYS models: solar panels at -4°/-34°
DIDIER	Freemac Didier models: solar panels at -60°/22°

File extension include

1n	Normal and tangential accommodation set at 1.0
8n	Normal and tangential accommodation set at 0.8
18	Normal accommodation set at 1.0, tangential at 0.8
81	Normal accommodation set at 0.8, tangential at 1.0
kp	Model set to use Knechtels and Pitts surface model
low	Low resolution model
s20	Molecular speed ratio set at 20.5
s26	Molecular speed ratio set at 26.5
t35	Component temperatures set to 350
xp2	Center of mass moved 2 inches +X axis
yp2	Center of mass moved 2 inches +Y axis
zp2	Center of mass moved 2 inches +Z axis

Analysis Codes

freemac.exe	Free molecular code. Implemented on PC and Unix
freemol	Free molecular code. Implemented on Unix system
par5	DSMC analysis code.

Matlab files

magoctr.m	Determines the spacecraft orbital path, orientation to the free stream and gravity gradient model. Output is magsav.mat file
makepath.m	Extracts orientation data from magsav file and converts to freepath.dat format
reacalb.m	Calibrates REA thrusters from telemetry data. Output is results.mat file
atmosph.m	Determines atmospheric torques once thrust level of REA's are manually entered. Output is atmcXXX.mat file. First two X's are last two digits of orbit number, last X is either a, b, or c to distinguish between nominal, low, or high cases.
dutycycl.m	Determines duty cycle rates from telemetry data.

Appendix E: Freemac TRASYS and Freemac Didier Magellan Geometry Models

E.1 Freemac TRASYS model: solar panels in -60°/22° configuration.

```
        72   35650.0     144.0     190.00       0.0       0.0    27.529
        20      90.0     -90.0       10.0      10.0       0.0      90.0
         0       1.0      23.5      225.0      1.35
 5  32   7       0.0       6.8       13.0       0.0       0.0     128.6
      0.0      90.0      90.0       90.0      90.0       0.0
         1     300.0       1.0        1.0       2.0       0.0
 5 120   8    63.039     5.185       70.0       0.0       0.0   105.746
    180.0      90.0      90.0       90.0      90.0       0.0
         1     300.0       1.0        1.0       2.0       0.0
 5 120   8    55.264      5.17     63.039       0.0       0.0   100.576
    180.0      90.0      90.0       90.0      90.0       0.0
         1     300.0       1.0        1.0       2.0       0.0
 5 120   8    46.198      5.17     55.264       0.0       0.0    95.406
    180.0      90.0      90.0       90.0      90.0       0.0
         1     300.0       1.0        1.0       2.0       0.0
 5 120   8     34.85      5.17     46.198       0.0       0.0    90.236
    180.0      90.0      90.0       90.0      90.0       0.0
         1     300.0       1.0        1.0       2.0       0.0
 1 120  35     34.85       0.0        0.0       0.0       0.0    90.236
      0.0      90.0      90.0       90.0      90.0     180.0
         1     300.0       1.0        1.0       1.0       0.0
 4 120  10      35.0       9.0        0.0       0.0      0.00     81.1
      0.0      90.0      90.0       90.0      90.0       0.0
         1     300.0       1.0        1.0       1.0       0.0
 1 120  20      35.0      18.0        0.0       0.0       0.0     81.1
    180.0      90.0      90.0       90.0      90.0       0.0
         1     300.0       1.0        1.0       1.0       0.0
 3  30  30     65.46     12.25        0.0     83.40       0.0   107.00
    28.624      90.0   118.624    118.624      90.0   151.376
         1     300.0       1.0        1.0       1.0       0.0
 3  30  30     12.25     65.46        0.0     83.40       0.0   107.00
    28.624      90.0   118.624       90.0     180.0      90.0
         1     300.0       1.0        1.0       1.0       0.0
 3  30  30     11.00     66.60        0.0     83.40    -12.25   107.00
    95.054    169.40    99.292     151.38      90.0     61.38
         1     300.0       1.0        1.0       1.0       0.0
 3  30  30     66.60     11.00        0.0     83.40     12.25   107.00
    95.054     10.60    99.292    118.091    100.60   149.633
         1     300.0       1.0        1.0       1.0       0.0
 3  30  30    66.378     12.25        0.0    73.744       0.0   112.269
   160.915     90.00    70.915    109.085     90.00   160.915
         1     300.0       1.0        1.0       1.0       0.0
 3  30  30     12.25    66.378        0.0    73.744       0.0   112.269
   160.915     90.00    70.915       90.0      0.00     90.00
         1     300.0       1.0        1.0       1.0       0.0
 2  25  10     24.50     11.00        0.0     83.40    -12.25   107.00
    61.376      90.0    28.624      90.00      0.00     90.00
         1     300.0       1.0        1.0       1.0       0.0
 2  66  50      65.5      49.4        0.0      20.2     -24.7     81.1
      0.0      90.0      90.0       90.0      90.0     180.0
         1     300.0       1.0        1.0       1.0       0.0
 2  66  40      65.5      38.6        0.0      20.2      24.7     81.1
     90.0       0.0      90.0       90.0      90.0     180.0
         1     300.0       1.0        1.0       1.0       0.0
 2  66  50      65.5      49.4        0.0     -18.4     -24.7     15.6
    180.0      90.0      90.0       90.0      90.0       0.0
```

```
         1      300.0       1.0       1.0       1.0       0.0
2  66  40       65.5      38.6       0.0      20.2     -24.7      15.6
      90.0      180.0      90.0      90.0      90.0       0.0
         1      300.0       1.0       1.0       1.0       0.0
5  32  10       2.628       9.0      4.65       0.0      24.7      30.4
       0.0       90.0      90.0      90.0       0.0      90.0
         1      300.0       1.0       1.0       2.0       0.0
5  32  25        2.00      25.0      9.50       0.0    -38.34     22.20
       0.0       90.0      90.0      90.0     160.0      70.0
         1      300.0       1.0       1.0       2.0       0.0
2 100 100       98.30     99.50      0.00    -80.00   -46.127     2.363
     90.00       68.00    158.00    180.00     90.00     90.00
         1      300.0       1.0       1.0       1.0       0.0
2 100 100       98.30     99.50      0.00    -80.00    46.127    39.837
     90.00      112.00     22.00    180.00     90.00     90.00
         1      300.0       1.0       1.0       1.0       0.0
5  32  50        3.00     47.95      5.50    -18.40      0.00     21.00
     90.00        0.00     90.00    180.00     90.00      90.0
         1      300.0       1.0       1.0       1.0       0.0
1  16   6        5.50       0.0       0.0    -66.35      0.00     21.00
     90.00        0.00     90.00      0.00     90.00      90.0
         1      300.0       1.0       1.0       1.0       0.0
2 100 100       98.30     99.50      0.00    178.30   -24.875    64.085
     90.00      150.00    120.00    180.00     90.00     90.00
         1      300.0       1.0       1.0       1.0       0.0
2 100 100       98.30     99.50      0.00    178.30    24.875   -21.885
     90.00       30.00     60.00    180.00     90.00     90.00
         1      300.0       1.0       1.0       1.0       0.0
5  32  50        3.00     46.15      5.50     20.20      0.00     21.00
     90.00        0.00     90.00      0.00     90.00      90.0
         1      300.0       1.0       1.0       1.0       0.0
1  16   6        5.50       0.0       0.0     66.35      0.00     21.00
     90.00        0.00     90.00     180.0     90.00      90.0
         1      300.0       1.0       1.0       1.0       0.0
1 120  20       38.45      18.0       0.0       0.0       0.0     15.60
       0.0       90.0      90.0      90.0      90.0     180.0
         1      300.0       1.0       1.0       1.0       0.0
4 120  20       38.45      20.0       0.0       0.0       0.0     15.60
       0.0       90.0      90.0      90.0      90.0     180.0
         1      300.0       1.0       1.0       1.0       0.0
1 120  25       38.45      25.6       0.0       0.0       0.0     -4.40
     180.0       90.0      90.0      90.0      90.0       0.0
         1      300.0       1.0       1.0       1.0       0.0
5 120  30       25.60      30.1      33.5       0.0       0.0     -4.20
       0.0       90.0      90.0      90.0      90.0     180.0
         1      300.0       1.0       1.0       1.0       0.0
1 120  24        23.2       0.0       0.0       0.0       0.0    -21.70
     180.0       90.0      90.0      90.0      90.0       0.0
         1      300.0       1.0       1.0       1.0       0.0
5 120  13       23.20      12.6      29.2       0.0       0.0    -21.70
       0.0       90.0      90.0      90.0      90.0     180.0
         1      300.0       1.0       1.0       2.0       0.0
1 120   5        33.5      29.2       0.0       0.0       0.0    -34.30
     180.0       90.0      90.0      90.0      90.0       0.0
         1      300.0       1.0       1.0       1.0       0.0
4  16  12         4.5      11.0       0.0    -55.00     55.00     -9.31
       0.0       90.0      90.0      90.0      90.0     180.0
         1      300.0       1.0       1.0       1.0       0.0
1  16   5         4.5       0.0       0.0    -55.00     55.00     -9.31
       0.0       90.0      90.0      90.0      90.0     180.0
         1      300.0       1.0       1.0       1.0       0.0
1  16   5         4.5       0.0       0.0    -55.00     55.00    -20.31
       0.0       90.0      90.0      90.0      90.0       0.0
         1      300.0       1.0       1.0       1.0       0.0
```

```
4  16  12      4.5      11.0       0.0     -55.00     -55.00     -9.31
       0.0     90.0      90.0      90.0       90.0      180.0
         1    300.0       1.0       1.0        1.0        0.0
1  16   5      4.5       0.0       0.0     -55.00     -55.00     -9.31
       0.0     90.0      90.0      90.0       90.0      180.0
         1    300.0       1.0       1.0        1.0        0.0
1  16   5      4.5       0.0       0.0     -55.00     -55.00    -20.31
       0.0     90.0      90.0      90.0       90.0        0.0
         1    300.0       1.0       1.0        1.0        0.0
4  16  12      4.5      11.0       0.0      55.00     -55.00     -9.31
       0.0     90.0      90.0      90.0       90.0      180.0
         1    300.0       1.0       1.0        1.0        0.0
1  16   5      4.5       0.0       0.0      55.00     -55.00     -9.31
       0.0     90.0      90.0      90.0       90.0      180.0
         1    300.0       1.0       1.0        1.0        0.0
1  16   5      4.5       0.0       0.0      55.00     -55.00    -20.31
       0.0     90.0      90.0      90.0       90.0        0.0
         1    300.0       1.0       1.0        1.0        0.0
4  16  12      4.5      11.0       0.0      55.00      55.00     -9.31
       0.0     90.0      90.0      90.0       90.0      180.0
         1    300.0       1.0       1.0        1.0        0.0
1  16   5      4.5       0.0       0.0      55.00      55.00     -9.31
       0.0     90.0      90.0      90.0       90.0      180.0
         1    300.0       1.0       1.0        1.0        0.0
1  16   5      4.5       0.0       0.0      55.00      55.00    -20.31
       0.0     90.0      90.0      90.0       90.0        0.0
         1    300.0       1.0       1.0        1.0        0.0
4  16  45      1.25     45.60      0.00      17.50      24.50     -3.00
    59.100   149.100    90.000    31.797     59.425     97.900
         1    300.0       1.0       1.0        1.0        0.0
4  16  45      3.00     44.20      0.00      17.50      24.50     -3.00
    43.600   133.600    90.000    46.955     44.212     98.200
         1    300.0       1.0       1.0        1.0        0.0
4  16  45      3.00     44.20      0.00      17.50     -24.50     -3.00
    43.600    46.400    90.000    46.955    135.788     98.200
         1    300.0       1.0       1.0        1.0        0.0
4  16  45      1.25     45.60      0.00      17.50     -24.50     -3.00
    59.100    30.900    90.000    31.797    120.575     97.900
         1    300.0       1.0       1.0        1.0        0.0
4  16  45      1.25     45.60      0.00     -17.50     -24.50     -3.00
    59.100   149.100    90.000   148.203    120.575     97.900
         1    300.0       1.0       1.0        1.0        0.0
4  16  45      3.00     44.20      0.00     -17.50     -24.50     -3.00
    43.600   133.600    90.000   133.045    135.788     98.200
         1    300.0       1.0       1.0        1.0        0.0
4  16  45      3.00     44.20      0.00     -17.50      24.50     -3.00
    43.600    46.400    90.000   133.045     44.212     98.200
         1    300.0       1.0       1.0        1.0        0.0
4  16  45      1.25     45.60      0.00     -17.50      24.50     -3.00
    59.100    30.900    90.000   148.203     59.425     97.900
         1    300.0       1.0       1.0        1.0        0.0
4  16  60      1.25     58.80      0.00      31.20       0.00    -33.00
    27.700   117.700    90.000    64.830     35.894     66.200
         1    300.0       1.0       1.0        1.0        0.0
4  16  60      1.25     56.50      0.00      31.20       0.00    -33.00
    21.800   111.800    90.000    68.412     23.089     82.200
         1    300.0       1.0       1.0        1.0        0.0
4  16  60      1.25     58.80      0.00       0.00     -31.20    -33.00
    62.300    27.700    90.000    35.894    115.170     66.200
         1    300.0       1.0       1.0        1.0        0.0
4  16  60      1.25     56.50      0.00       0.00     -31.20    -33.00
    68.200    21.800    90.000    23.089    111.588     82.200
         1    300.0       1.0       1.0        1.0        0.0
4  16  60      1.25     58.80      0.00     -31.20       0.00    -33.00
```

```
    27.700   117.700    90.000   115.170   144.106    66.200
         1     300.0       1.0       1.0       1.0       0.0
4   16  60      1.25     56.50      0.00    -31.20      0.00    -33.00
    21.800   111.800    90.000   111.588   156.911    82.200
         1     300.0       1.0       1.0       1.0       0.0
4   16  60      1.25     58.80      0.00      0.00     31.20    -33.00
    62.300    27.700    90.000   144.106    64.830    66.200
         1     300.0       1.0       1.0       1.0       0.0
4   16  60      1.25     56.50      0.00      0.00     31.20    -33.00
    68.200    21.800    90.000   156.911    68.412    82.200
         1     300.0       1.0       1.0       1.0       0.0
4   16  60      1.25     58.80      0.00      0.00     31.20    -33.00
    62.300   152.300    90.000    35.894    64.830    66.200
         1     300.0       1.0       1.0       1.0       0.0
4   16  60      1.25     56.50      0.00      0.00     31.20    -33.00
    68.200   158.200    90.000    23.089    68.412    82.200
         1     300.0       1.0       1.0       1.0       0.0
4   16  60      1.25     58.80      0.00     31.20      0.00    -33.00
    27.700    62.300    90.000    64.830   144.106    66.200
         1     300.0       1.0       1.0       1.0       0.0
4   16  60      1.25     56.50      0.00     31.20      0.00    -33.00
    21.800    68.200    90.000    68.412   156.911    82.200
         1     300.0       1.0       1.0       1.0       0.0
4   16  60      1.25     58.80      0.00      0.00    -31.20    -33.00
    62.300   152.300    90.000   144.106   115.170    66.200
         1     300.0       1.0       1.0       1.0       0.0
4   16  60      1.25     56.50      0.00      0.00    -31.20    -33.00
    68.200   158.200    90.000   156.911   111.588    82.200
         1     300.0       1.0       1.0       1.0       0.0
4   16  60      1.25     58.80      0.00    -31.20      0.00    -33.00
    27.700    62.300    90.000   115.170    35.894    66.200
         1     300.0       1.0       1.0       1.0       0.0
4   16  60      1.25     56.50      0.00    -31.20      0.00    -33.00
    21.800    68.200    90.000   111.588    23.089    82.200
         1     300.0       1.0       1.0       1.0       0.0
```

Freemac Didier model: solar panels in -60°/22° configuration.

```
        82    35650.0      144.0     190.00        0.0        0.0        0.0
        20       90.0      -90.0        1.0       10.0        0.0       90.0
         0        1.0       27.5      225.0       1.40
 5  32   8        0.0        5.4      9.968        0.0        0.0     99.761
     180.0       90.0       90.0       90.0       90.0        0.0
         1      300.0        1.0        1.0        2.0        0.0
 5 180  10     65.321       5.08       72.0        0.0        0.0     76.881
     180.0       90.0       90.0       90.0       90.0        0.0
         1      300.0        1.0        1.0        2.0        0.0
 5 180  10     57.428       5.08     65.321        0.0        0.0     71.801
     180.0       90.0       90.0       90.0       90.0        0.0
         1      300.0        1.0        1.0        2.0        0.0
 5 180  10     47.723       5.08     57.428        0.0        0.0     66.721
     180.0       90.0       90.0       90.0       90.0        0.0
         1      300.0        1.0        1.0        2.0        0.0
 5 180  10     34.720       5.08     47.723        0.0        0.0     61.641
     180.0       90.0       90.0       90.0       90.0        0.0
         1      300.0        1.0        1.0        2.0        0.0
 1  60  15     34.720        0.0        0.0        0.0        0.0     61.641
       0.0       90.0       90.0       90.0       90.0      180.0
         1      300.0        1.0        1.0        1.0        0.0
 4 180  20     34.720     12.550        0.0        0.0       0.00     61.641
       0.0       90.0       90.0       90.0       90.0      180.0
         1      300.0        1.0        1.0        1.0        0.0
 1 180  32     34.720      19.30        0.0        0.0        0.0     49.091
     180.0       90.0       90.0       90.0       90.0        0.0
         1      300.0        1.0        1.0        1.0        0.0
 2  64  36     63.90       38.60        0.0      19.30      24.70     49.091
      90.0        0.0       90.0       90.0       90.0      180.0
         1      300.0        1.0        1.0        1.0        0.0
 2  64  48     63.90       49.40        0.0      19.30     -24.70     49.091
       0.0       90.0       90.0       90.0       90.0      180.0
         1      300.0        1.0        1.0        1.0        0.0
 2  64  36     63.90       38.60        0.0      19.30     -24.70    -14.809
      90.0      180.0       90.0       90.0       90.0        0.0
         1      300.0        1.0        1.0        1.0        0.0
 2  64  48     63.90       49.40        0.0     -19.30     -24.70    -14.809
     180.0       90.0       90.0       90.0       90.0        0.0
         1      300.0        1.0        1.0        1.0        0.0
 1 180  40     36.60       19.30        0.0        0.0        0.0    -14.809
       0.0       90.0       90.0       90.0       90.0      180.0
         1      300.0        1.0        1.0        1.0        0.0
 4 180  30     36.60       16.80        0.0        0.0        0.0    -14.809
       0.0       90.0       90.0       90.0       90.0      180.0
         1      300.0        1.0        1.0        1.0        0.0
 1 180  16     36.60       28.40        0.0        0.0        0.0    -31.649
     180.0       90.0       90.0       90.0       90.0        0.0
         1      300.0        1.0        1.0        1.0        0.0
 5 180  56     28.40       33.27      31.70        0.0        0.0    -31.649
       0.0       90.0       90.0       90.0       90.0      180.0
         1      300.0        1.0        1.0        1.0        0.0
 1 180  30     19.40        0.0        0.0        0.0        0.0    -53.569
     180.0       90.0       90.0       90.0       90.0        0.0
         1      300.0        1.0        1.0        1.0        0.0
 1 120   5     31.70       27.4        0.0        0.0        0.0    -64.919
       0.0       90.0       90.0       90.0       90.0        0.0
         1      300.0        1.0        1.0        1.0        0.0
 5 120  20     19.40     11.350       27.4        0.0        0.0    -53.569
       0.0       90.0       90.0       90.0       90.0      180.0
```

```
         1      300.0        1.0        1.0        2.0        0.0
5  32  10        2.7       10.5        4.7        0.0       24.7    -1.179
      0.0       90.0       90.0       90.0        0.0       90.0
         1      300.0        1.0        1.0        2.0        0.0
5  32  32        0.0       32.7       9.38        0.0      -33.4    -7.519
     90.0       68.9       21.1       90.0      158.9       68.9
         1      300.0        1.0        1.0        2.0        0.0
5  32  50        0.00      75.90       10.0      45.40        0.0    10.181
     90.0        0.0       90.0       62.0       90.0       28.0
         1      300.0        1.0        1.0        1.0        0.0
4  32  45        4.75      47.60        0.0     -19.30        0.0    -8.529
     90.0       90.0      180.0      180.0       90.0       90.0
         1      300.0        1.0        1.0        1.0        0.0
6  16  16        6.00       0.0        0.0     -66.90        0.0    -8.529
     90.0        0.0       90.0        0.0       90.0       90.0
         1      300.0        1.0        1.0        1.0        0.0
4  16  50        2.00     107.30        0.0     -66.90        0.0    -8.529
     90.0       90.0      180.0      180.0       90.0       90.0
         1      300.0        1.0        1.0        1.0        0.0
6  16  16        2.00       0.0        0.0    -174.20        0.0    -8.529
     90.0        0.0       90.0        0.0       90.0       90.0
         1      300.0        1.0        1.0        1.0        0.0
4  32  45        4.75      47.60        0.0      66.90       0.00    -8.529
     90.0       90.0      180.0      180.0       90.0       90.0
         1      300.0        1.0        1.0        1.0        0.0
6  16  16        6.00       0.0        0.0      66.90       0.00    -8.529
     90.0        0.0       90.0      180.0       90.0       90.0
         1      300.0        1.0        1.0        1.0        0.0
4  16  50        2.00     107.30        0.0      66.90       0.00    -8.529
     90.0        0.0       90.0        0.0       90.0       90.0
         1      300.0        1.0        1.0        1.0        0.0
6  16  16        2.00       0.0        0.0     174.20        0.0    -8.529
     90.0        0.0       90.0      180.0       90.0       90.0
         1      300.0        1.0        1.0        1.0        0.0
2  50  50       99.40      97.26       0.00     178.20    -24.315    35.586
    90.00      150.00     120.00     180.00      90.00      90.00
         1      300.0        1.0        1.0        1.0        0.0
2  50  50       99.40      97.26       0.00     -78.80     -45.09   -24.749
    90.00       68.00     158.00     180.00      90.00      90.00
         1      300.0        1.0        1.0        1.0        0.0
2  50  50       99.40      97.26       0.00     178.20     24.315   -48.544
    90.00       30.00      60.00     180.00      90.00      90.00
         1      300.0        1.0        1.0        1.0        0.0
2  50  50       99.40      97.26       0.00     -78.80      45.09    11.791
    90.00      112.00      22.00     180.00      90.00      90.00
         1      300.0        1.0        1.0        1.0        0.0
4  32  11        5.9        5.2        0.0      57.20      55.50   -43.249
      0.0       90.0       90.0       90.0       90.0      180.0
         1      300.0        1.0        1.0        1.0        0.0
1  32   6        5.9        0.0        0.0      57.20      55.50   -43.249
      0.0       90.0       90.0       90.0       90.0      180.0
         1      300.0        1.0        1.0        1.0        0.0
1  32   6        5.9        0.0        0.0      57.20      55.50   -48.449
      0.0       90.0       90.0       90.0       90.0        0.0
         1      300.0        1.0        1.0        1.0        0.0
4  32  54        1.1     54.074        0.0     29.550        0.0   -64.919
  152.901     62.901       90.0     65.721     36.527     64.511
         1      300.0        1.0        1.0        1.0        0.0
4  32  36        1.1     36.338        0.0     51.785     43.452   -41.649
  116.779     26.779       90.0    151.445    116.313     79.696
         1      300.0        1.0        1.0        1.0        0.0
4  32  51        1.1     51.751        0.0     29.550        0.0   -64.919
  158.377     68.377       90.0     68.760     23.946     79.456
         1      300.0        1.0        1.0        1.0        0.0
```

```
4  32  52       1.1     52.320       0.0     48.298     47.297    -55.449
   110.176    20.176       90.0   157.389    109.829    100.428
          1     300.0        1.0       1.0        1.0        0.0
4  32  34       2.7     34.681       0.0     19.867     27.345    -35.149
   133.840    43.840       90.0    44.888     47.127    100.802
          1     300.0        1.0       1.0        1.0        0.0
4  32  54       1.1     54.533       0.0     44.438     50.941    -41.649
   115.704    25.704       90.0   144.577    113.095    115.259
          1     300.0        1.0       1.0        1.0        0.0
6  16  16       2.7      0.0         0.0     44.438     50.941    -41.649
   133.840    43.840       90.0   135.112    132.873     79.198
          1     300.0        1.0       1.0        1.0        0.0
5  16  11       0.0     11.2         2.80    59.30      56.30     -48.449
        0.0     90.0       90.0      90.0     90.0      180.0
          1     300.0        1.0       1.0        1.0        0.0
5  16  11       0.0     11.2         2.80    55.00      60.80     -48.449
        0.0     90.0       90.0      90.0     90.0      180.0
          1     300.0        1.0       1.0        1.0        0.0
4  32  11       5.9      5.2         0.0     57.20     -55.50     -43.249
        0.0     90.0       90.0      90.0     90.0      180.0
          1     300.0        1.0       1.0        1.0        0.0
1  32   6       5.9      0.0         0.0     57.20     -55.50     -43.249
        0.0     90.0       90.0      90.0     90.0      180.0
          1     300.0        1.0       1.0        1.0        0.0
1  32   6       5.9      0.0         0.0     57.20     -55.50     -48.449
        0.0     90.0       90.0      90.0     90.0        0.0
          1     300.0        1.0       1.0        1.0        0.0
4  32  54       1.1     54.074       0.0     29.550        0.0    -64.919
    27.099    62.901       90.0    65.721    143.473     64.511
          1     300.0        1.0       1.0        1.0        0.0
4  32  36       1.1     36.338       0.0     51.785     -43.452    -41.649
    63.221    26.779       90.0   151.445     63.687     79.696
          1     300.0        1.0       1.0        1.0        0.0
4  32  51       1.1     51.751       0.0     29.550        0.0    -64.919
    21.623    68.377       90.0    68.760    156.054     79.456
          1     300.0        1.0       1.0        1.0        0.0
4  32  52       1.1     52.320       0.0     48.298     -47.297    -55.449
    69.824    20.176       90.0   157.389     70.171    100.428
          1     300.0        1.0       1.0        1.0        0.0
4  32  34       2.7     34.681       0.0     19.867     -27.345    -35.149
    46.160    43.840       90.0    44.888    132.873    100.802
          1     300.0        1.0       1.0        1.0        0.0
4  32  54       1.1     54.533       0.0     44.438     -50.941    -41.649
    64.296    25.704       90.0   144.577     66.905    115.259
          1     300.0        1.0       1.0        1.0        0.0
6  16  16       2.7      0.0         0.0     44.438     -50.941    -41.649
   133.840   136.160       90.0   135.112     47.127     79.198
          1     300.0        1.0       1.0        1.0        0.0
5  16  11       0.0     11.2         2.80    59.30      -56.30     -48.449
        0.0     90.0       90.0      90.0     90.0       180.0
          1     300.0        1.0       1.0        1.0        0.0
5  16  11       0.0     11.2         2.80    55.00      -60.80     -48.449
        0.0     90.0       90.0      90.0     90.0       180.0
          1     300.0        1.0       1.0        1.0        0.0
4  32  11       5.9      5.2         0.0     -57.20     -55.50     -43.249
        0.0     90.0       90.0      90.0     90.0       180.0
          1     300.0        1.0       1.0        1.0        0.0
1  32   6       5.9      0.0         0.0     -57.20     -55.50     -43.249
        0.0     90.0       90.0      90.0     90.0       180.0
          1     300.0        1.0       1.0        1.0        0.0
1  32   6       5.9      0.0         0.0     -57.20     -55.50     -48.449
        0.0     90.0       90.0      90.0     90.0        0.0
          1     300.0        1.0       1.0        1.0        0.0
4  32  54       1.1     54.074       0.0     -29.550       0.0     -64.919
```

```
   152.901     62.901      90.0    114.279    143.473     64.511
         1      300.0       1.0        1.0        1.0       0.0
4  32  36        1.1     36.338        0.0    -51.785    -43.452    -41.649
   116.779     26.779      90.0     28.555     63.687     79.696
         1      300.0       1.0        1.0        1.0       0.0
4  32  51        1.1     51.751        0.0    -29.550       0.0    -64.919
   158.377     68.377      90.0    111.240    156.054     79.456
         1      300.0       1.0        1.0        1.0       0.0
4  32  52        1.1     52.320        0.0    -48.298    -47.297    -55.449
   110.176     20.176      90.0     22.611     70.171    100.428
         1      300.0       1.0        1.0        1.0       0.0
4  32  34        2.7     34.681        0.0    -19.867    -27.345    -35.149
   133.840     43.840      90.0    135.112    132.873    100.802
         1      300.0       1.0        1.0        1.0       0.0
4  32  54        1.1     54.533        0.0    -44.438    -50.941    -41.649
   115.704     25.704      90.0     35.423     66.905    115.259
         1      300.0       1.0        1.0        1.0       0.0
6  16  16        2.7      0.0         0.0    -44.438    -50.941    -41.649
    46.160    136.160      90.0     44.888     47.127     79.198
         1      300.0       1.0        1.0        1.0       0.0
5  16  11        0.0     11.2         2.80    -59.30     -56.30     -48.449
       0.0      90.0      90.0         90.0     90.0      180.0
         1      300.0       1.0        1.0        1.0       0.0
5  16  11        0.0     11.2         2.80    -55.00     -60.80     -48.449
       0.0      90.0      90.0         90.0     90.0      180.0
         1      300.0       1.0        1.0        1.0       0.0
4  32  11        5.9      5.2         0.0    -57.20      55.50     -43.249
       0.0      90.0      90.0         90.0     90.0      180.0
         1      300.0       1.0        1.0        1.0       0.0
1  32   6        5.9      0.0         0.0    -57.20      55.50     -43.249
       0.0      90.0      90.0         90.0     90.0      180.0
         1      300.0       1.0        1.0        1.0       0.0
1  32   6        5.9      0.0         0.0    -57.20      55.50     -48.449
       0.0      90.0      90.0         90.0     90.0        0.0
         1      300.0       1.0        1.0        1.0       0.0
4  32  54        1.1     54.074        0.0    -29.550       0.0    -64.919
    27.099     62.901      90.0    114.279     36.527     64.511
         1      300.0       1.0        1.0        1.0       0.0
4  32  36        1.1     36.338        0.0    -51.785     43.452    -41.649
    63.221     26.779      90.0     28.555    116.313     79.696
         1      300.0       1.0        1.0        1.0       0.0
4  32  51        1.1     51.751        0.0    -29.550       0.0    -64.919
    21.623     68.377      90.0    111.240     23.946     79.456
         1      300.0       1.0        1.0        1.0       0.0
4  32  52        1.1     52.320        0.0    -48.298     47.297    -55.449
    69.824     20.176      90.0     22.611    109.829    100.428
         1      300.0       1.0        1.0        1.0       0.0
4  32  34        2.7     34.681        0.0    -19.867     27.345    -35.149
    46.160     43.840      90.0    135.112     47.127    100.802
         1      300.0       1.0        1.0        1.0       0.0
4  32  54        1.1     54.533        0.0    -44.438     50.941    -41.649
    64.296     25.704      90.0     35.423    113.095    115.259
         1      300.0       1.0        1.0        1.0       0.0
6  16  16        2.7      0.0         0.0    -44.438     50.941    -41.649
   133.840    136.160      90.0     44.888    132.873     79.198
         1      300.0       1.0        1.0        1.0       0.0
5  16  11        0.0     11.2         2.80    -59.30      56.30     -48.449
       0.0      90.0      90.0         90.0     90.0      180.0
         1      300.0       1.0        1.0        1.0       0.0
5  16  11        0.0     11.2         2.80    -55.00      60.80     -48.449
       0.0      90.0      90.0         90.0     90.0      180.0
         1      300.0       1.0        1.0        1.0       0.0
```

Appendix F: Freemac File Formats

Input Files:

freedat.dat	Input free stream and geometry file
freepath.dat	Input θ and ϕ attitude list

Output Files:

matout.out	Output force and moment coefficients in Matlab format
tecout.plt	Output force and moment coefficients in Tecplot format
freesnap.PLT	Output graphic file of pressure and shear in Tecplot format
elemchk.dat	Output force and moment coefficients of each component in freedat.dat

Freedat.dat

freedat.dat is a fixed format ASCII data file consisting of a three line header followed by a list of components. A numbered column bar is shown for convenience, all variables should be right justified.

header data:

```
12345678901234567890123456789012345678901234567890123456789012345678901234567890
      NC      AREF      LREF       PPL       XBO       YBO       ZBO
     NDS      TMIN      PMIN      TDEL      PDEL      TMAX      PMAX
    IMOD     CPXYZ        SR      TINF      GAMM
```

NC	Number of Components in model
AREF, LREF	Reference Area and Length
PPL	Boundary radius
XBO, YBO, ZBO	Center of Mass of model
NDS	Number of panel division, used in shadowing routine
TMIN, PMIN, TDEL	No longer used
PDEL, TMAX, PMAX	
IMOD	
CPXYZ	Flag to calculate center of pressure (1=yes, 0=no)
SR	Molecular speed ratio
TINF	Ambient free stream temperature
GAMM	Gamma value

component:

```
12345678901234567890123456789012345678901234567890123456789012345678901234567890

ID ND1 ND2          D1          D2          D3          XCO          YCO          ZCO
       AXX          AXY         AXZ         AYX         AYY          AYZ
       DUM          TMP         NAC         TAC         SIDE         SMOD
```

ID	Component ID number
ND1, ND2	Number of surface division, determine surface discretization
D1, D2, D3	Component dimensions
XCO, YCO, ZCO	Body axis location of component axis origin
AXX, AXY, AXZ	Degree angles between component x axis and body axes
AYX, AYY, AYZ	Degree angles between component y axis and body axes
DUM	No longer used
TMP	Component temperature
NAC, TAC	Normal and tangential accommodation coefficients
SIDE	Number of active sides (1.0 or 2.0)
SMOD	Surface model (0.0=constant accom. 1.0=K-P, 2.0=Nocilla)

Freepath.dat

freepath.dat contains the θ and ϕ used when solving for an attitude trajectory.

```
12345678901234567890123456789012345678901234567890123456789012345678901234567890

  NDP
       TIME       THETA          PHI
```

NDP	Number of trajectory points
TIME	Time index, optional, else put 0.0
THETA	θ in degrees
PHI	f in degrees

Matout.out and Tecout.PLT

Matout.out is an ASCII file formatted for use by Matlab containing the aerodynamic characteristics determined by freemac. Tecout.PLT is a Tecplot format ASCII file containing the same information as matout.out. The information presented, from left to right in the files are: time, θ and ϕ in degrees, drag coefficient, the force coefficients in the body axis x, y, and z, and the moment coefficients in the body axis x, y, and z.

Freesnap.PLT

Freesnap.PLT contains the location, pressure and shear coefficient data determined for each element determined by freemac in a Tecplot format that can be imaged.

Elemchk.dat

Elemchk.dat is an ASCII file that contains the force and moment coefficients determined by freemac for each of the components in a model. The coefficient output is in the same order as they are listed in the corresponding freedat.dat file. A final line is added that presents the summation of the previous lines.

References

1. National Aeronautics and Space Administration, "Magellan: The Unveiling of Venus, "JPL 400-345 8/89, March 1993, pp. 23.

2. D.T. Lyons, "Aerobraking Magellan: Plan versus Reality," Advances in the Astronautic Sciences, 87, part II, 1994, pp. 663-680.

3. D.T. Lyons and F.C. Hurlbut, "Measuring the Lift Coefficients in Free Molecular Flow while Aerobraking Magellan", 18th International Symposium on Rarefied Gas Dynamics, University of British Columbia, Vancouver, Canada, July 26-31, 1992.

4. R.C. Espiritu and R.H. Tolson, "Determining Upper Atmosphere Characteristics using Magellan Attitude Control Data," AAS/AIAA Spaceflight Mechanics Meeting, Albuquerque, NM, 2/13-16/95, AAS Paper 95-152.

5. R. Fredo, "A Numerical Procedure for Calculating the Aerodynamic Coefficients for Complex Spacecraft Configurations in Free-Molecular Flow," Master's Thesis, Penn. State Univ., June 1980.

6. R. Fredo and M. Kaplan, "Procedure for Obtaining Aerodynamic Properties of Spacecraft," AIAA-81-4214, Journal of Spacecraft, vol. 18, no. 4, July-August, 1981.

7. M.S. Woronowicz and D.F.G. Rault, "Direct Simulation Monte Carlo Prediction Of On-Orbit Contaminant Deposit Levels for HALOE," NASA TM-109069, August 1994.

8. R.H. Tolson, M. Patterson, and D.T. Lyons,"Magellan Windmill and Termination Experiments," Spaceflight Dynamics, Cépaduès-Éditions, pp. 265, Toulouse, June 95.

9. D.F.G. Rault, "Aerodynamic Characteristics of Magellan Spacecraft in Venus Upper Atmosphere," AIAA 93-0723, 31st Aerospace Sciences Meeting and Exhibit, Reno NV, January 11-14, 1993.

10. A.S. Carpenter, "Control of the Magellan Space Craft During Aerobraking.", AAS 93-016, 16th Annual AAS Guidance and Control Conference. Keystone, CO, Feb. 1993.

11. D.T. Lyons, "Magellan: Planetary Constants and Models," JPL D-2300, Rev. E, April 1, 1992, sect. 2-1.

12. C.A. Croom and R.H. Tolson, "Venusian Atmospheric and Magellan Properties From Attitude Control Data," NASA CR-4619, August 1994.

13. G.M. Keating, A.J. Kliore, and V.I. Moroz, "Venus International Reference Atmosphere,"Advances in Space Research, vol. 5, No. 11, 1985.

14. "Tecplot Version 6 User's Manual", Central Scientific Computing Complex Document G-19B, Amtec Engineering, Inc. P.O. Box 3633 Bellevue, WA 98009-3633.

REPORT DOCUMENTATION PAGE

Form Approved
OMB No. 0704-0188

1. AGENCY USE ONLY (Leave blank)	2. REPORT DATE	3. REPORT TYPE AND DATES COVERED
	March 1998	Contractor Report

4. TITLE AND SUBTITLE
Magellan Aerodynamic Characteristics During the Termination Experiment Including Thruster Plume-Free Stream Interaction

5. FUNDING NUMBERS
NCC1-104

242-80-01-01

6. AUTHOR(S)

Francisco J. Cestero
Robert H. Tolson

7. PERFORMING ORGANIZATION NAME(S) AND ADDRESS(ES)

The George Washington University
Joint Institute for Advancement of Flight Sciences
NASA Langley Research Center
Hampton, VA 23681-2199

8. PERFORMING ORGANIZATION REPORT NUMBER

9. SPONSORING / MONITORING AGENCY NAME(S) AND ADDRESS(ES)

National Aeronautics and Space Administration
Langley Research Center
Hampton, VA 23681-2199

10. SPONSORING / MONITORING AGENCY REPORT NUMBER

NASA/CR-1998-206940

11. SUPPLEMENTARY NOTES
The information submitted in this report was offered as a thesis by the first author in partial fulfillment of the requirements for the Degree of Master of Science, The George Washington University, JIAFS. Langley Technical Monitor: Dr. D. F. G. Rault

12a. DISTRIBUTION / AVAILABILITY STATEMENT
Unclassified - Unlimited
Subject Category 18
Distribution Nonstandard
Availability: NASA CASI (301) 621-0290

12b. DISTRIBUTION CODE

13. ABSTRACT *(Maximum 200 words)*

Results are presented on the aerodynamic characteristics of the Magellan spacecraft during the October 1994 Termination Experiment, including the effects of the thruster engine exhaust plumes upon the molecular free stream around the spacecraft and upon the aerodynamics coefficients. As Magellan passed through the Venusian atmosphere, the solar arrays were turned in opposite directions relative to the free stream creating a torque on the spacecraft. The spacecraft control system was programmed to counter the effects of this torque with attitude control engines to maintain an inertially fixed attitude. The orientation and reaction engine telemetry returned from Magellan are used to create a model of the aerodynamic torques. Geometric models of the Magellan spacecraft are analyzed with the aid of both free molecular and Direct Simulation Monte Carlo codes. The simulated aerodynamic torques determined are compared to the measured torques. The Direct Simulation Monte Carlo method is also used to model the attitude engine exhaust plumes, the free stream disturbance caused by these plumes, and the resulting torques acting on the spacecraft compared to no-exhaust plume cases. The effect of the exhaust plumes was found to be sufficiently large that thrust reversal is possible.

14. SUBJECT TERMS
Magellan mission, aerothermodynamics, transition flow

15. NUMBER OF PAGES
117

16. PRICE CODE
A06

17. SECURITY CLASSIFICATION OF REPORT	18. SECURITY CLASSIFICATION OF THIS PAGE	19. SECURITY CLASSIFICATION OF ABSTRACT	20. LIMITATION OF ABSTRACT
Unclassified	Unclassified	Unclassified	

NSN 7540-01-280-5500

Standard Form 298 (Rev. 2-89)
Prescribed by ANSI Std. Z39-18
298-102